

**DEBRISFALL ASSESSMENT IN MOUNTAIN
CATCHMENTS FOR LOCAL END-USERS**
Contract No EVG1 - CT-1999-00007

GRANULAR FLOWS AND NUMERICAL MODELLING OF LANDSLIDES

Giovanni B. Crosta¹,
Francesco Calvetti², Silvia Imposimato²
Dennis Roddeman³, Paolo Frattini¹, Federico Agliardi¹

¹Dip. Scienze Geologiche e Geotecnologie, Università degli Studi di Milano Bicocca

²Dip. Ingegneria Strutturale, Politecnico di Milano

³FEAT, Finite Element Applications Technology



CONTENTS

1. INTRODUCTION	3
2. GRANULAR MATERIALS	3
3. CLASSIFICATION OF FLOWS.....	8
4. DRY GRANULAR FLOWS.....	12
4.1. Morphological and sedimentological characteristics of Rock avalanches.....	12
4.2. Experimental work	13
4.3. The Distinct Element model.....	16
4.4. General features of the numerical simulations	16
4.5. Numerical model.....	17
4.5.1. Numerical Parameters.....	17
4.5.2. Contact parameters	17
4.5.3. Numerical damping.....	18
4.5.4. Small scale simulations.....	18
4.6. Sensitivity analysis	21
4.6.1 Contact parameters	21
4.6.2. Numerical damping.....	23
4.7. Parameter Calibration	23
4.8. Large scale simulations	30
4.8.1. Description of the val Pola rock avalanche	30
4.8.2. Numerical simulations	31
4.9. Discussion	34
4.10. Critical review of results	36
5. AN EXAMPLE OF DEPTH AVERAGED MODEL.....	36
5.1. Val Pola rock avalanche.....	38
5.2. Sesa landslide.....	41
5.2.1. Landslide dynamics.....	45
6. FINITE ELEMENT MODELLING.....	46
7. EMPIRICAL AND SEMIEMPIRICAL RELATIONSHIPS	51
7.1. Empirical relationships for debris flows.....	52
8. REFERENCES	62

1. INTRODUCTION

Gravity-driven flows of grain-fluid mixtures with free upper surfaces are quite common geomorphologic processes. These phenomena can show different characteristics (eg.: dilatancy, internal friction, particles collision, fluidization, particle size segregation, variable pore pressure, etc.) and can interest very different volumes, types of materials and environments. Among the various processes that can be observed in nature the most interesting are: debris flows, debris avalanches, pyroclastic flows, rapid mudflows, mass falls and rock avalanches. Distinctions among the different phenomena can be done by considering the presence and abundance of each phase (solid, air and water), the properties of the solid phase.

Rock avalanches and mass rock falls are commonly dry mass movements in which pore fluid play a negligible role and for which an exceptional runout is usually observed. Debris flows and rapid mudflows are formed by liquid-saturated debris, coarse and fine respectively, and can originate both along open slopes or within a drainage channel. Debris flows may include a wide range of sediment sizes and their mechanical characteristics vary significantly with differences in water and silt and clay content, and sediment size and sorting (COSTA, 1984). The term debris flow is often broadly interpreted to include rapid mudflows, lahars, flow-tills, wet grain flows and wet rock avalanches, with or without a viscous interstitial fluid. Pyroclastic flows are gas-charged phenomena differently linked to the volcanic activity. All these phenomena travel very large distances, generally much larger than one would expect on the basis that the loss in potential energy, from initiation to runout, is balanced by the work done due to basal sliding.

Many researchers are involved in the modeling of granular flows and modeled mathematically these types of processes by using different rheological rules and modeling approaches. We don't want to develop here any specific approach but simply we want to summarize some of the most recent results published in the literature. The application of some numerical technique will be also discussed or presented.

As a consequence we will make use of the published contributions of investigators that have been involved most recently on this subject and especially on the study of granular flows as natural slope instability phenomena.

2. GRANULAR MATERIALS

A granular material is an assembly of a large number of discrete solid components that are dispersed in one or more fluids. The granular flow may behave like a solid or a fluid showing very different behaviour and features both during and after movement. Dispersed single-phase flows are those for which the interstitial fluids play a minor role during flow and in the transportation of momentum. If the mass or volume of the interstitial fluid is comparable to that of the solids the fluid-solid interactions are significant. Therefore, the motion of the fluid through the pores can provide the driving force for the flow of the solid phase. This behaviour is quite well known in soil mechanics but the description of the dynamic behaviour of flowing granular materials can involves aspects pertaining to traditional fluid mechanics, soil mechanics, plasticity theory and rheology.

Granular materials show distinctive features that are not relevant for other single phase fluids or materials. Granular materials can behave differently accordingly to the type and the amount of applied stress and the grain size distribution of the material or the water content. As a consequence, it has been observed by various investigators that these mixtures can rapidly change their behaviour from solid-like to fluid-like because of small changes in boundary conditions. Flow freezing, inverse or direct gradation, levees, front snouts and tilting are among the effects of such rapid changes. Three simple fluid models have been proposed initially for these flows to explain these different behaviour, namely: Newtonian flow, both laminar or turbulent, Bingham and

Herschel Bulkley (non linear) fluid flow (in laminar regime) and dilatant grain shearing flow, especially within the inertial regime

The most distinctive features of granular materials are, namely: dilatancy, Coulomb-like behaviour, particle size segregation, fluidization, grain collision.

Dilatancy is the result of the passage from the initial dense state of a material, when at rest, to the open or dilated packing typical of a flowing ensemble of particles. REYNOLDS (1885) termed this particle over riding behaviour as dilatancy. Dilatancy and compaction are typical of the initiation and deposition phases, respectively. Nevertheless, when a granular material is flowing the volume is usually preserved and only minor changes are observed.

When grains are poured on a rough horizontal plane from a fixed source point they pile up in a heap. The angle at the base of the material is called angle of repose and represents a limiting value for equilibrium of the material. The behaviour of the material can be explained according to the Mohr-Coulomb yield criterion. This criterion relates the shear strength on a plane within the material with the normal stress acting on it through the coefficient of friction and cohesion. Generally, it is assumed that the angle of internal friction and the angle of dilatancy are equal (associated flow rule). Various investigators support the validity of Coulomb's model. This model considers deformation as independent by the shear rate in granular mixtures. According to IVERSON & DENLINGER (2001), the intergranular stresses satisfy the COULOMB rule (1776) whereas the changes in flow behaviour are the result of different actions related to pore fluids, topographic features and inertial forces. This can be reasonably accepted also in very rapid granular flows, for which a collisional mechanism dominates (SAVAGE, 1984, SAVAGE & HUTTER, 1989)

An esteem of the role of Coulomb friction and grain collisions on gravity-driven granular flows can be done through a criterion defined by SAVAGE (1984, SAVAGE & HUTTER, 1989) by means of dimensional analysis. IVERSON (1997) generalized this approach to account for the presence of pore fluid at equilibrium pressure. The proposed criterion makes use of a dimensionless parameter, N_{SAV} (Savage number), to describe stresses in steady, uniform flows:

$$N_{SAV} = \frac{\dot{\gamma}^2 \delta}{g}$$

modified by Iverson in:

$$N_{SAV} = \frac{\rho_s}{(\rho_s - \rho_f)} \frac{\dot{\gamma}^2 \delta}{g}$$

or

$$N_{SAV} = \frac{\rho_s \dot{\gamma}^2 \delta^2}{(\rho_s - \rho_f) g H}$$

where ρ_s and ρ_f are the mass densities of the solid grains and intergranular fluid, respectively, $\dot{\gamma}$ is the bulk shear rate (du/dy where u is the velocity parallel to the slope of the basal flow surface), δ is the grain diameter, g is the gravitational acceleration, and H the flow thickness. Therefore, N_{SAV} represents the ratio of stresses connected to grain collision to those due to the gravitational grain contact. Generally (SAVAGE & HUTTER, 1989, IVERSON, 1997, IVERSON & DENLINGER, 2001), it is assumed that if $N_{SAV} > 0.1$ grain collisions have a strong effect on flow dynamics. In presence of a fluid within pores, pore fluid pressure can influence the stress state within the material inducing changes in frictional resistance. This is known as the effective stress principle (TERZAGHI, 1936) in soil mechanics and it applicable both to slow and rapid deformations.

BAGNOLD (1954) and other researchers performed shear cell experiments with different approaches and showed that an equation identical to the Coulomb equation for cohesionless materials ($c = 0$) describes the relationship between bulk intergranular normal and shear stresses even in collision-

dominated flows with $N_{SAV} \rightarrow \infty$. Bagnold (1954) also found that bulk normal stresses in rapid, collision-dominated flows depend on shear rate. This dependence is absent in slower, friction-dominated flows. The difference between bulk normal stresses in rapid ($N_{SAV} > 0.1$) gravity-driven flows with free upper surfaces and slower flows can be ascribed to grain collisions which tend to decrease mixture density by dilation of the solid phase. Bagnold's experiments also assessed the role of viscous fluid stresses in granular mixtures. He distinguished contributions of grain collision and viscous stresses in steady, uniform shear flows on the basis of a dimensionless parameter, N_B :

$$N_{BAG} = \left(\frac{v_s^{1/3}}{v_*^{1/3} - v_s^{1/3}} \right)^{1/2} \frac{\rho_s \dot{\gamma} \delta^2}{\mu} = \frac{\lambda^{1/2} \rho_s \dot{\gamma} \delta^2}{\mu}$$

where $\lambda = \left(\frac{v_s^{1/3}}{v_*^{1/3} - v_s^{1/3}} \right) = \left\{ \left(\frac{v_*}{v_s} \right)^{1/3} - 1 \right\}^{-1}$ is the linear concentration of solid particles and it is

usually defined as the ratio between the particles diameter and their reciprocal distance and for highly packed structures $\lambda = \infty$.

N_{BAG} depends on the same properties used for N_{SAV} and also depend on v_s , the volume fraction (concentration) of the granular solids that is generally assumed equal to the one of the undisturbed surface of the channel (commonly between 0.6 and 0.7); v_* , the maximum (close-packed, dense flow; $v_* = \pi/3\sqrt{2}=0.74$ for a cannon-ball closely packed structure for spherical particles) value of v_s ; and μ , the viscosity of the intergranular fluid. Values of N_{BAG} smaller than - 40 indicate a "macroviscous" regime, in which bulk normal and shear stresses are both proportional to the shear rate. Values of $N_{BAG} > 450$ indicate a collision-dominated regime in which bulk normal and shear stresses are both proportional to $\dot{\gamma}^2$ (BAGNOLD, 1954; SAVAGE AND SAYED, 1984). A transitional condition exists in between these two values.

One more scaling number has been proposed by IVERSON & LAHUSEN, 1993, to indicate dominance of frictional or viscous stresses. This scaling number is called Friction number, N_{FRIC} , and is defined as:

$$N_{FRIC} = \frac{v_s (\rho_s - \rho_f) g H \tan \phi}{(1 - v_s) \dot{\gamma} \mu}$$

Most debris flows and rock avalanches appear to have a $v_s > 0.5$, not far from the dense flow limit, whereas little is known about grain concentrations in moving pyroclastic flows. However, trade-offs between differing stress generation mechanisms are summarized by variations in N_{SAV} , N_{BAG} and related dimensionless parameters. Furthermore, changes in the effective viscosity and density of the fluid phase can be observed during flows by the presence of fine particles carried in suspension. These fine particles may be regarded as part of the fluid phase rather than solid phase if the time required for "Stokesian" settling of the particles (viscous settling in the absence of interaction with other particles) exceeds the flow duration. By this rationale, finer particles (silts and clays) can be considered as part of the fluid phase in many water-saturated debris flows (IVERSON, 1997a). Larger particles constitute the granular solids.

Type of interaction	Scaling Term	Type of Mechanism	Source theory
Solid, inertial	$v_s \rho_s \dot{\gamma}^2 \delta^2$	collision	Granular flow dynamics
Solid, quasi-static	$v_s (\rho_s - \rho_f) g H \tan \phi$	friction	Mohr-Coulomb
Fluid, quasi-static	$v_f \dot{\gamma} \mu$	Viscous deformation	Newtonian viscous flow

Solid-fluid, quasi static	$\frac{\dot{\gamma} \mu \delta^2}{k}$	Viscous drag	Mixture theory (Darcian flow)
---------------------------	---------------------------------------	--------------	-------------------------------

A quantitative interpretation of these scaling terms and scaling numbers is important but critical values have not been yet determined through appropriate experiments especially for natural debris flows. Critical values are generally based on experiments with mixtures of single sized particles in a simple viscous fluid (eg. BAGNOLD, 1954). The main problem consist in, namely:

- The wide range in grain size that usually characterizes debris flows. As a consequence, it is difficult to estimate the most representative value for the particle diameter, δ
- Interstitial fluids in debris flows are usually characterized by a mixture of water and suspended particles (sand, silt, clay). As a consequence, interstitial fluids behave as non Newtonian fluids and the major problem is still where to draw the limit between solid and fluid behavior and how to choose the representative value for viscosity, μ

Scaling number	Value	Mechanism	Source
N_{BAG}	>100	Collisional	Bagnold (1954), Iverson (1997)
	< 10	Viscous	
N_{SAV}	>0.1/tan ϕ	Collisional	Savage and Hutter (1989)
	<0.01/tan ϕ	Frictional	
N_{FRIC}	>1000	Frictional	Iverson and LaHusen (1993)
	<1000	Viscous	
N_{LIQ}	< 50	Liquified	Iverson & LaHusen, (1989), Iverson (1997)
	>>50	Minimal Pore fluid effect	

One of the consequences of this scaling approach is also the possibility to classify the flows according to their strain rate and partially on their physical characteristics as the silt and clay content. We will see that some researchers applies this approach in flow classifications (COUSSOT, 1992, COUSSOT & MEUNIER, 1996). In a more general term we can use the diagram sketched in the figure where the dominant mode of shear resistance and momentum transport in debris flows is hypothesized to be a function of strain rate and silt-and-clay content.

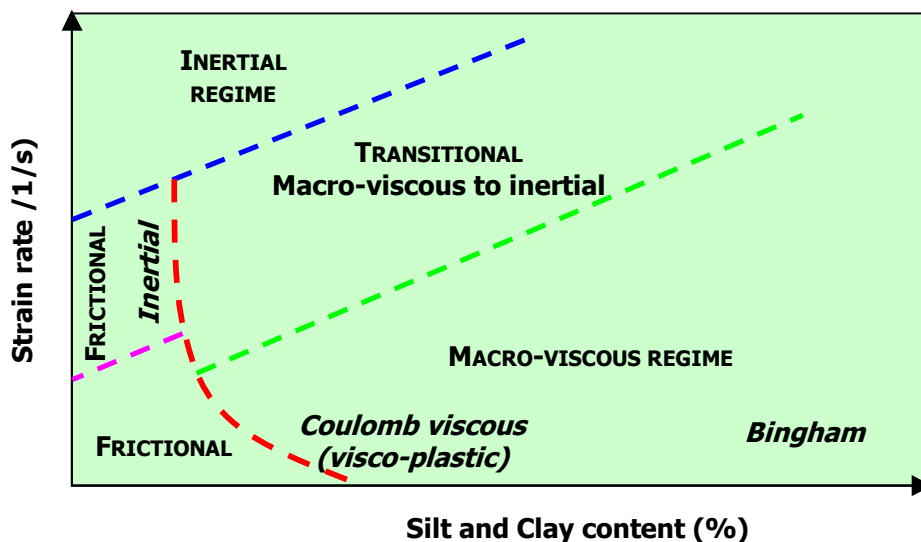


Figure 2.1. Classification of flow regimes as a function of strain rate and content in fines

Several postulates have been proposed to explain the exceptional mobility or *fluidization* of rapid flow movements (e.g. hovercraft action or air cushion entrapping at the base, rock melting, fluidization aided by the presence of fine dust, mechanical and acoustic fluidization, vaporization, etc.). One of the most widely accepted explanation is that in a very thin layer, immediately above the sliding surface, the strong shearing gives rise to enhanced collisions of the particles, leading to an increase of the mean particle distance and thus reducing the effective friction angle (CAMPBELL, 1990, IVERSON, 1997). One way to handle this situation is to ignore the thickness of the boundary layer and to introduce a basal Mohr-Coulomb type friction law with a bed friction angle $\delta < \phi$. Alternatively, one may resolve the boundary layer with a theory that accounts for the dilatation due to the particle collisions.

Many investigators (JENKINS & SAVAGE, 1983, LUN et al., 1984, CAMPBELL, 1990, WALTON, 1993, IVERSON et al., 1997) speak about a phenomenon, known as granular temperature, important when soil deformation rates exceed quasi-static limits. Granular temperature, T , is a measure of the degree of agitation of solid grains which is also directly related with changes in the mixture bulk density and in the particle interlocking and mobility. Granular temperature derives its name from the analogy between grain fluctuation kinetic energy and the molecular kinetic energy that determines the thermodynamic temperature of a gas.

The main difference between gas and granular temperature consists in the impossibility to maintain granular temperature in the absence of energy exchange with the environment, because grain velocity fluctuations cause energy dissipation due to grain interactions and pore fluid flow. Granular temperature can be generated and maintained only by a continual conversion of bulk translational energy to grain fluctuation energy. Bulk translational energy in debris flows is supplied by down-slope travel of the moving mass, and conversion of bulk translational energy to grain fluctuation energy occurs as grains shear along irregular surfaces (IVERSON et al., 1997)

Granular temperature has been defined by CAMPBELL (1990) and IVERSON et al. (1997) as the ensemble average of grains' velocity fluctuations, v' , about their mean velocities:

$$T = \langle v'^2 \rangle = \langle (\vec{v} - v_x)^2 \rangle$$

where \vec{v} is the instantaneous velocity of a solid grain, v_x , is its average down-slope velocity, and $\langle \rangle$ denotes the ensemble average of all grains. According to this definition, the granular temperature may be interpreted as twice the fluctuation kinetic energy per unit mass of grains.

The mechanics of the granular temperature generation differs from the ones of acoustic fluidization or dispersive stress. Acoustic fluidization, as presented by MELOSH (1979, 1987) occurs when propagating elastic waves briefly but repeatedly reduce grain contact stresses. This reduction allows the Coulomb rule to be satisfied and to permit the flow of the granular mixture.

On the contrary, granular temperature spreads through the mixture by a conduction process rather than a wave-propagation process (CAMPBELL, 1990). Furthermore, granular temperature extends the ideas presented by BAGNOLD (1954) about grain interactions. In fact, granular temperature can occur also in an environment where gravity is still active.

Particle size separation or *particle size segregation* has been described almost everywhere in granular deposits, and its phenomenology is understood but the theoretical state of its description is still fairly meagre. Particle size segregation is commonly experienced any time someone wishes to mix different types of particles. In fact, the homogeneous mixing of several sorts of grains is almost impossible to be obtained, Factors that can give rise to separation are differences in size, density and shape and differences in resilience (i.e. interaction forces) during impact.

Particle size separations are often observed in avalanche-, debris- and pyroclastic flow deposits. Generally, it is observed that large particles move to the front and to the top surface whilst small particles accumulate at the bottom and in the rear part of the flowing material. Deposition profiles in pyroclastic flow or turbidity flow deposits show a repetitive occurrence of flow units with the

finer particles at the bottom and particle size increasing as one moves higher up (coarsening upward) until a level is reached where a new flow unit commences. Each flow unit, corresponding to the passage of a flow, is characterised by reverse (or inverse) grading.

A simple mathematical model (SAVAGE & LUN, 1988) allows the quantification of the process of gravity separation of fine from coarse spherical particles during the shearing flow of an initially randomly mixed material down an inclined chute. The model is restricted to shear flow of a cohesionless granular material which consists of bimodal spherical particles. During the shearing motion the particles experience continued rearrangements that are assumed to be random.

At any instant, there will be a distribution of void spaces in the granular material and if a void space at a certain depth is sufficiently large, then a particle from a position immediately above can fall into it. For a given realization of the solid concentration, the probability of finding a hole that a small particle can fall into is obviously larger than the probability of finding a hole that a large particle can fall into. This will lead to a tendency for particles to segregate. This mechanism is clearly dependent on the orientation of the flowing material due to the action of gravity and it is called the random fluctuating sieve mechanism.

This gravity-induced size-dependent void infilling mechanism is insufficient to explain the phenomenon of inverse grading, because there exists a net mass flux perpendicular to the direction of the shearing motion towards the bed. Therefore, a second mechanism must exist to transfer particles from one position to another. This will give rise to a counter flow so as to accommodate for the mass loss in the transverse direction of motion that would otherwise exist. SAVAGE & LUN (1988) propose a squeeze expulsion mechanism that cannot be gravity driven nor be size dependent. This mechanism is due to the fluctuating contact forces on an individual particle. These contact forces induce unbalanced forces such that a particle is squeezed out of its own position into a position above or below.

3. CLASSIFICATION OF FLOWS

It is well known that in technical literature an enormous variety of processes are classified in a generic way as "slope instability" phenomena, which is misleading. This confusion remains even if more specific terms are used. This is the case for the term "flow", which can indicate quite different complex processes and mechanisms (flows in bedrock, earth and mud flows, debris flows, rock avalanches (VARNES, 1978); flow slides (HUTCHINSON, 1992). A general kinematic term describing these landslides is composite flows (WP/WLI, 1993)). In this report we disregard the bedrock, earth or slow mud flows, to concentrate our attention on debris flows, rapid mudflows and rock avalanches which are characterised by flow features and transport of large mass of solids (mass movements). Nevertheless, this set of phenomena presents different characteristics. For example, debris flows are saturated or close to saturation and they show distributed velocity profiles resembling the flow of fluids. On the contrary, rock avalanches contain mostly stronger material in almost dry conditions and with limited internal deformation. These rock avalanches seem to move on a thin basal layer with strong concentration of shear strain.

Five different classifications for flow processes are reported in the following figures (PIERSON & COSTA, 1987, LOWE, 1979, BEVERAGE & CULBERTSON, 1979, COUSSOT, 1992; COUSSOT & MEUNIER, 1996). As suggested by PIERSON and COSTA (1987), it is possible to couple rheological and geomorphological terms for a better and more complete description of flows and mass movements (figure). They proposed to discern among the vast range of processes by taking into account the sediment concentration and the mean velocity, and by analysing the most probable acting element (water, air, solid) and mechanism (flow with different viscosity, granular and inertial flow). Again, for our present interest, we can neglect flows characterised both by low sediment or solid volumetric concentration (normal and hyper-concentrated streamflows) and by high sediment concentration but very low mean velocity. On the contrary, we are interested in debris and grain flows, debris and rock avalanches (**shaded area in Figure**). These classes of slope instability have either relatively high sediment volumetric concentration and average velocity (at the

transition between viscous and granular flow) or a firm granular or inertial regime. All these processes are among the most dangerous and damaging of all landslide phenomena, also because of the difficulties in reducing their destructive potential by stabilisation. As a consequence is vital to perform a risk analysis to predict, among other features, the maximum run-out (distance reached by the movement), the velocity of mise-en-place, the geometry of the deposit (thickness, width, length, shape).

Figure 3.1. Classification of gravitational sediment flows according to LOWE

FLOW BEHAVIOUR	FLOW TYPE		SEDIMENT SUPPORT MECHANISM
FLUID	FLUIDAL FLOW	TURBIDITY CURRENT	FLUID TURBULENCE
		FLUIDIZED FLOW	ESCAPING PORE FLUID (FULL SUPPORT)
PLASTIC (BINGHAM)	DEBRIS FLOW	LIQUEFIED FLOW	ESCAPING PORE FLUID (PARTIAL SUPPORT)
		GRAIN FLOW	DISPERSIVE PRESSURE
		COHESIVE DEBRIS FLOW	MATRIX STRENGTH MATRIX DENSITY

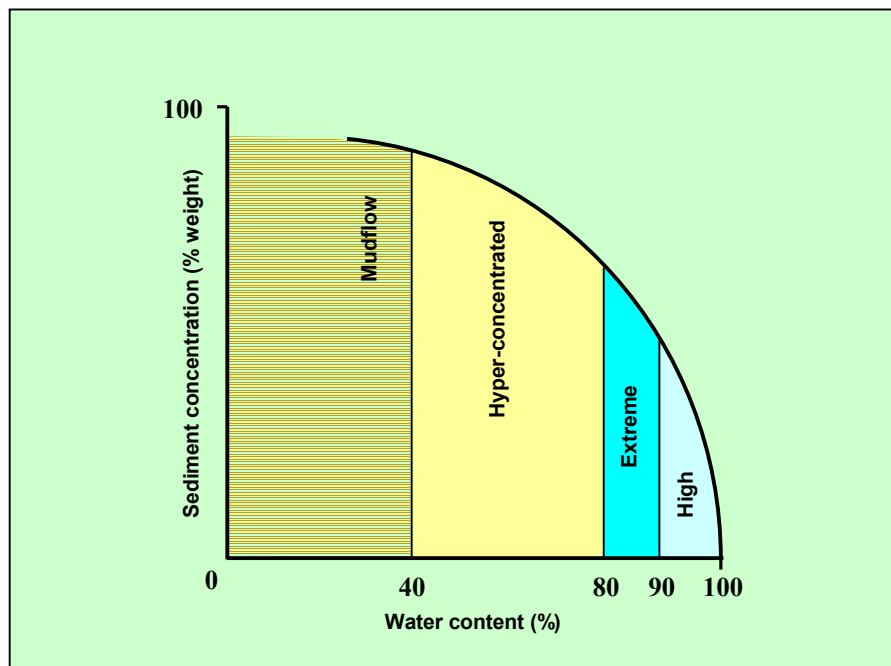


Figure 3.2. Flow classification after BEVERAGE & CULBERTSON (1979),

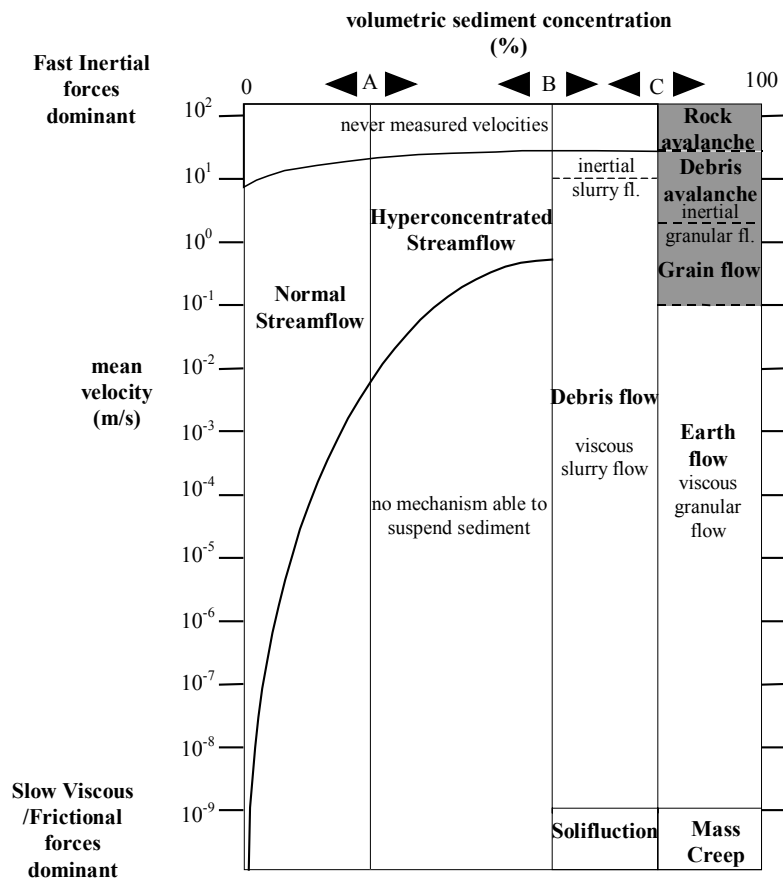


Figure 3.3. Geomorphological-rheological classification of flows [PIERSON and COSTA, 1987]

Figure 3.4. Rheological classification according to COUSSOT (1992)

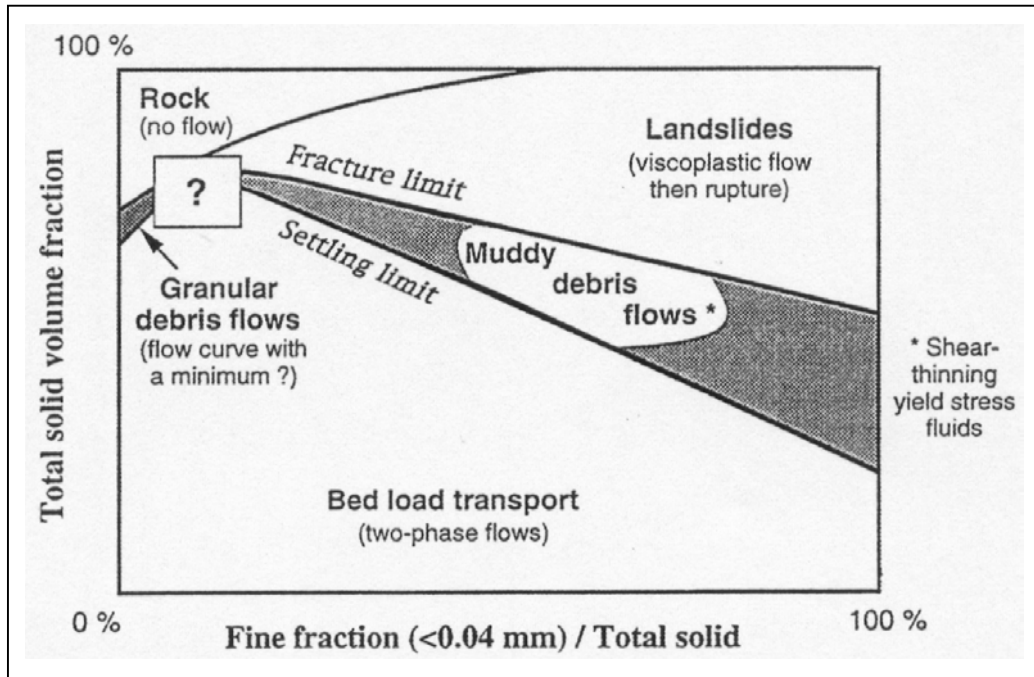
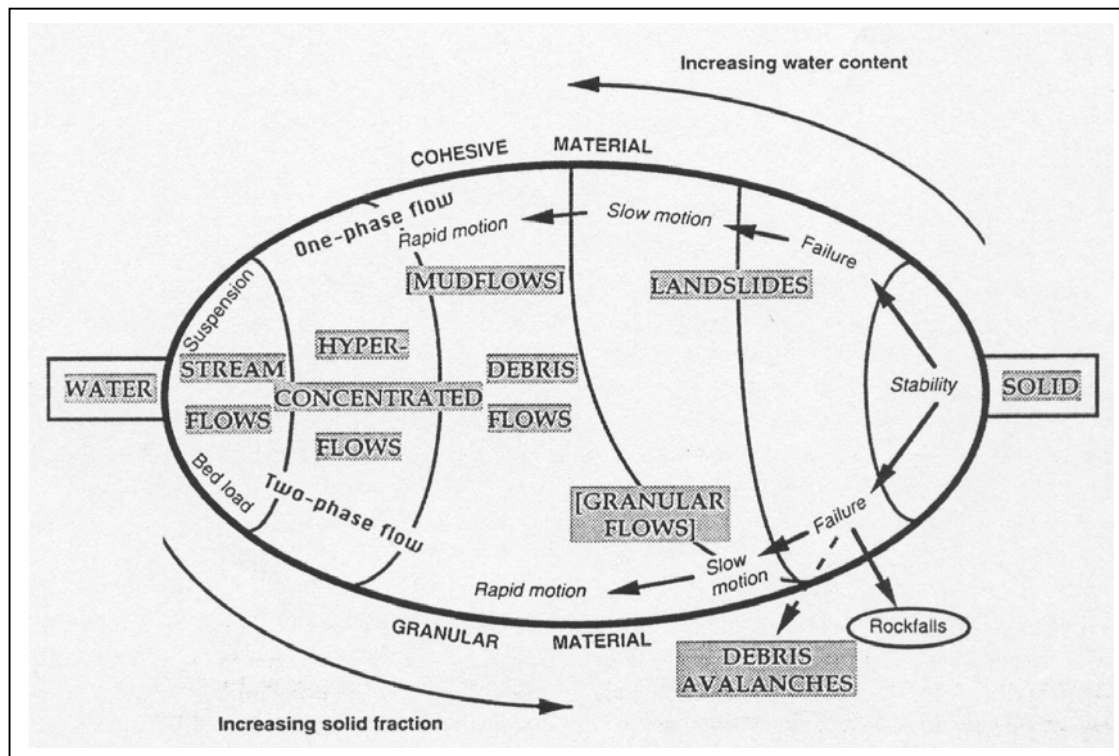


Figure 3.5 Rheological classification according to COUSSOT & MEUNIER (1996)



TAKAHASHI (1991, 1999) describes different flow regimes distinguishing also viscous from inertial (stony, muddy, hybrid) debris flows. Macro-viscous debris flows are characterized by a laminar flow and can be modeled through equations identical to those used for clear water laminar flows by inserting a specific value for viscosity. In presence of a pore fluid formed by clear water, the macro-viscous flow regime occurs when the concentration in solid particles is very high ($> 55\%$).

On the contrary, if the interstitial fluid is viscous (e.g.: high clay content) the macro-viscous regime can occur at lower solid particle concentrations.

Stony debris flows, also known as mature debris flows, are characterized by sediment particles distributed along the entire flow depth. Because of the high solid concentration (> 20%) grains are frequently in contact and internal stresses, due to friction and impact between particles, and large solid particles can float at the flow surface. Turbulence is still limited within the flow and laminar conditions are dominant because the shear stress is controlled by inter particle contacts that provide a high viscosity. On the other hand, small particles are maintained into suspension within the interstitial fluid because of its turbulence. The final consequence consists in a much denser interstitial fluid with respect to water.

Immature debris flows are characterized by a higher concentration in solids, at the bottom layer of the flow, and a diluted solid fraction (finer particles) suspended in the upper part of the flow. In this case as in the previous one, shear stresses are connected to interparticle contacts. Eventually, it must be suggested that immature debris flows can develop at the very origin of stony debris flows or at the very end, when friction and collisions are unable to maintain a homogeneous distribution of solid particles within the entire flow depth.

Turbulent mudflows are characterized by turbulent shear stresses within the interstitial fluid comparable in magnitude to those generated by inter-particle contacts. These flows are usually characterized by large eddies and large scale turbulence.

Hybrid stony and muddy debris flows are characterized by a mature or immature flow in the lower part of the flow, whereas the upper part shows a strong turbulence with finer particles in suspension (muddy debris flow).

4. DRY GRANULAR FLOWS

4.1. Morphological and sedimentological characteristics of Rock avalanches

The knowledge of the main morphological and sedimentological characteristics, typical of the broad class of granular flows, is imperative for modelling purposes. In fact, these features help in the understanding of the processes and are essential when studying phenomena which are generally too fast, or occur in remote areas. At the same time, indirect observations from slide events provide only some post-event information with few indications about real behavior of the moving mass.

Debris flows, with a high volumetric concentration in solids (v_s) and minimum content in fine particles, are usually characterized by steep nose or front areas, along route lateral deposits, floating of large blocks due to sieve effect (also called inverse grading), long run-out both along laterally confined and unconfined paths. Rock avalanches are equally peculiar for some of their features. They usually involve large volumes of rock material (> $1 \times 10^6 \text{ m}^3$), and their very large run-out is considered volume dependent, increasing with the volume of involved material (HUTCHINSON, 1992; ERISMANN, 1979; SCHEIDEGGER, 1973). The thickness of the deposit is usually small with respect to its length and local morphological conditions (initial drop height, slope length and inclination, geometrical relationship between the originating slope and the area of expansion, etc.) can be very effective in controlling the distribution of the material. Very low friction coefficients are calculated by comparing the run-out to the drop height, as reported in literature (ERISMANN, 1979).

The deposit is generally formed by angular blocks with a high degree of interlocking. Large blocks are spread at the accumulation surface. The material is usually able to overcome wide and high obstacles as also witnessed by its run-up potential (almost 300 m of elevation for the val Pola rock-avalanche).

On the basis of such a series of features, a long series of explanations or models have been presented to justify the high mobility of rock avalanches and debris flows. For rock-avalanches, in particular, we can list: hovercraft or air-layer effect (SHREEVE, 1968), air escaping or fluidization, mechanical and/or acoustical fluidization (MELOSH, 1979), dispersive stresses (BAGNOLD, 1954),

rock melting along the sliding surface, or water vaporization (GOGUEL, 1978) block rolling or vibration along the surface of movement (PARISEAU and VOIGHT, 1978), aero-planning from topographical irregularities, granular agitation within the entire thickness or in a basal stratum (CAMPBELL, 1989).

4.2. Experimental work

As above stated, we can usually use post-event, or after-the-fact observations, and this fact is at the base of many experimental and numerical modelling studies. As a consequence there is still no complete understanding of the phenomena and of the parameters (total mass, material bulk and grain density, characteristics of particle collision, surface roughness and slope geometry, strength parameters, etc.) that really control the development of the flow, as well as the geometry of the deposits and the distribution of the mass, or the ability to erode from or deposit material along the slope.

SAVAGE and HUTTER (1991) and HUTTER *et al.* (1995), up to now, are the most systematic and important sources of experimental observations concerning granular flows down an inclined plane. This is true even if other investigators (Iverson, 1997, Iverson *et al.*, 1992, Iverson & LaHusen, 1993) started to run tests of very large size. These tests have been performed on granular mixtures in presence of water and monitoring flow geometry, stresses, velocity and pore pressures.

Experiments by SAVAGE AND HUTTER (1991) have been performed in a chute (Fig.4.1) consisting of three 100 mm large different portions: an initial straight one, with inclination of 40°, 50° or 60°, an intermediate curved one and a final horizontal straight one. The chute had a PVC bottom, that could be covered with different materials (sand paper, sheets with glued particles of the same size as the ones used as flowing material) and plexiglass side walls. A rotating gate was located at the uppermost sector of the inclined portion of the chute to contain and release the granular material.

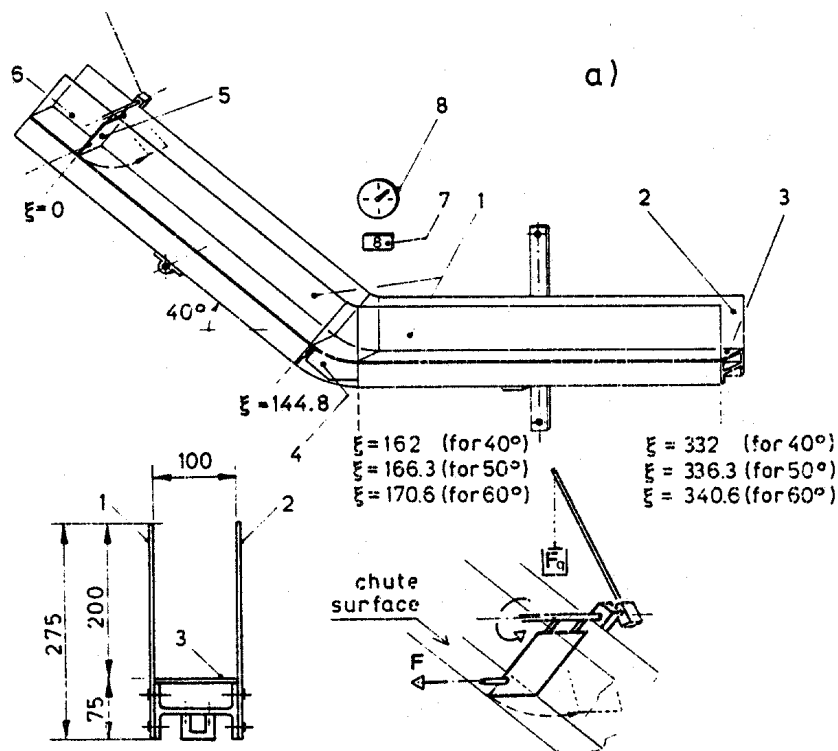


Figure 4.1. Schematic views of the experimental chute [HUTTER *et al.*, 1995]

In this kind of experiments the selection of the granular material is a critical point. It should allow for variation of: specific gravity, interparticle and particles/bed angles of friction, impact properties. Spherical glass beads (particle density, $\rho = 2860 \text{ kg m}^{-3}$, bulk density = 1730 kg m^{-3} , diameter = 3 mm) and disc-like shaped plastic particles (vestolen plastic, particle density, $\rho = 950 \text{ kg m}^{-3}$, bulk density = 540 kg m^{-3} , diameter = 4 mm, thickness = 2.5 mm) have been adopted by HUTTER *et al.* (1995). Each of the reference experiments involved: deposition of the granular material up-slope of the gate, time recording, material release by gate opening and pictures taking or filming (Fig.1.3). The effects of the following variables on the resulting flow were considered: type of material, total mass of granular material (ranging between 500 g to 5000 g), angle of chute inclination (40° , 50° , 60°) and roughness of the chute bottom surface.

From pictures taken during the flow (Fig.4.2), after each test data have been collected about:

- position of the rear (X_R) and front (X_F) ends of the mass;
- length of the flowing mass along the chute (L);
- maximum thickness (H_{Max}) of the deposit and position (X_{Max}) of the thickest section.

The assessment of X_R has always been easier than that of X_F , because of the longitudinal dispersion of isolated particles, at the front of the flowing mass.

The authors also measured the mean velocity of the front and rear ends along the path (V_F and V_R), as well as a general description of the mass geometry along the falling path. Photographs allowed to show: the minor influence of initial shape on the experimental results, the particle agitation at the rear and front ends, the small shear distortion present within the granular mass in motion with a maximum at the bottom of the moving mass.

The results have been presented by HUTTER *et al.* (1995) in terms of X_F , X_R , L , V_F and V_R vs. time curves, which are plotted together with bars indicating the value reliability (Fig.4.3). Unfortunately, in front of the large number of performed experiments, only the results of one experiment conducted with vestolen disks (#87) are reported in detail by HUTTER *et al.* (1995). The corresponding results will be compared to those obtained with a DEM model.

According to HUTTER *et al.* (1995) the following conclusions can be retained:

- the mass motion is insensitive to minor changes in the internal angle of friction and material stiffness,
- differences in the shape of the deposits are imputable more to the particle shape than to their density or elastic properties,
- different total masses have a weak influence on the geometry of the deposit (length, rear and front end position).

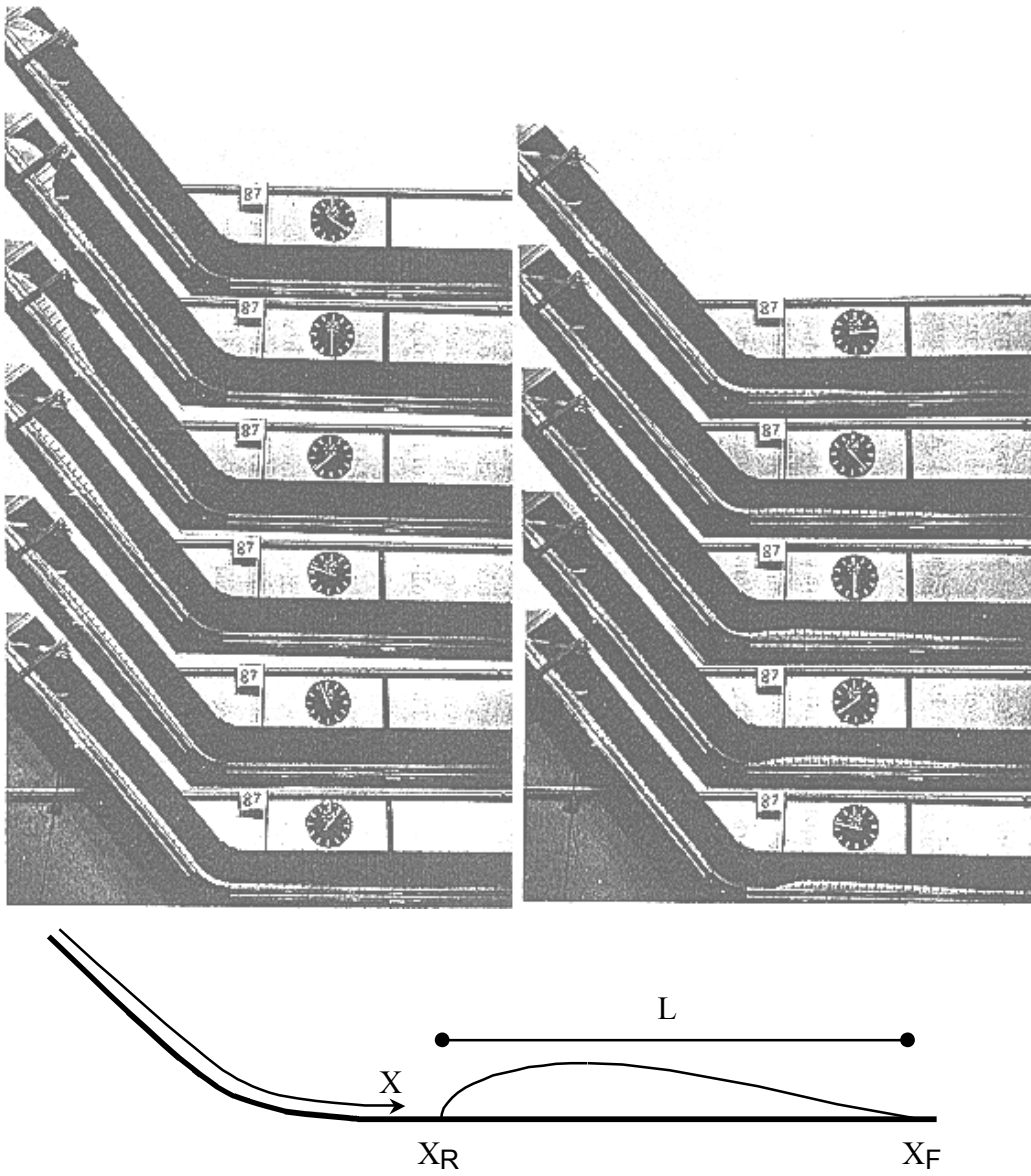


Figure 4.2. Pictures of a flow experiment with schematic reconstruction of the flowing mass geometry [after HUTTER *et al.*, 1995]

4.3. The Distinct Element model

The numerical model employed to reproduce the described experiments represents a particular application of a commercial 2D Distinct Element Method code (PFC-2D) (ITASCA, 1996), which is commonly used to model granular assemblies of purely frictional or bonded circular particles (disks).

The original version of the DEM (CUNDALL, 1971) was devoted to the modeling of rock-block systems, and it was lately applied to the modeling of granular materials (CUNDALL and STRACK, 1979).

It is here recalled that in DEM the global behavior of an assembly of particles connected by a network of contacts is obtained by writing the equation of motion of each component .

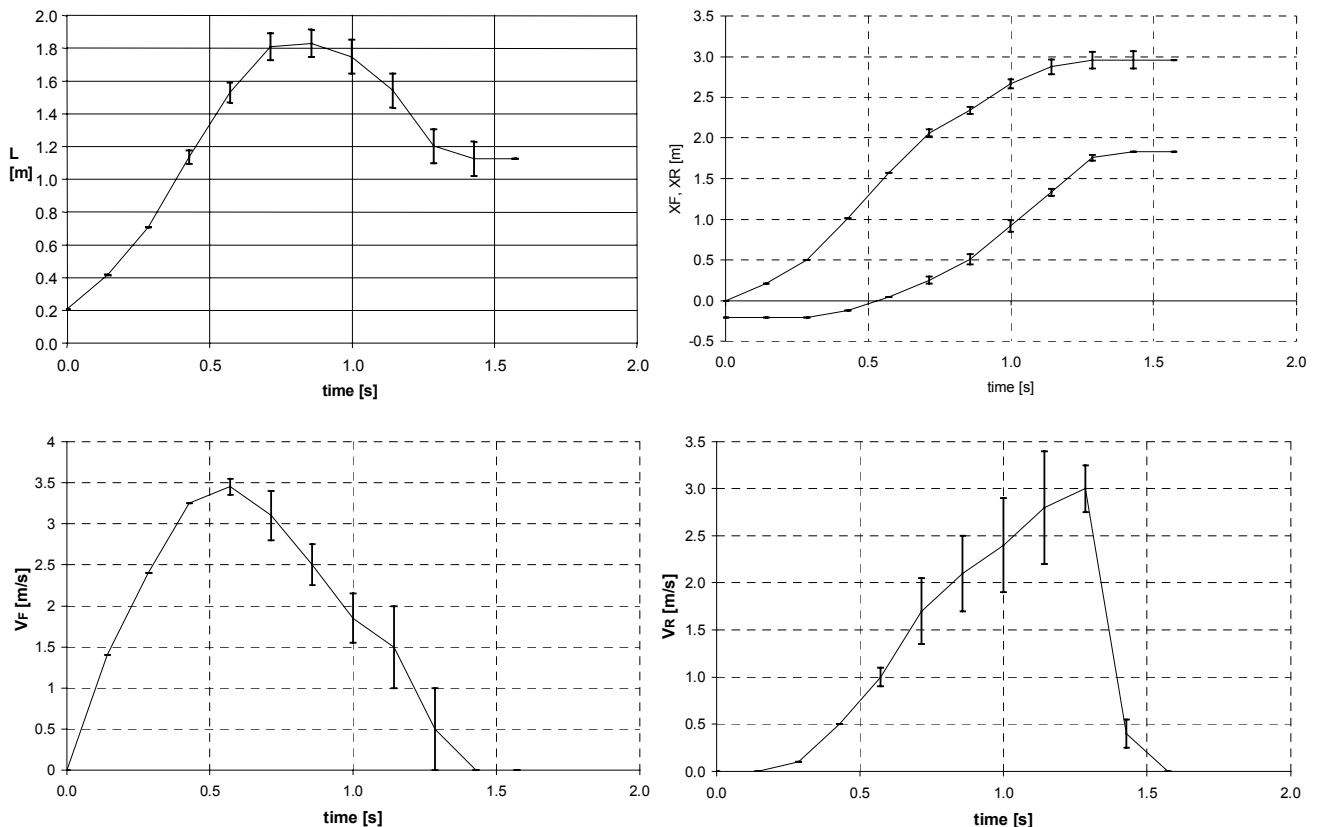


Figure 4.3. X_R and X_F vs. time; b: L vs. time; a: V_F vs. time; a: V_R vs. time [after HUTTER *et al.*, 1995].

4.4. General features of the numerical simulations

Before gaining insight into the numerical model features it is necessary to point some key-points connected with the choice of a 2D DEM tool.

In general, the use of a 2D code has several consequences: on the kinematics of the flowing mass, and therefore on the force transmission within the granular mass. Moreover, the 3D behaviour of the flow and, in particular, the lateral expansions cannot be modelled.

Next, the flowing mass is composed of rigid disk. This fact has several consequences. First of all, the shape of the elements may be substantially different from that of the blocks involved in a rock avalanche. Secondly, the behaviour of the system is ruled by contact properties only (elastic compliance and Coulomb's friction). In addition, it is not possible to reproduce the progressive surface damage and wearing of grains during the flow. The only source of energy dissipation is related to the inter-particle sliding mechanism: other sources of dissipation, related to the non elasticity of the impacts between grains cannot be directly modeled. This is the reason why a numerical damping is introduced in the model. Although in general the damping is introduced to accelerate the convergence of the numerical solution, in the case of a dynamic particle flow

simulation, the numerical damping controls the coefficient of restitution for the individual grain-to-grain interaction.

It is also necessary to report that it is impossible to take into account many of the mechanisms invoked to explain the observed high mobility of rock avalanches and debris flows. This point will be discussed on the basis of the results of the numerical simulations.

In conclusion, the authors are aware that the numerical model is very simple if compared with the real phenomenon; nevertheless, as it will be shown in the following, the numerical results can be considered satisfactory. In our opinion, this is due to the model capability to catch the basic aspects of the phenomenon, which resides in the discrete and frictional nature of the flowing material.

4.5. Numerical model

The numerical model reproduces the experimental set-up as close as possible. Of course the main discrepancy regards the differences between plane strain conditions (those of the experiments) and the two dimensional nature of the numerical model. The numerical model is intended as a slice of the laboratory one, with a thickness equal to that of the vestolen disks employed by HUTTER *et al.* (1995). Of course the out of plane movements are not considered at all: in particular the out-of-plane rotations of the experimental disks cannot be modelled. This is a quite noticeable difference.

4.5.1. Numerical Parameters

In order to perform a DEM simulation the following parameters must be defined:

- density (unit mass) of the elements;
- mechanical properties of contacts (stiffness and friction);
- numerical damping.

While the first one is of immediate comprehension, the others deserve a more accurate description.

4.5.2. Contact parameters

The compliance of contacts is represented by a system of elastic springs (Fig.4.4). The procedure implemented in PFC-2D to calculate the normal and tangential contact forces (F_N and F_T) from the normal and tangential relative displacements (U_N and U_T) of two disks in contact is the following:

$$F_N = U_N \cdot k_N . \quad (2.1.a)$$

$$\Delta F_T = \Delta U_T \cdot k_T . \quad (2.1.b)$$

where k_N and k_T are the stiffness of the elastic springs of Fig.2.1. Please note that the normal force is calculated on the basis of the current normal displacement (overlapping of particles), whereas the tangential force is calculated incrementally. Non reversible sliding occurs if the Coulomb condition is met:

$$F_T = F_N \cdot \tan(\Phi) \quad (2.1.c)$$

where φ is the interparticle friction angle.

In the employed code, the elastic behaviour of contacts can be either linear or non linear: in this case k_N and k_T are calculated according to Hertz's law starting from the elastic parameters (Young modulus, E , and shear modulus, G) of the simulated material. Where not specified, in this work linear elastic contacts have been used.

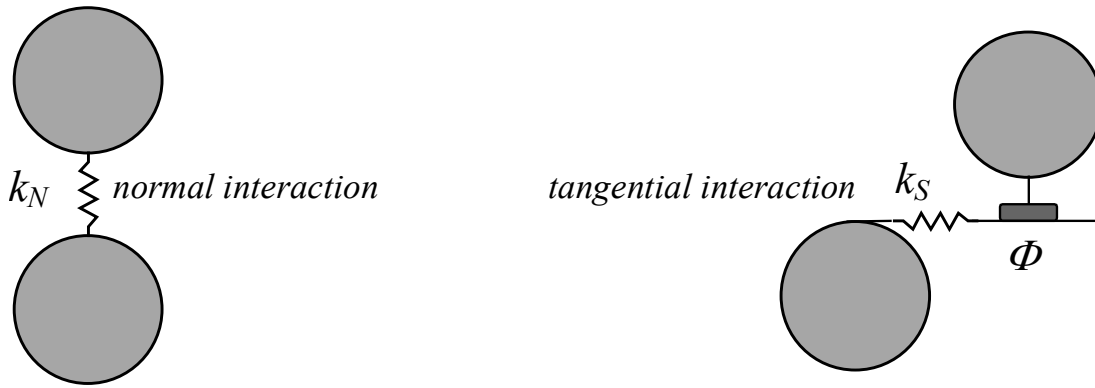


Figure 4.4: Representation of contacts

4.5.3. Numerical damping

In a DEM model composed of rigid disks with elastic springs the only energy dissipation source is frictional contact sliding. In general, this dissipation is not sufficient to avoid oscillations around the equilibrium state. For this reason a numerical damping is introduced. In previous versions of several DEM codes damping was introduced by applying to each degree of freedom a force (moment) proportional to the corresponding speed (viscous damping).

On the contrary, PFC-2D is implemented with a "non-viscous" damping (CUNDALL, 1987); the 2D equation of motion is written (and solved in a finite difference time marching scheme) for each disk in the following way:

$$[F_x(t)/m](1 - \delta \operatorname{sgn} \dot{x}) = \ddot{x} \quad (2.2.a)$$

$$[F_y(t)/m](1 - \delta \operatorname{sgn} \dot{y}) = \ddot{y} \quad (2.2.b)$$

$$[M(t)/I](1 - \delta \operatorname{sgn} \dot{\omega}) = \ddot{\omega} \quad (2.2.c)$$

where: F_x , F_y and M are the forces and moment acting on the particle; m and I are the particle mass and moment of inertia; δ is a non dimensional damping parameter, and the following notation applies:

$$\operatorname{sgn} k = \begin{cases} +1 & \text{if } k > 0 \\ -1 & \text{if } k < 0 \\ 0 & \text{if } k = 0 \end{cases} \quad (2.2.d)$$

Following (2.2) the consequences of using a non zero δ value is that along a general degree of freedom accelerations are reduced and decelerations are amplified.

The effects of the damping parameter on the results of the numerical simulations will be widely discussed in section 3.

4.5.4. Small scale simulations

The experiments described in Section 1 are first reproduced. A numerical model of the experimental chute is built.

The geometry and initial configuration of the numerical model are based on a 2D reproduction of the laboratory conditions. The numerical disks have properties based on those of the plastic ones employed by HUTTER *et al.* (1995) (Table 4.2).

Of course, given the 2D nature of the model, the numerical chute represents a thin slice of the real one. It is important to underline that the individual mass of particles is unchanged passing from the experiments to the numerical simulations.

The numerical chute is formed of one inclined and one horizontal "wall" element, with a rounded connection (Fig.4.6). The disks are generated in the upper part of the chute, upstream of an additional wall, which reproduces the experimental releasing device (Fig.4.5). Before the flow is triggered by removing the release wall, the gravity force is applied and the disk deposit in order to

match the bulk density deduced from the experiments. In order to shorten this unessential phase the damping parameter δ is set to 0.5 (50%).

Table 4.2

<i>shape</i>	<i>disk</i>
<i>radius</i>	<i>2 mm</i>
<i>thickness</i>	<i>2.5mm</i>
<i>unit mass</i>	<i>950 kg/m³</i>
<i>interparticle friction angle</i> ϕ	<i>29°</i>

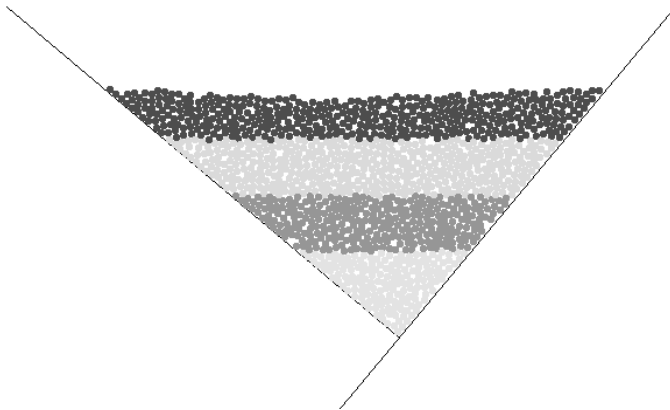


Figure 4.5. Initial configuration of the granular mass

During each simulation, traces of the following variables are recorded:
 global kinetic energy (E_K); in order to make comparisons between different simulations the global kinetic energy is normalised with respect to the initial (before release) potential energy of the granular mass;

position (X_G) and velocity (V_G) of the centre of mass of the flowing mass;

number of disk-to-disk contacts (N_C); in order to make comparisons between different simulations the number of contacts is normalised with respect to the number of disks (the "co-ordination number" is obtained);

position and velocity of the front and rear ends of the flowing mass (V_{F_f} , V_{R_f} , X_{F_f} , X_{R_f}): as in the laboratory, these measurements are not clearly defined: therefore, two different techniques are tested, the first one based on the direct observation of the flowing numerical mass, the other based on an automatic calculation

A representative series of pictures of the flowing mass is reproduced in the following (Fig. 4.6; for a comparison with the experiments see Fig.4.1). It is worth noting that the front and the back of the flowing mass are characterised by a large dispersion of particles. This situation is in agreement with the experimental observations by HUTTER *et al.* (1995). From the inspection of pictures, one can also conclude that the initial and final part of the flow are characterised by a quite compact granular mass configuration, in which the predominant interaction mechanism is continuous (with time) contact. On the contrary, during the central part of the flow (from 0.6 to 1.4 seconds after the release) the particles are far more dispersed, and the predominant disk-to-disk interaction mechanism is impact.

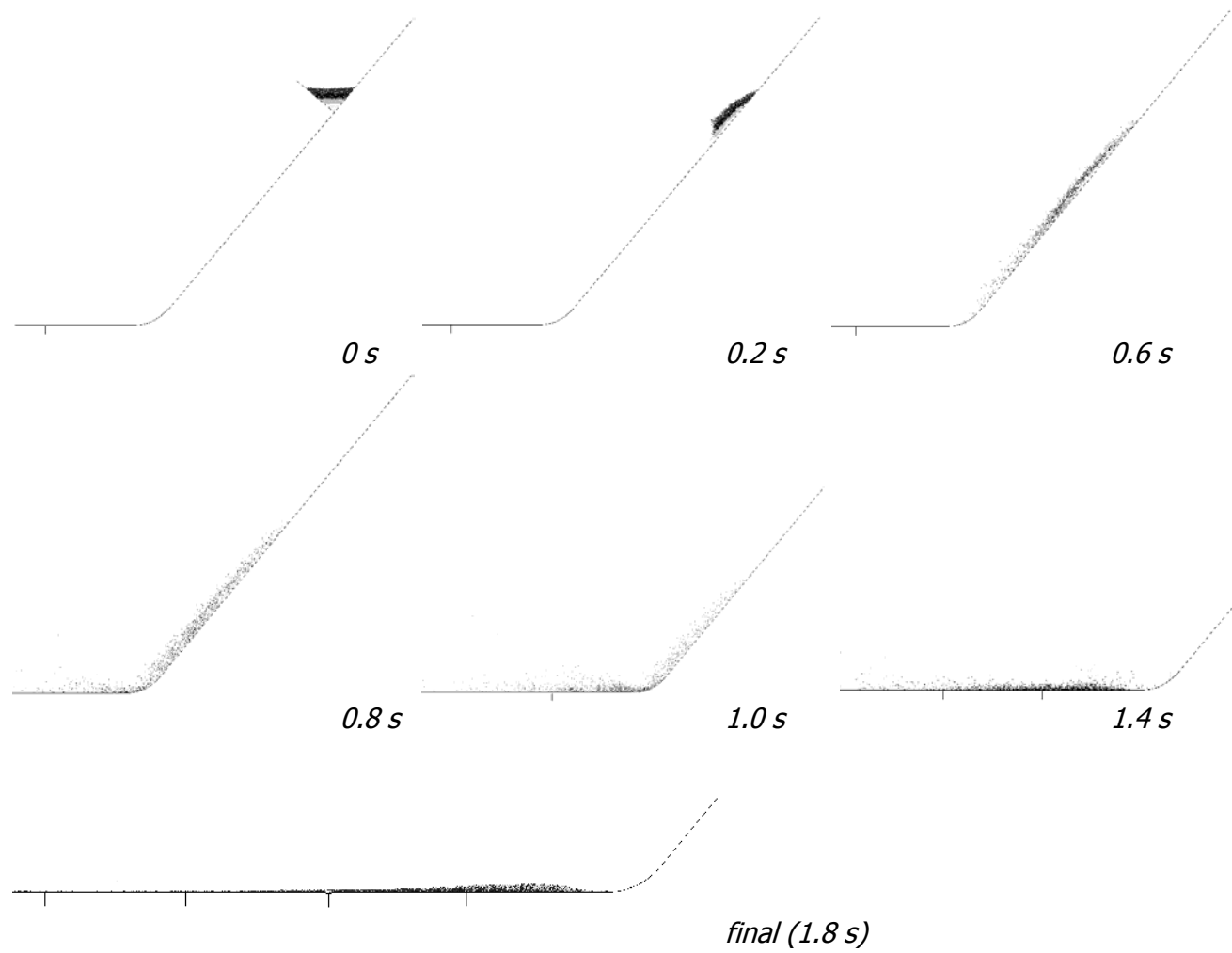


Figure 4.6: Granular mass configuration during flow

4.6. Sensitivity analysis

A preliminary analysis of the influence of the numerical parameters was performed on a reference numerical model, based on the experiment #87, in which: the inclination of the chute is 50°; the granular mass is composed of 1256 disks with radius of 2 mm and thickness of 2.5 mm; the equivalent global mass is 1.5 kg (the actual global mass of the numerical elements is 1/40 of the equivalent one, since the numerical model represents a 2.5 mm thick slice of the 100 mm wide experimental chute, see Fig.4.1). In this phase, both contact parameters and numerical damping are changed, and the effects of their variation on the results is analysed.

4.6.1 Contact parameters

Contact stiffness

The influence of the contact stiffness is analysed first. In principle, it would be possible to perform simulations where contacts obey to Hertz law. Two problems arise, linked with the time required to perform simulations. The use of non linear elastic contacts turns into a less efficient calculation (ITASCA, 1996). In addition, the use of the elastic parameters of the plastic material composing the laboratory disks would involve the use of a very small time-step. This is due to the very small mass of the individual disks, and it turns into time consuming simulations. In order to overcome these problems the following procedure was followed:

one simulation with realistic (high modulus and non linear) contact stiffness was performed. The corresponding average time-step was measured;

starting from the consideration that time-step depends on the contact stiffness (ITASCA, 1996), an equivalent stiffness was calculated for the linear contact model;

simulations are performed with lower values of stiffness (both for the linear and Hertz contact stiffness), and the influence of this parameter on results is considered (Table 4.3).

The obtained results show a negligible influence of the contact stiffness value (the centre of mass run-out varied less than 1% from the average value). The intermediate value among the linear stiffness ones was retained, since the lower one corresponded to an excessive particle overlapping, which is in contrast with the DEM principles.

Table 4.3

Contact model	$K_N = K_S$ (N/m)	E; G (N/m ²)
Linear elastic	$1 \times 10^2 \div 1 \times 10^4$	
Hertz		$7 \times 10^2 \div 7 \times 10^4$; $3 \times 10^2 \div 3 \times 10^4$

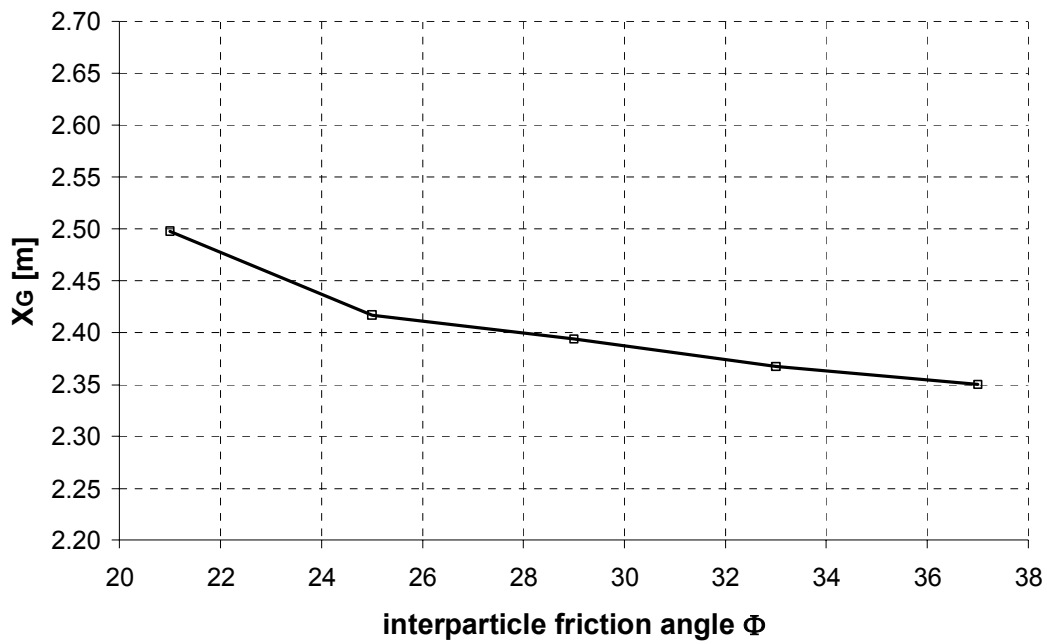
Contact friction

The influence of this parameter is analysed in the range between 21° and 37°. During this series of simulations the base friction angle was set to 23°.

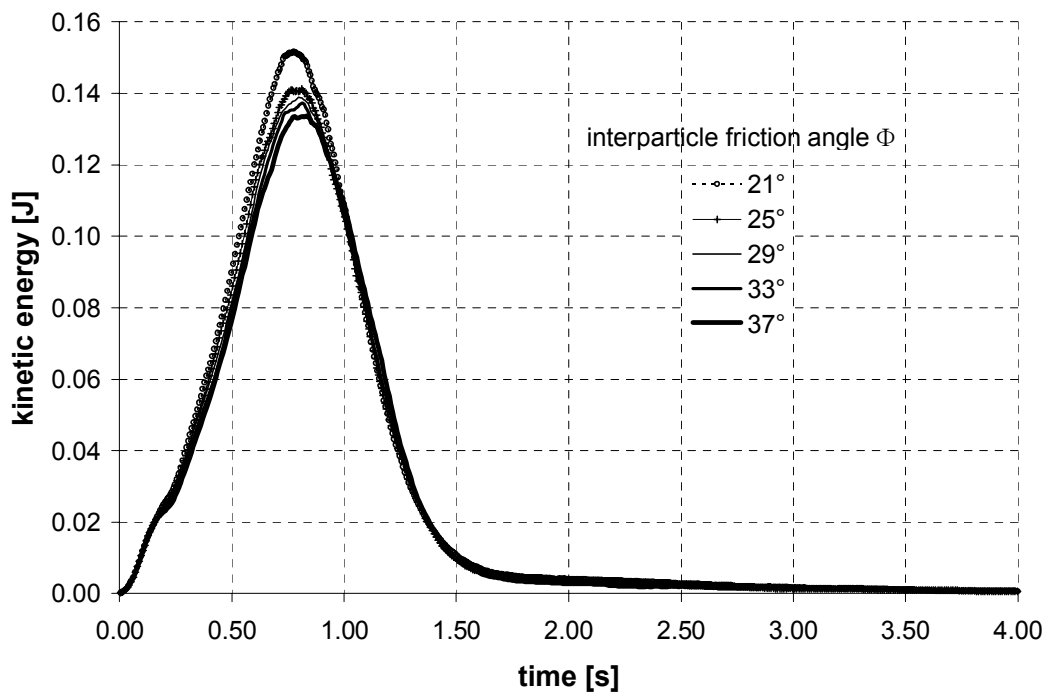
As it could be expected, the obtained results show a regular dependency on the interparticle friction angle: in particular, the centre of mass run-out (final value of X_G) and the mobilised kinetic energies decrease under increasing contact friction (Fig.4.7). In good agreement with the micromechanical investigations performed by several authors, this effect is less evident for high values of contact friction: in fact, a well established evidence is that this phenomenon is linked to the progressive importance gained by particle rotations under increasing contact friction.

Chute friction angle

The influence of this parameter is analysed in the range between 20° and 35°. During this series of simulations the interparticle (disk-disk) friction angle was fixed to 29° (that of the experimental disks). The interpretation of these results is similar to that regarding the interparticle friction angle. The only final X_G vs. base friction curve is reported (Fig.4.8).



a



b

Figure 4.7: Influence of interparticle friction. a: centre of mass run-out, X_G ; b: kinetic energy vs. time curves.

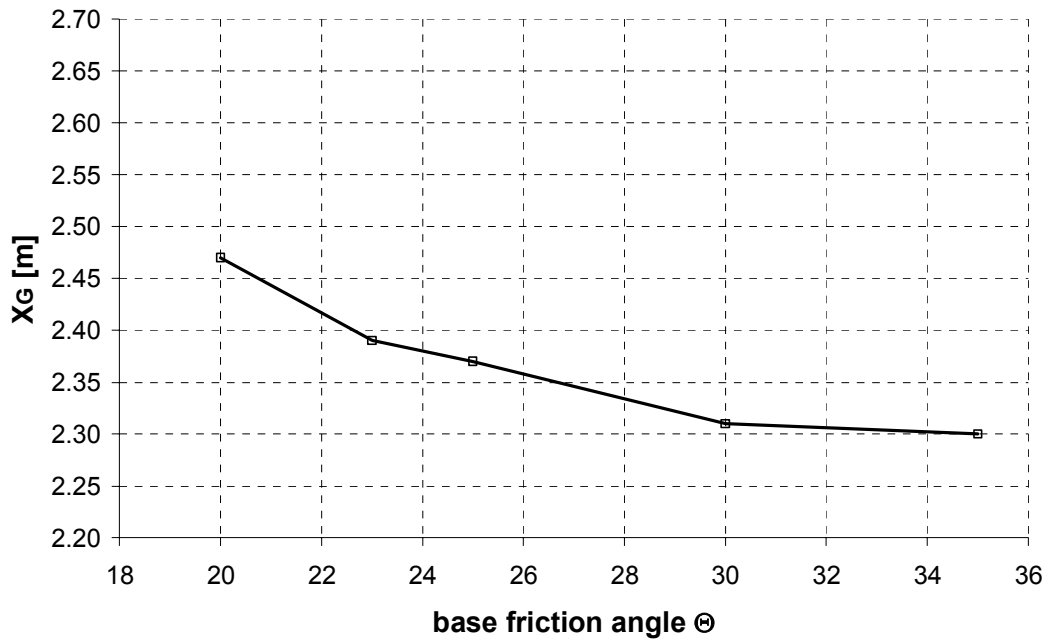


Figure 4.8: Influence of base friction on the centre of mass run-out, X_G .

4.6.2. Numerical damping

In this paragraph, the influence of the numerical damping parameter, δ , is analysed. It is necessary to recall the fact that this parameter is not clearly related to any physical mechanism. For this reason, the realistic value must be obtained by back-analysis of the experimental data. A preliminary sensitivity analysis was performed, which consisted in a series of numerical simulations with δ ranging from 0 to 0.1. It is here recalled that the largest employed value corresponds to a reduction (increase) of 10% of the accelerations (decelerations) calculated from the application of the second Newton's law. The results are presented in terms of X_G and kinetic energy vs. time curves (Fig.4.9).

The influence of δ on the shape and position of the deposit is shown in Fig. 4.10, from which it is evident that even a small damping variation turns into a qualitative change of the shape of the deposit. The higher δ value corresponds to a more compacted deposit and to a smaller run-out.

The damping parameter δ affects the kinematics of the flowing mass in an evident way, and far beyond than expected: in fact, all the employed values are quite small. In order to make a comparison, for the free fall of a single disk the effects of a 10% damping value would result in a 10% reduction of the distance travelled, at any given time. In addition, the use of far larger damping values (up to 0.7) does not affect in a significant way the results of quasi-static simulations of compression tests on an assembly of disks. In that case the main effect of damping is that of reducing the undesired oscillations of the system around the static equilibrium state.

It follows that in the case of granular flows the damping influence is related to the nature of the modelled phenomenon, where impacts between particles are predominant. In fact, during a parallel research it was recently observed (BAMBOZZI, 1999) that for the normal impact of a single disk on a planar surface the coefficient of restitution is linearly depending on the adopted δ parameter (being 1 for δ equal to zero).

4.7. Parameter Calibration

It is first recalled that HUTTER *et al.* (1995) report a detailed description of results only for one flow experiment (#87): the calibration of the numerical model is therefore based on the reproduction of that experiment. The following procedure was adopted:

the interparticle friction, the base friction, the unit mass and the size of the disks, and the initial bulk density of the granular material are directly picked from the data reported by HUTTER *et al.* (1995) for the corresponding experimental values; the global mass of the granular material is 1/40 of that used in the reference experiment (1.5/40 kg), since the numerical model represents a slice of the 10 cm wide experimental chute (Fig. 4.1), with a thickness equal to the disk one (2.5 mm); the contact stiffness is given the intermediate value.

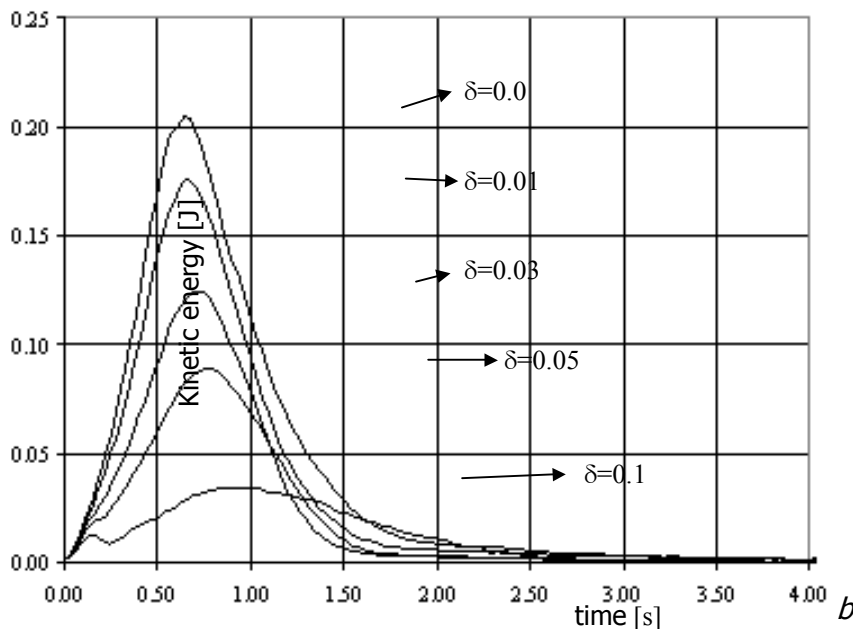
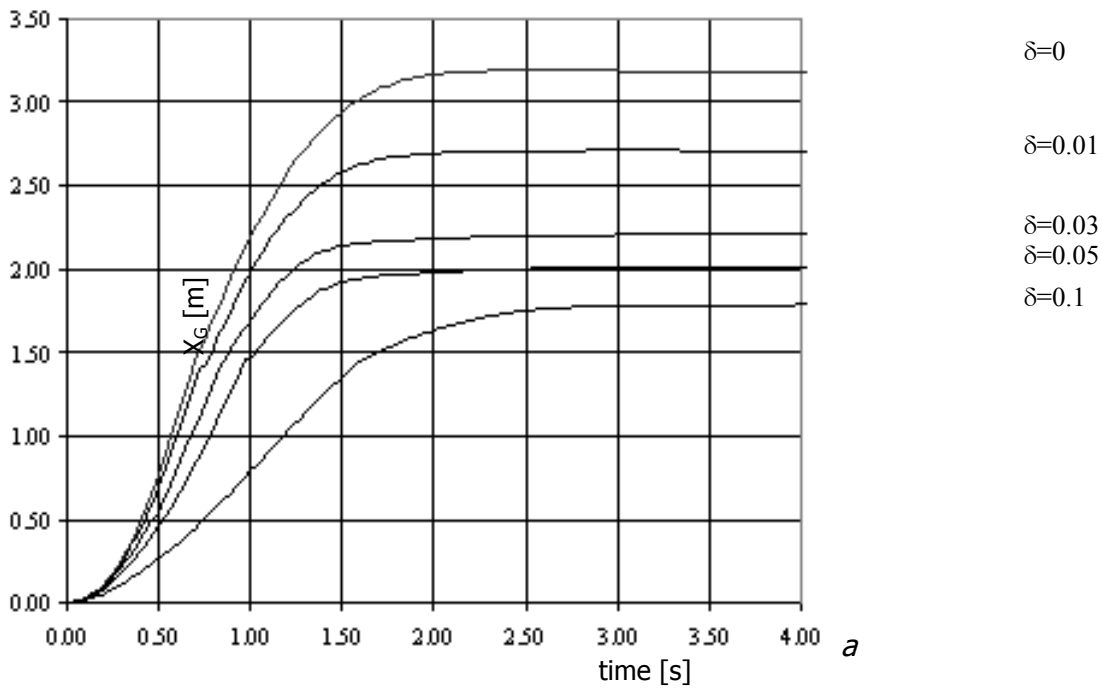


Figure 4.9: Influence of numerical damping.
a: centre of mass position, X_G ; b: kinetic energy.

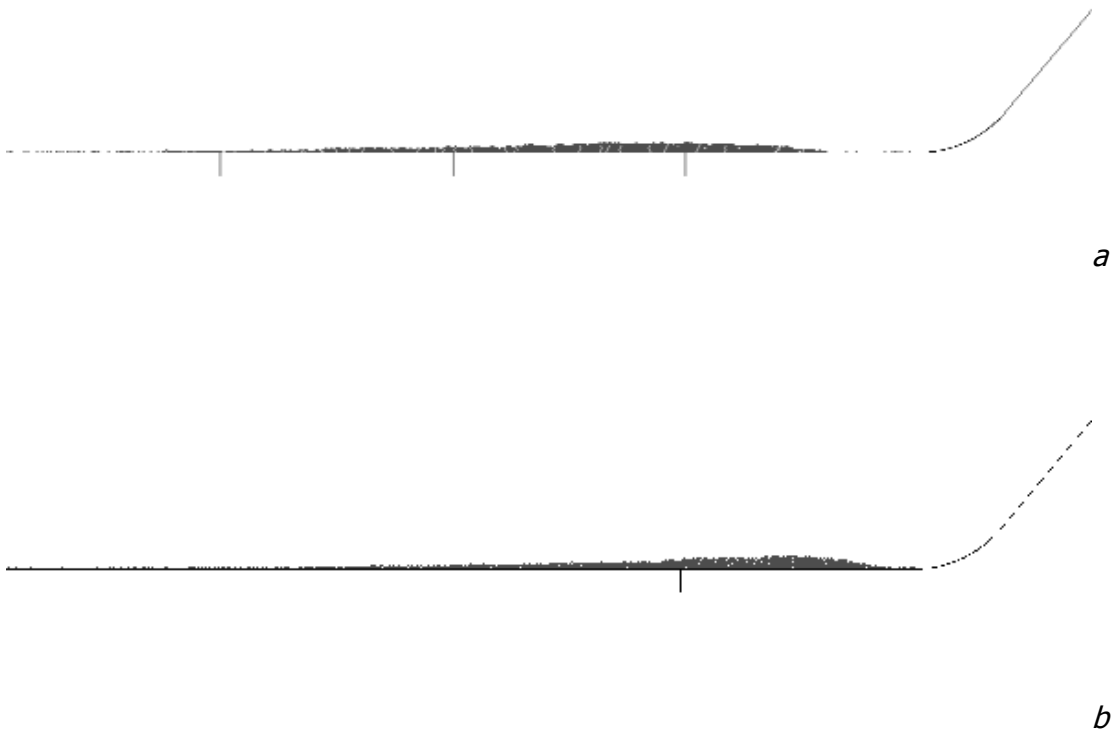


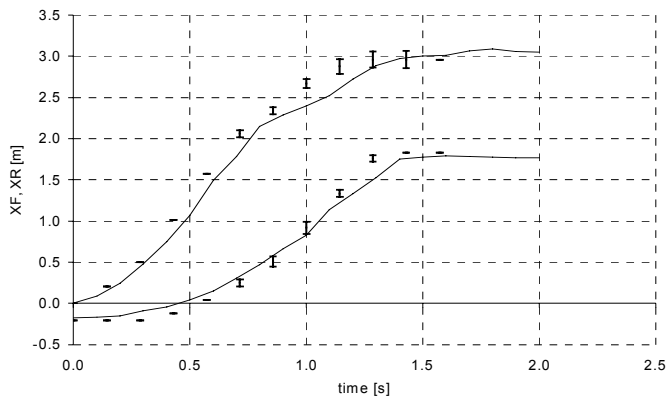
Figure 4.10: Position and shape of the deposit: a: $\square = 2\%$; b: $\square = 3\%$.

As a consequence, the only damping parameter is calibrated in order to reproduce the experimental measurements. The comparison of the position and shape of the deposit is used for a first evaluation of the damping parameter: on this basis the value $\delta = 0.03$ was retained. Then, the parameter calibration is verified by comparing the position and velocity of the front and rear ends of the flowing mass and its length along the chute (V_F , V_R , X_F , X_R , L).

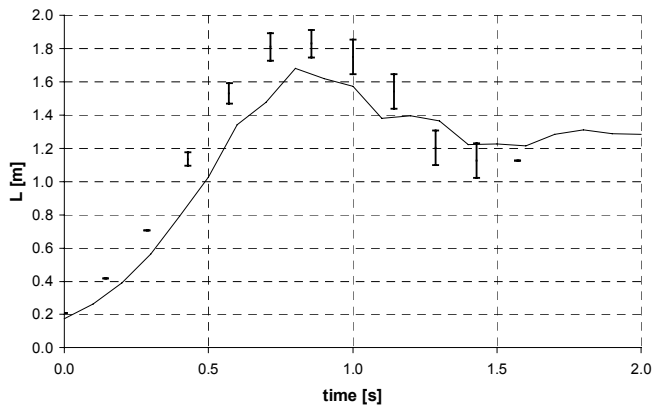
The evaluation of the variables V_F , V_R , X_F , X_R , L was performed following two different techniques: direct inspection of the pictures taken during the numerical flow, and automatic calculation. As previously reported, the first procedure becomes difficult for the central phase of the flow, given the dispersion of particles. This point was observed by HUTTER *et al.* (1995) too. The second procedure is based on the automatic tracking of the particles position: X_F , X_R are located in correspondence of the centre of mass of the first (last) 100 particles within the flowing mass. If desired, a threshold distance may be introduced to exclude from the calculation the particles that escape too far from the bulk of granular mass. It is interesting to note that if a threshold distance equal to the error estimated by HUTTER *et al.* (1995) for their inspection technique is adopted, the two procedures give almost equal results.

In Fig. 4.11 the comparison between the experimental and the numerical results corresponding to $\delta = 0.03$ (3%) is presented.

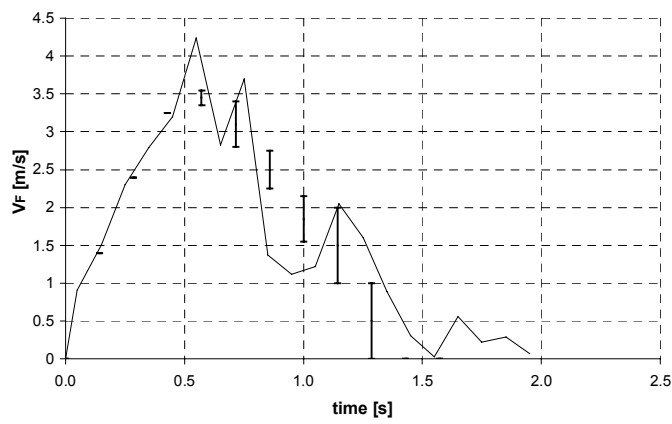
From the analysis of the obtained results the capability of the model to reproduce the experimental flow can be considered satisfactory, at least for what regards the small scale situation. In section 4 the numerical model will be used to reproduce a real scale phenomenon, the well known Val Pola rock avalanche.



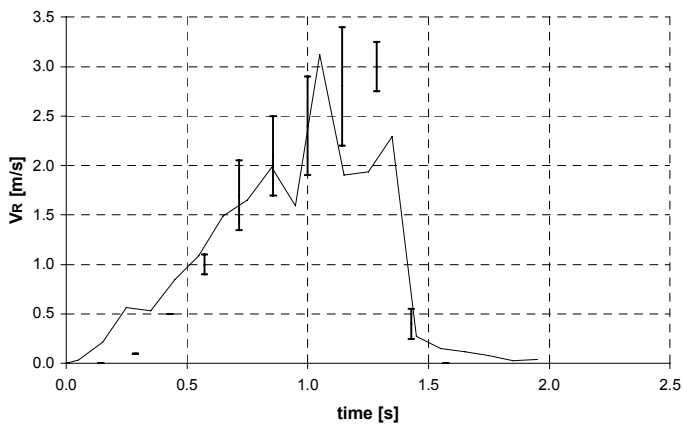
a



b



c



d

Figure 4.11. a: X_R and X_F vs. time; b: L vs. time; c: V_F vs. time; d: V_R vs. time. (experiments: error bars; simulations: solid lines)

Investigation of the flow mechanisms

The numerical model was then used to assess the influence of external parameters, such as the inclination of the chute and the number of particles involved in the flow. In the following the mechanical and numerical parameters calibrated are retained.

Influence of the geometry

The results obtained for the calibrated reference model are compared to those corresponding to a different inclination of the chute channel ($\alpha= 40^\circ$ and 60°). A quite regular trend is obtained, in which an increase of inclination turns into an increase of the maximum kinetic energy (from 22 % to 35% of the initial potential energy) and a shortening of the flow phenomenon (Fig. 4.12). This is due to increasingly rapid accelerations just after triggering of the flow, and increasingly rapid decelerations when the flowing mass reaches the horizontal part of the channel. As it could be expected, an increase of α has a positive influence on the final X_G . The measured values are 2.16, 2.39 and 2.49 m, for a chute inclination of 40° , 50° and 60° , respectively.

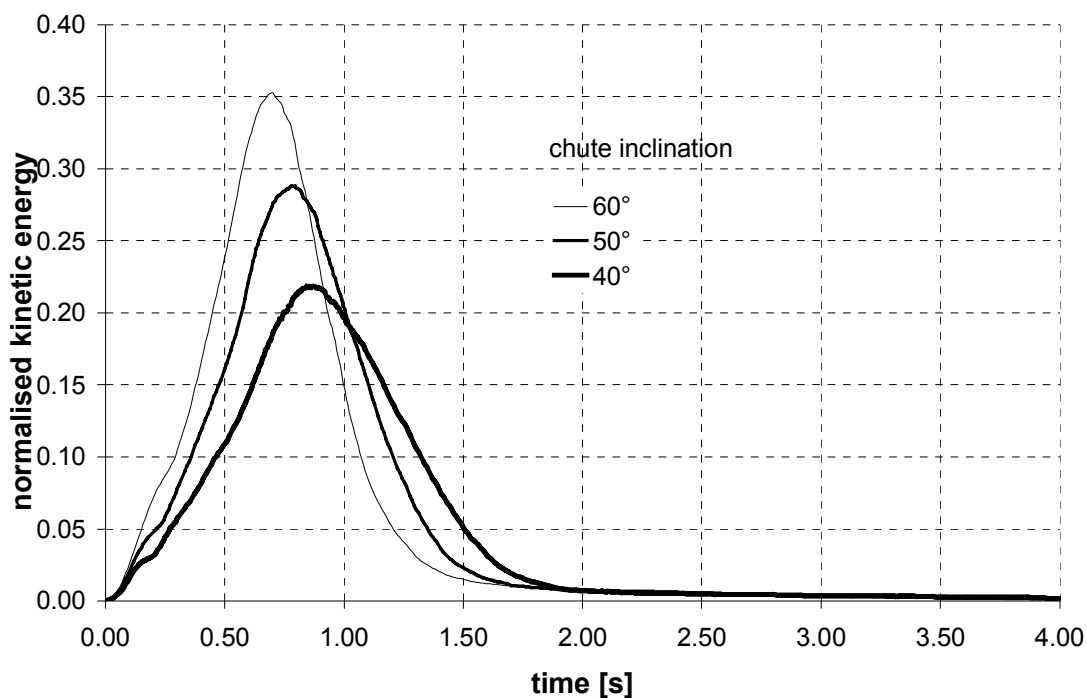


Figure 4.12: Influence of the chute inclination on normalised kinetic energy.

Influence of global mass/number of particles

The importance of the flowing mass is considered in this paragraph. This parameter is of great importance, since it seems that in many recorded cases, the longest run-out correspond to the larger masses.

The global mass of the flowing material can be changed either by acting on the number of disks, or by changing their size: these two conditions, which are analysed separately, are in principle different, since the second one modifies the mass of the single element and its dynamic behaviour.

Number of elements variation (fixed disk size).

Two numerical models are built, with a number of elements (and global mass) equal to the half and the double of the reference one. The corresponding results are shown in Fig. 4.13.

The general trend is that an increase of the number of elements turns into larger energy dissipation as the normalized kinetic energy reaches lower values. This result is confirmed by a progressive reduction of the run-out of the center of mass (X_G) which reaches 2.71, 2.38 and 2.17 m for the 628, 1256 and 2512 disk simulations, respectively.

The analysis of the co-ordination number vs. time curve allows to give an interpretation of this effect: the larger the number of particle, the larger the average number of contacts in the central

and final part of the flow. This means that an increase of the number of disks turns into a more compacted flow configuration. A simple explanation could be that the ratio between the number of particles on the free surface of the flowing mass (which are less confined) and the overall number of particles increases if the global mass decreases. This effect is similar to the specific surface reduction for increasing volume of a solid body.

Disk size variation (fixed number of elements)

In this case two models are built with 628 disks having radius of 2 and 2.84 mm, which corresponds to an equivalent mass of 0.75 and 1.5 kg. The obtained results are shown in Fig. 4.14.

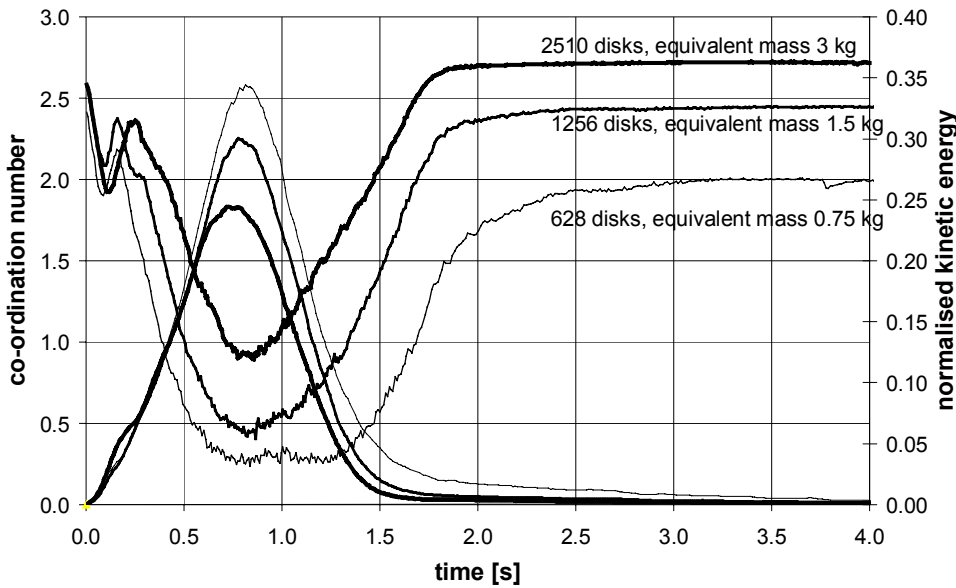


Figure 4.13: Mass change by number of elements variation; influence on kinetic energy and co-ordination number

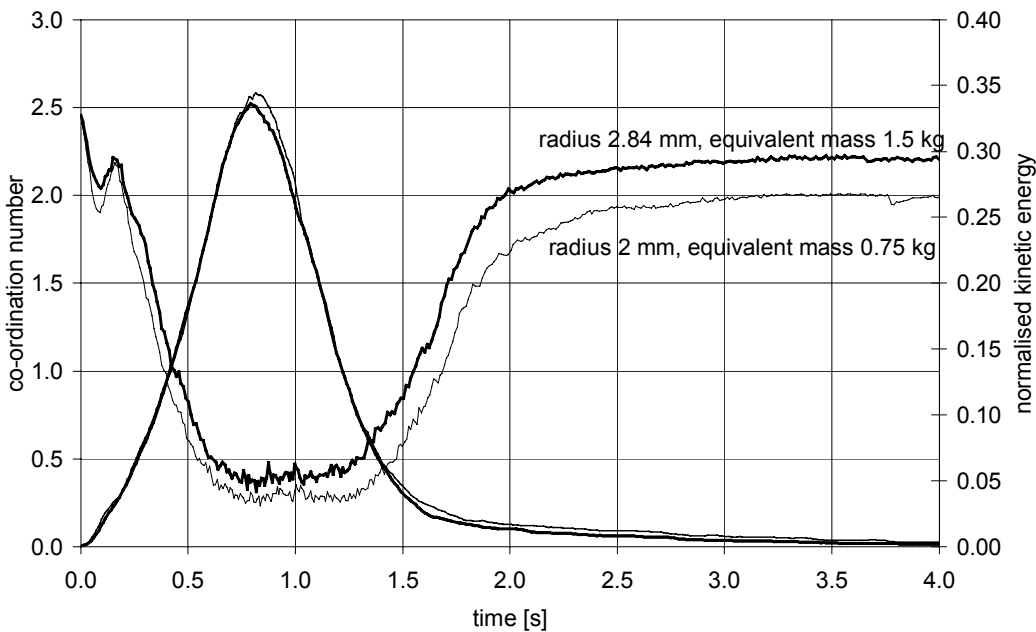


Figure 4.14: Mass change by size of elements variation; influence on kinetic energy and co-ordination number

In this case, the results are not significantly influenced by a mass variation; only the co-ordination number of the deposit is slightly lower, and the mobilised kinetic energy a little higher, for the simulation conducted with smaller particles.

As a conclusion, it seems that the relevant parameter is the number of elements, despite of their size, which has a minor influence.

In order to have a confirmation, three additional simulations were performed, in which the number and size of elements changed, in order to keep the equivalent mass unchanged (1.5 kg). The employed disks have a radius of 1.4, 2, 2.84 mm. The number of elements in the granular mass is 2512, 1256 and 630, respectively.

The previously observed trend is confirmed if the kinetic energy vs. time curves are plotted (Fig. 4.15)

The same conclusions arise from the inspection of the position and shape of the deposit for the simulations performed with the largest and smallest elements (Fig. 4.16). It is interesting to note that the comparison between Fig. 4.10 and Fig. 4.16 suggests that an increase of the number of elements has the same effects of an increase of the damping parameter (which controls energy dissipation).

Additional simulations are in due course, in order to verify whether these results depend on the employed investigation tool, or they are simply due to the relatively small number of particles involved in the presented simulations. It is in fact possible that the supposed volume dependency of the run-out can be observed only above a certain "critical volume".

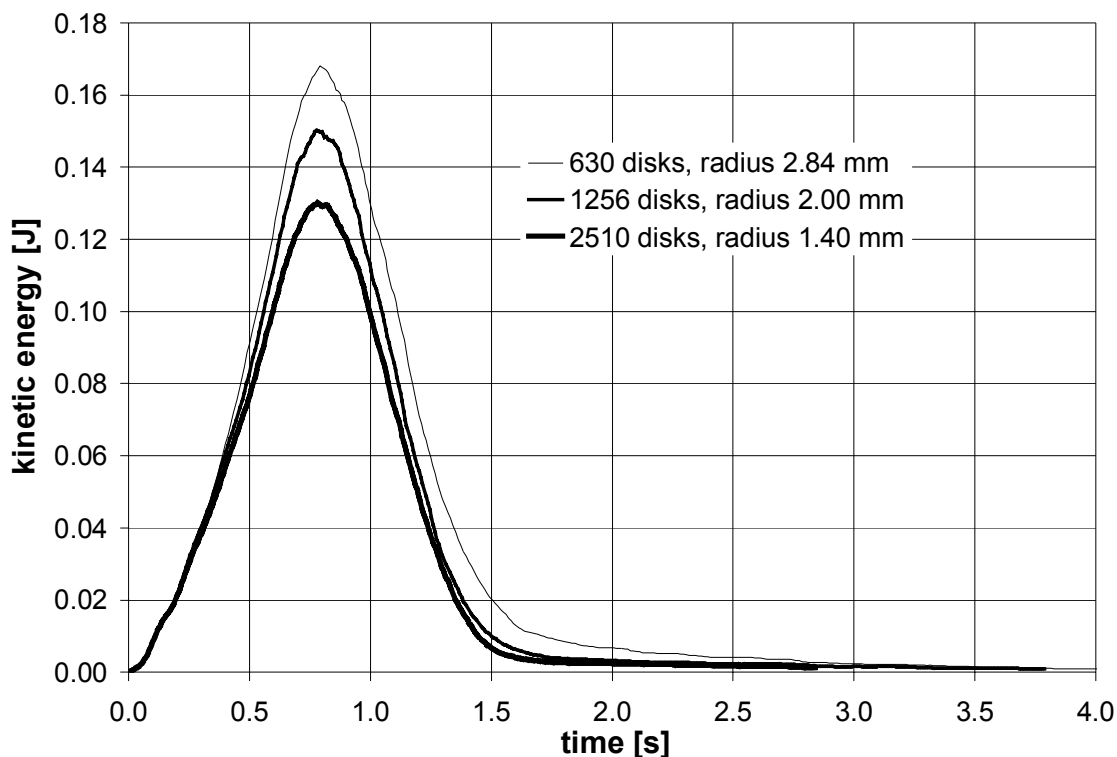


Figure 4.15: Influence of the number of elements on the kinetic energy (equivalent mass 1.5 kg).

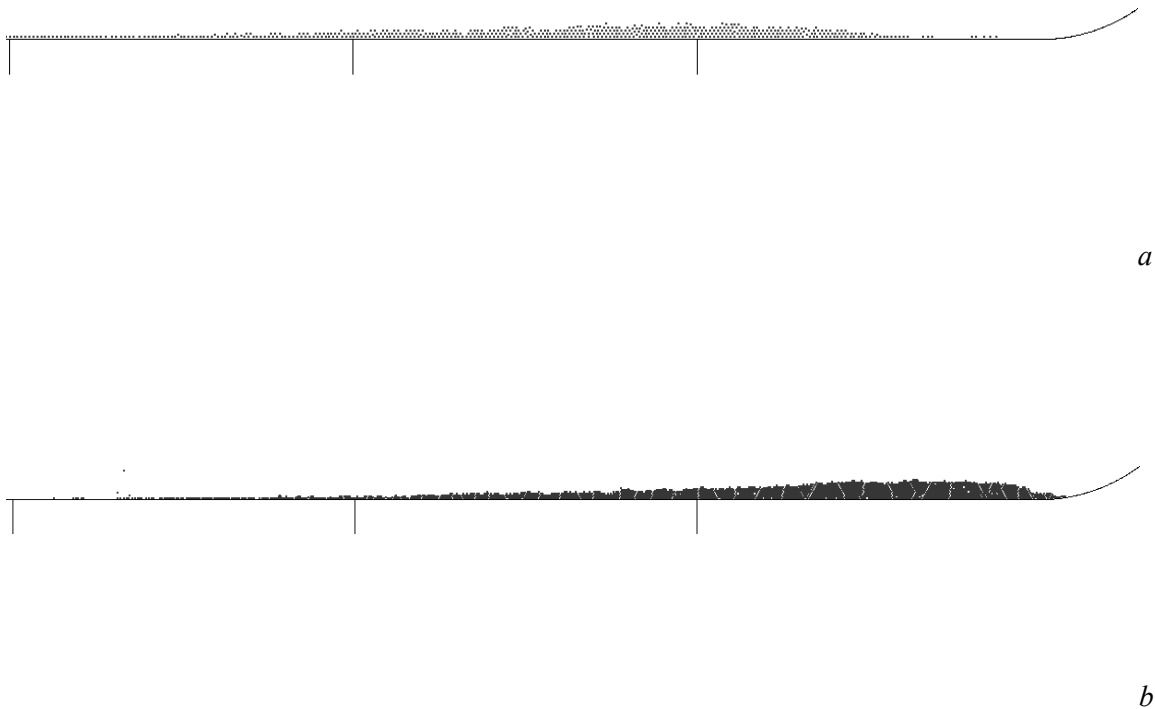


Figure 4.16. Influence of the number of elements on the shape and position of the deposit (equivalent mass 1.5 kg). a: 628 (big) disks; b: 2512 (small) disks.

4.8. Large scale simulations

In this section we will try to extend the use of the DEM model to the reproduction of a real event, which was selected because of its relevance and possibility .

4.8.1. Description of the val Pola rock avalanche

The val Pola rock avalanche (July 28th, 1987) is the most catastrophic event that occurred in the Alps in recent times (see figure 4.17). The rock avalanche involved about 40-50 Mm³ of rock and debris, 32-45 Mm³ of which originated from the main landslide body (composed of highly fractured and altered rock), and about 8 Mm³ were scraped along its falling path. The total drop amounted at about 1200 metres and the total duration of the event was about 70 seconds (CROSTA, 1991). After the event, 2.4 km² of the valley bottom were covered with coarse debris with a maximum thickness up to almost 90 m. The deposit was 1200 m wide, transversally to the valley, and spread laterally 2500 m along the valley bottom. The falling mass climbed on the opposite valley flank with a total run-up of about 300 m. Thanks to its importance, its location and the continuous monitoring, it is possible to collect enough data for a relatively significant analysis. Up to now, relatively few studies involved the dynamic analysis of the falling mass (COSTA, 1991; CROSTA, 1991; AMARÙ and CROSTA, 1996).

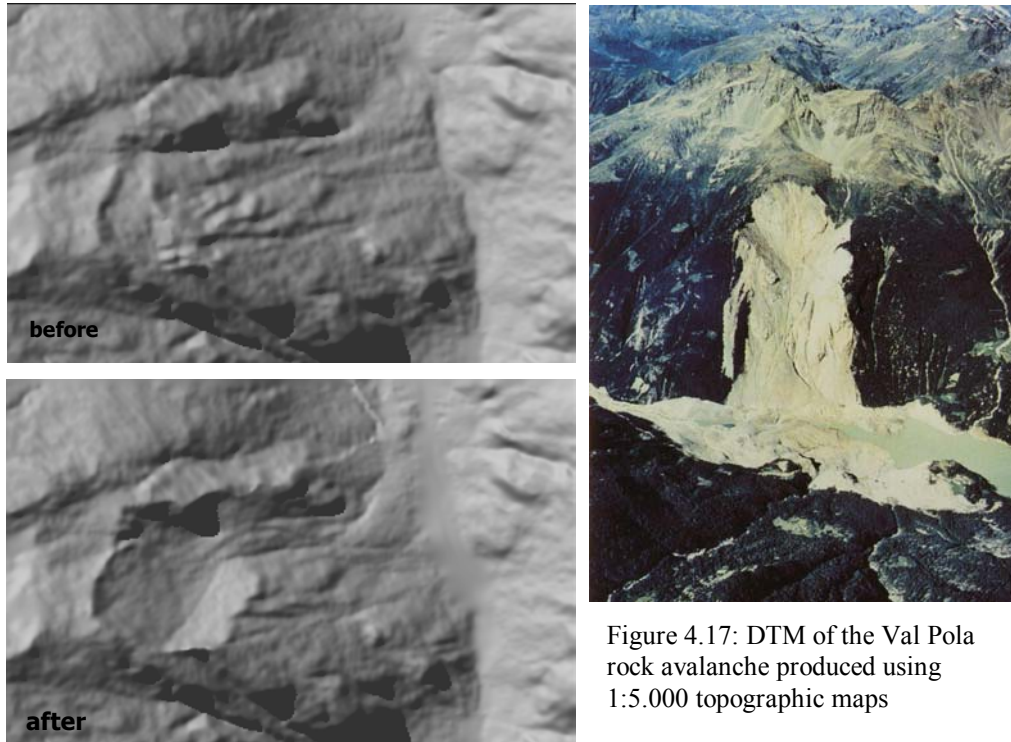


Figure 4.17: DTM of the Val Pola rock avalanche produced using 1:5.000 topographic maps

4.8.2. Numerical simulations

From a DEM point of view, the reproduction of a real scale rock avalanche involves some amplifications of the problems encountered for the simulation of small scale experiments. First of all, given the 2D nature of the employed code, it was necessary to choose the relevant section of the mountain side. Moreover, the rock blocks in the failed mass have irregular shape size and composition. As a consequence, the use of circular elements may seem not realistic. In addition, the choice of size and mechanical properties of the numerical disks is not univocal. In the following, the procedures adopted in the present work will be discussed.

Definition of the numerical model

In order to perform a numerical simulation a section of the slope was built, starting from the available 1:10000 topographic map. In the numerical model the mountain sides are represented by "wall" elements. Then, the particles composing the failed mass are randomly generated in the shaded region of Fig.4.18.

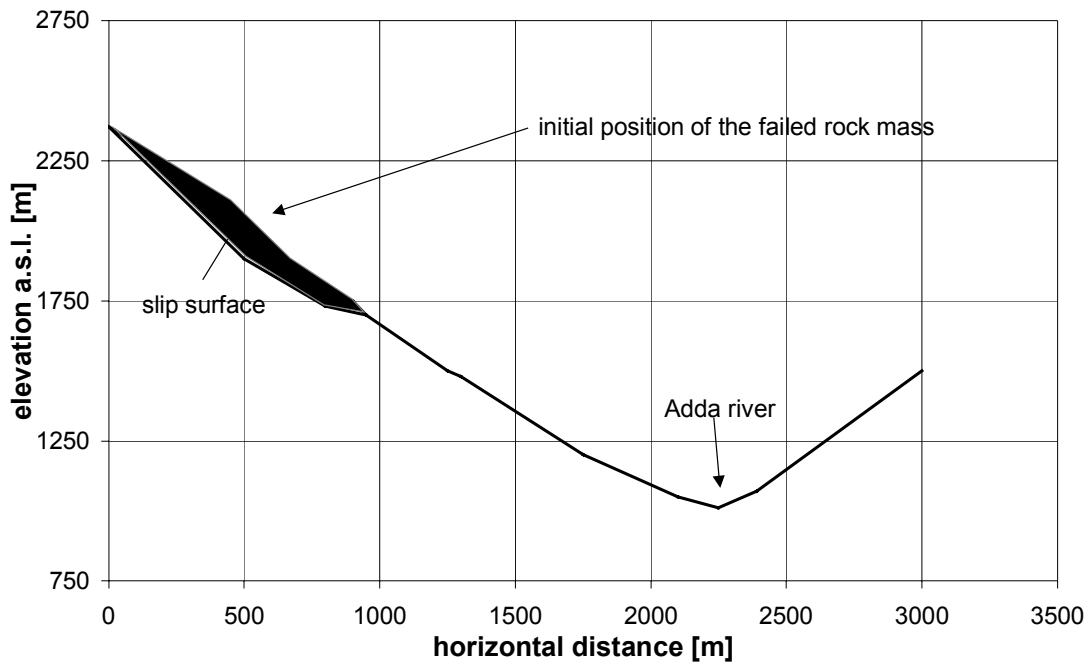


Figure 4.18: Numerical reconstruction of the slope section.

The mechanical and geometrical properties of the elements are evaluated according to the following considerations:

- on the basis of in-situ observations of the deposit, the chosen disk diameter ranges from 3.8 and 4.8 m, with a uniform distribution. Following this choice, the number of particles is 5308;
- the interparticle friction and the base friction are set to 45° , which is the residual friction angle of the joints in the involved rock mass ("Gabbro di Sondalo"), the unit mass of the elements is that of the composing rock;
- the contact stiffness is obtained in a way similar to that described above, starting from the stiffness of the composing rock. In this case, it was not necessary to reduce the calculated stiffness. In fact, given the relevant mass of the individual disks, the time step is sufficiently large to avoid excessively time consuming calculations;
- the numerical damping is the same used for the reproduction of the small scale experiments ($\delta = 3\%$). The reliability of this strong assumption will be evaluated after the simulations.

Before the flow, disks deposit under gravity force. In this phase a 50% damping value is used. In order to reproduce an initially intact rock mass configuration, the disks are bonded together by assigning high values of cohesion and tensile strength to the interparticle contacts.

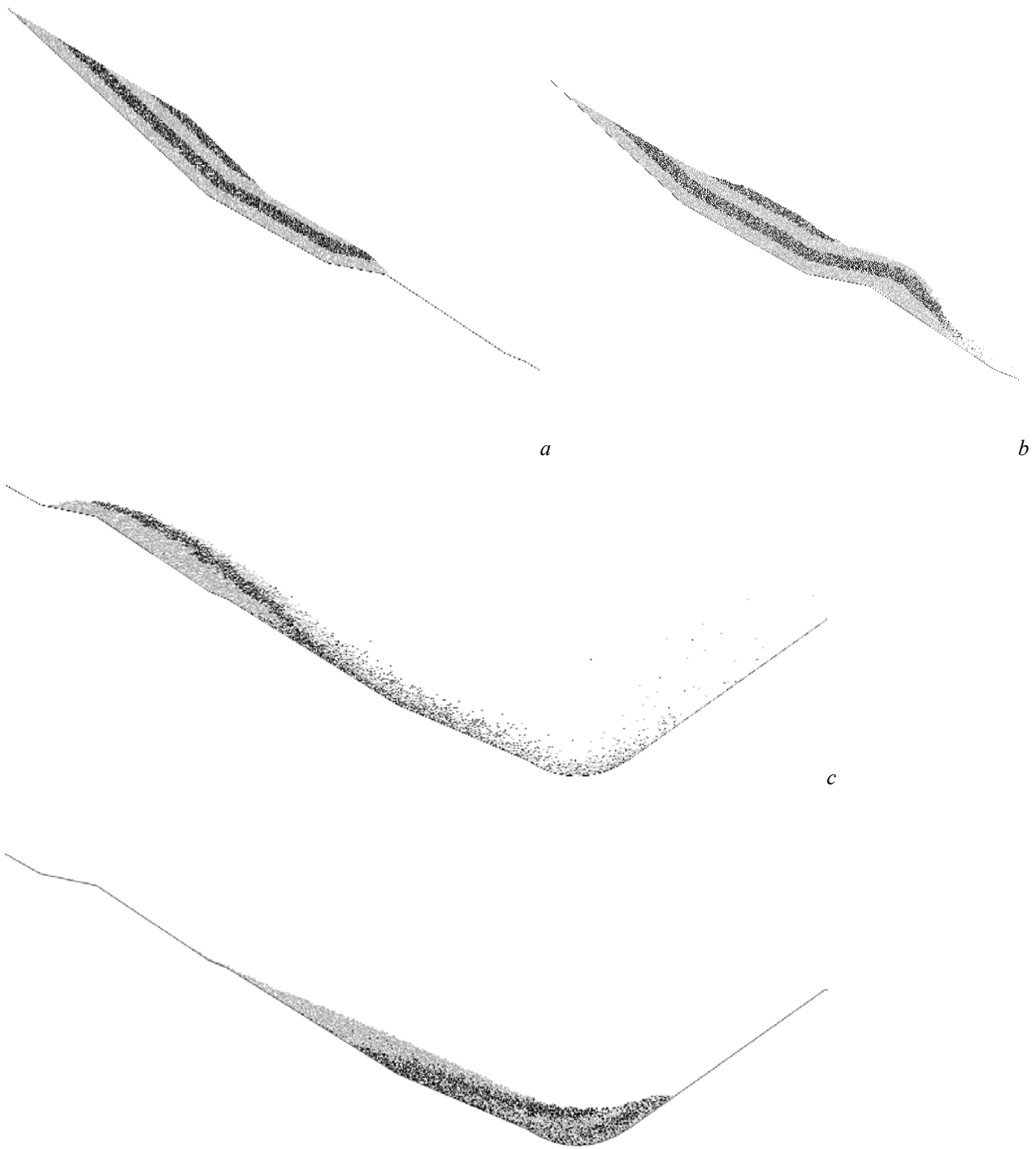


Figure 4.19: Configuration of the avalanche. a: initial; b: after 20 seconds; c: after 50 seconds (maximum run-out); d: final.

Description of the simulations

Two different simulations are performed. In the first one the avalanche is triggered by suddenly setting the cohesion and the tensile strength of contacts to zero. Given the nature of the material involved in the actual failure, this procedure is conservative. In the second simulation, the same parameters are progressively reduced until inception of the flow. This should better reproduce the effects of an initially damaged (fractured and altered) rock mass. In this case, during the avalanche, the remaining contact bonds are progressively destroyed.

In terms of observed behaviour, the first simulation corresponds to a more disperse flow, with higher global kinetic energy. This is due to an increase of the agitation of particles, since the velocity and position of the centre of mass are similar for the two simulations. In addition, other relevant parameters, as the maximum run-out and the position and shape of the deposit are not much affected by the procedure followed to trigger the avalanche. In the following, where not specified, results are commented with reference to the first simulation.

It is important to note that none of the model parameters was back analysed to match the in-situ observations. For this reason, the presented simulations represent a "prediction" more than a "reproduction". In fact, the same procedure could be applied to any unstable mountain side, for a preliminary risk evaluation.

4.9. Discussion

In order to have a visual idea of the simulated avalanche, the configuration of the rock mass is shown for different values of time elapsed since the inception of motion (Fig.4.19).

During the first seconds of simulation the flow is quite slow, and the mass moves in an ordered way (Fig.4.2.b): this is probably due to the fact that the bottom part of the slip line has a small inclination (about 15°). The subsequent progressive acceleration starts from the upper layers of the mass, which are the first one that reach the bottom of the valley and remount on the opposite flank, with a maximum climb of about 300 m (Fig.4.19 c). In this phase the measured speed reaches 100 m/s for some isolated elements, while the maximum speed of the centre of mass is about 40 m/s. It is important to note that the maximum run-out is in good agreement with the reconstruction of the real event based on in-situ observations (CROSTA, 1991). The deposit is characterised by the vertical inversion of the original layers (this point will be discussed later on). Its position, and the trajectory followed by the centre of mass are depicted in Fig.4.20. The maximum thickness of the deposit is about 100 m, with a climb of about 150 m on the opposite valley side.

The comparison with the actual situation is presented in Fig.4.21. The two simulations give results which are similar, and very close to the actual deposit. The main discrepancy regards the thickness of the deposit, which is smaller for the actual case. This difference is certainly due to the 2D nature of the numerical code that inhibits lateral expansion of the flow.

In order to get a more detailed description of the flow kinematics, the position of six sample disks was tracked during the simulation. From the inspection of Fig.4.22 the following points can be listed:

- the smallest run-out correspond to the disks (#1 and #5) that were initially located close to the slip line. These points maintain the original horizontal order;
- the disks initially belonging to the same vertical section (#3, #4 and #5) travel a distance that decreases with the initial depth.
- the disk initially located at the nose of the failed mass (#6) has a short run-out.

These evidences confirm the visual analysis of the pictures taken during the flow (Fig.4.2), from which it seems that the acceleration starts from the superficial layers.

A last consideration regards the time duration of the simulated rock avalanche, which is about 100 s, to be compared to the actual value of about 70 s. This discrepancy is not considered important, since the only in-situ measurement is based on the recordings of a seismic station, located 150 km

away from val Pola, in Switzerland. In our opinion, it is possible that the slower part of the flow (initial and final) did not give rise to measurable seismic waves.

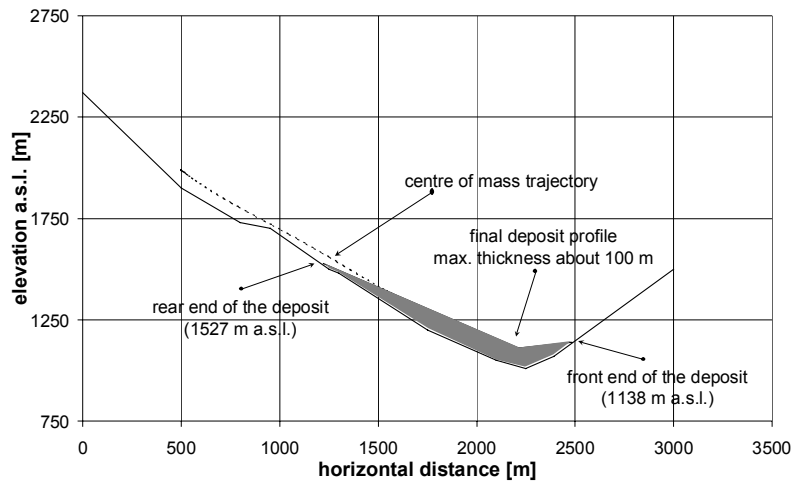


Figure 4.20: Position and shape of the deposit, with trajectory of the centre of mass.

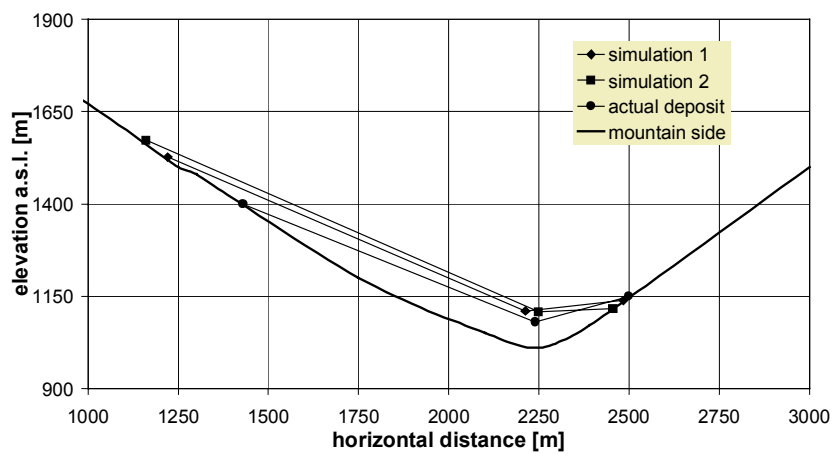


Figure 4.21: comparison between the deposit configuration.

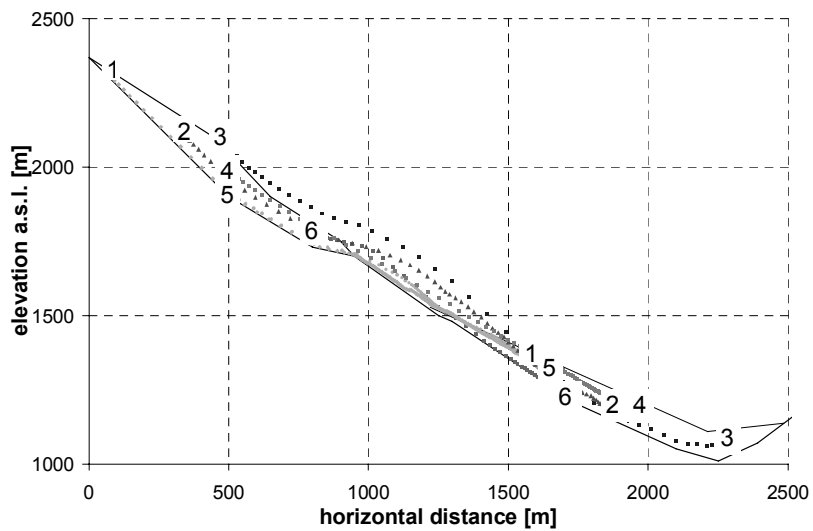


Figure 4.22: Initial and final position (with trajectories) of the sample elements

4.10. Critical review of results

The Authors are aware that the DEM models used in the present work are the result of an important process of simplification of several features involved with dry granular flows. In the text, it was already reported that several aspects that are often invoked to explain in-situ observations cannot be implemented in a DEM model.

On the other side, the obtained results can be considered satisfactory, even in the light of the simplicity of the parameter calibration procedure. This conclusion holds for the small scale simulations as well as for the large scale ones. In particular, the only parameter which is not related to any physical mechanism (numerical damping) has a quite regular influence on the results. The strong hypothesis that the damping parameter calibrated on small scale experiments could be used for the large scale rock avalanche, was not contradicted by the results. It is important to underline that the simulations of the val Pola event can be considered a prediction, at least for what regards the run-out assessment.

Of course, the solution of some problems is still an open point. In particular, in the presented simulations the increase of the run-out for increasing involved mass was not observed. Additional simulations are in due course, in order to verify whether this is an intrinsic limitation, or it is simply due to the relatively small number of particles involved in the presented simulations.

Other simulations are planned, in which a 3D DEM code will be employed. In this way, it is believed that the lateral spreading of rock avalanches and debris flows could be reproduced.

5. AN EXAMPLE OF DEPTH AVERAGED MODEL

According to HUNGR (1995), dynamic models of landslides fall into two large categories, namely: lumped mass models (KOERNER, 1976, PERLA et al., 1980, HUTCHINSON, 1986), which idealize the slide motion as a single point, and continuum mechanics models. The main limitation of a lumped mass model lays in being unable to account for internal deformations and to model the motion of the flow front. Each of the existing continuum mechanics models is associated with a specific rheological formula (e.g.: Newtonian or Bingham rheology). The frictional rheology, characterized by the dependence of the resisting basal stress on the normal stress, has been the most commonly adopted in lumped mass models. Furthermore, the large part of these models used an Eulerian framework with a fixed reference grid. Nevertheless, a moving Lagrangian reference system is much more advantageous in describing highly unsteady motion.

SAVAGE & HUTTER (1989) adopted a two dimensional Lagrangian frictional model to simulate the flow of a dry granular material. This model was the first one able to account for the nonhydrostatic internal stress states that are more specific of the flow of a granular material.

HUNGR (1995) developed starting from the approach by SAVAGE & HUTTER (1989) a universal model, called DAN (Dynamic Analysis). The model is based on a Lagrangian solution of the equations of motion and allows the selection of a variety of material rheologies. These rheologies can be varied along the slide path or within the slide mass. Furthermore, this model allows for the internal rigidity of relatively coherent slide material, moving on a thin liquefied basal layer, which can contrast with the fluidity of the basal layer. Eventually, it take into consideration the effects of lateral confinement along the path.

The moving landslide mass is replaced by an equivalent fluid whose bulk properties approximate the behavior of the prototype and are retained constant for the entire flow depth. These properties are too difficult to be evaluated in the laboratory or directly in situ and therefore a back analysis approach must be preferred.

For the original model we send the reader to the original paper by HUNGR (1995), whereas we show some of the modifications that we developed and an application to the Val Pola rock avalanche and to the Sesa landslide (CROSTA, 2001).

In the model, a earth pressure coefficient, k , is defined as the ratio between the tangential and normal stress in the flowing mass (see figure 5.1). The magnitude of k depends on strain according to equation: $K = K_j + S_c \Delta \epsilon_j$ where S_c is the stiffness coefficient: $(k_p - k_a)/0.05$ for compression and $(k_p - k_a)/0.025$ for unloading. The k_a and k_p coefficient values can be computed at each point within a flow (e.g. for each discrete block). The coefficients are computed differently for blocks where the depth averaged flow locally diverges or converges ($\partial v_x/\partial x + \partial v_y/\partial y > 0$ or $\partial v_x/\partial x + \partial v_y/\partial y < 0$) or whether an element of granular material is being elongated or compressed ($\partial u/\partial x > 0$ or < 0). The k coefficient, also expressed as

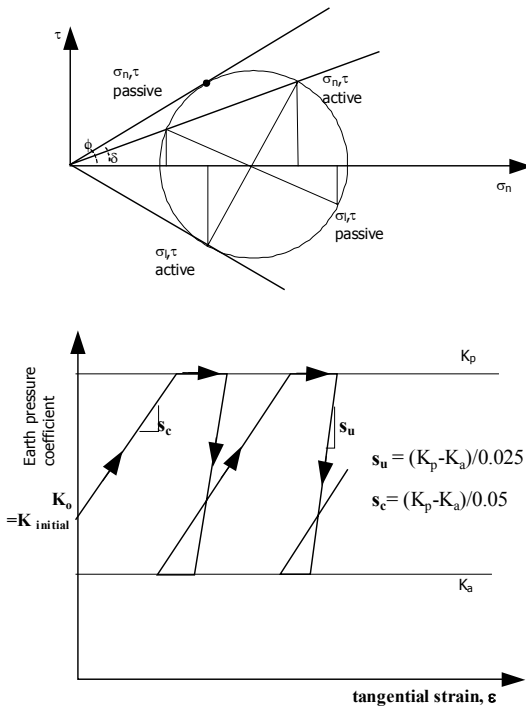


Figure 5.1: Earth pressure coefficients and stiffness coefficients

a) $k_{act/pass}$ is computed as:

$$k_{act/pass} = 2 \frac{1 \mp (1 - \cos^2 \phi_{int} (1 + \tan \phi_{bed}))^{1/2}}{\cos^2 \phi_{int}} - 1$$

in which "-" in " \mp " applies to the active coefficient for diverging flow, k_{act} , and "+" applies to the passive coefficient for converging flow, k_{pass} (figure 5.2). The main difference between this couple of coefficients and those described by RANKINE (1857) consists in the fact that they are derived by assuming that Coulomb failure occurs simultaneously along the bed ($\phi = \phi_{bed}$) and within the overlying material ($\phi = \phi_{int}$). This equation reduces to that by Rankine in case of $\phi_{bed} = 0$. As described by IVERSON (1997), generally, lateral stresses in regions of converging flow exceed bed-normal stresses, whereas lateral stresses in regions of diverging flow are less than bed-normal stresses.

Lateral normal stresses where flow converges exceed those where flow diverges by a factor of 2 to 10. If the bed has maximum roughness ($\phi_{int} = \phi_{bed}$) the coefficients reduce to a single case:

$$K_{act/pass} = \frac{1 + \sin^2 \phi_{int}}{1 - \sin^2 \phi_{int}}$$

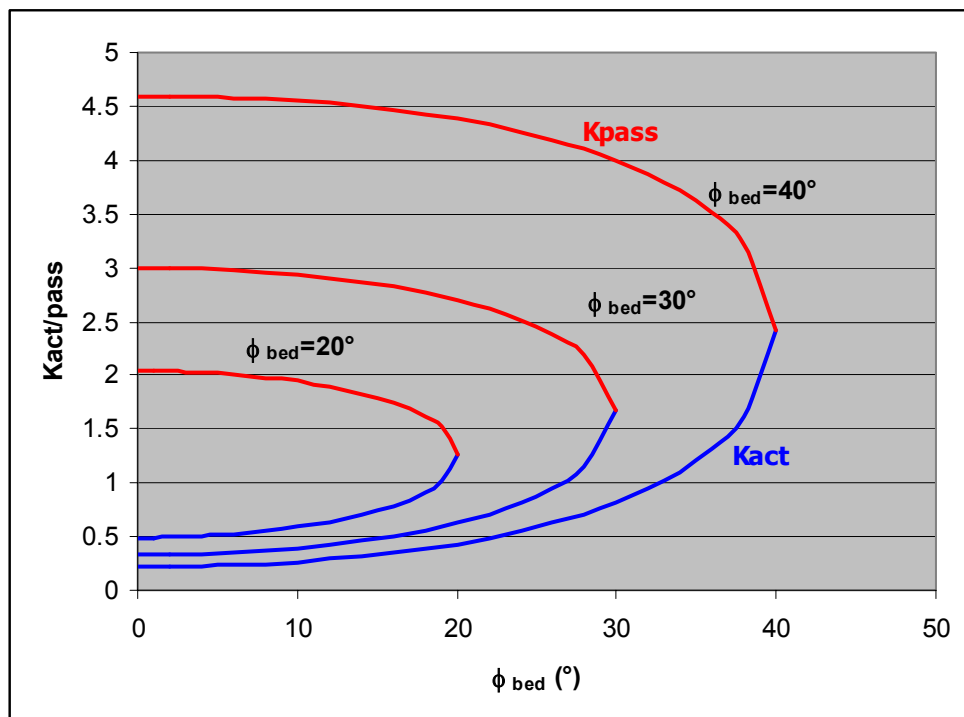


Figure 5.2: Values of $K_{act/pass}$ plotted vs ϕ_{bed} computed according to IVERSON et al. (1997)

This unique value points out that in these conditions a slab of Coulomb material can move downslope with zero velocity divergence, ie no thinning and no thickening.

The basal flow resistance force, T , depends on the rheology of the material and is a function of different parameters. The relationship between T and the other parameters is based on the assumption that the shear stress on tangential planes increases linearly with normal depth. This assumption together with a specified rheological constitutive equation determines the velocity vs depth distribution profile and an expression for T .

Rheological model	Rheological function	Notes
Plastic flow	$T = cA_i$	$c = \text{constant shear strength}$
Friction flow	$T = A_i \gamma H_i (\cos \alpha + a_d/g)(1-r_u) \tan \phi$	$a_c = v_i^2/R = \text{centrifugal acceleration}; R = \text{vertical curvature radius}, r_u = \text{pore pressure coefficient}$
Newtonian laminar flow	$T = 3A_i v_i \mu / H$	<i>Poiseuille equation, $\mu = \text{dynamic viscosity}$</i>
Turbulent flow	$T = A_i \gamma v_i^2 n^2 H_i^{-1/3}$	<i>Manning equation, $n = \text{roughness coefficient}$</i>
Bingham flow	$V_i = (H_i/6\mu)(2T/A_i - 3\tau + \tau^3 A_i^2/T^2)$	$\tau = \text{constant yield strength}, \mu = \text{Bingham viscosity}$
Coulomb viscous flow	$T = \gamma H_i (\cos \alpha + a_d/g)(1-r_u) \tan \phi$	
Voellmy fluid	$T = A_i (\gamma H_i (\cos \alpha + a_d/g) \tan \phi + (\gamma v_i^2/\xi))$	<i>VOELLMY (1955), $\xi = \text{turbulence coefficient}$</i>

The original model as proposed by HUNGR (1995) as been modified to take in account for:

- mass exchange between adjacent blocks as a consequence of excessive difference in height by considering slope and frictional resistance
- mass entrainment by considering a maximum soil thickness and the equilibrium between soil strength and shear stresses applied to the soil.
- mass deposition, controlled by a minimum value of flow velocity.

5.1. Val Pola rock avalanche

In the following figures (figures 5.3, 5.4) the results of the simulations for the Val Pola rock avalanches are reported. The adopted angle of internal friction is equal to 36° whereas a Voellmy model has been used for the thin shear zone, with friction angle of 15° , $r_u = 0.1$ and turbulence coefficient of 500 m/s^2 . These properties allowed to obtain a final result reasonably acceptable with respect to observed behaviour (geometry of accumulation, total time). Eventually, these data can be compared with those obtained for a lumped mass model of the sledge type according to three different assumed geometries for the energy line. It must be stressed that energy lines are here thought as broken lines with different segments characterized by a different slope. Differences in slope are motivated by differences in the rate of energy utilization because of slope geometry, changes in slope curvature, presence of different soil covers, etc..

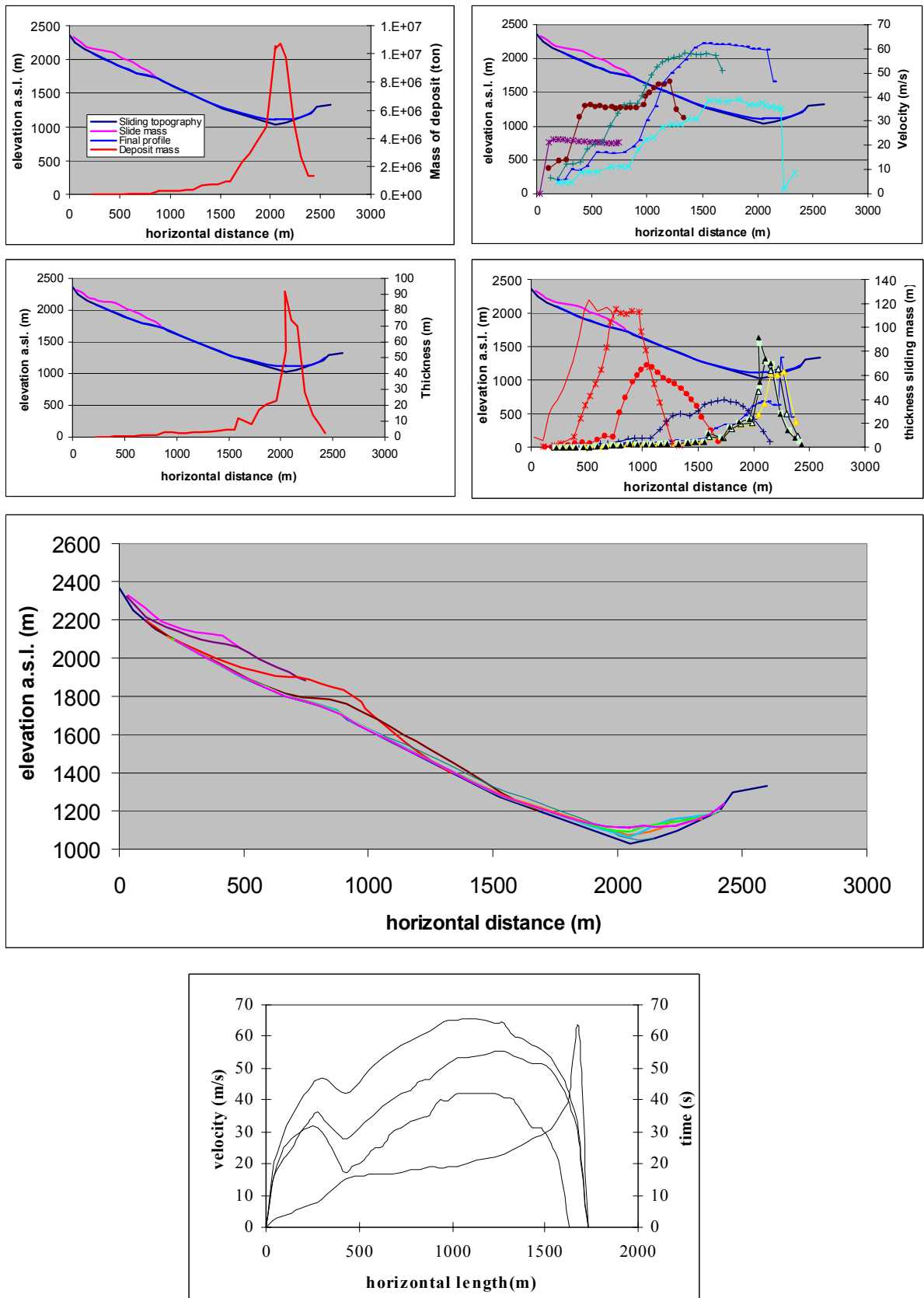


Figure 5.3: Results of the simulation for the Val Pola Landslide by means of the modified DAN model, considering mass exchange between adjacent blocks, and of the energy line approach

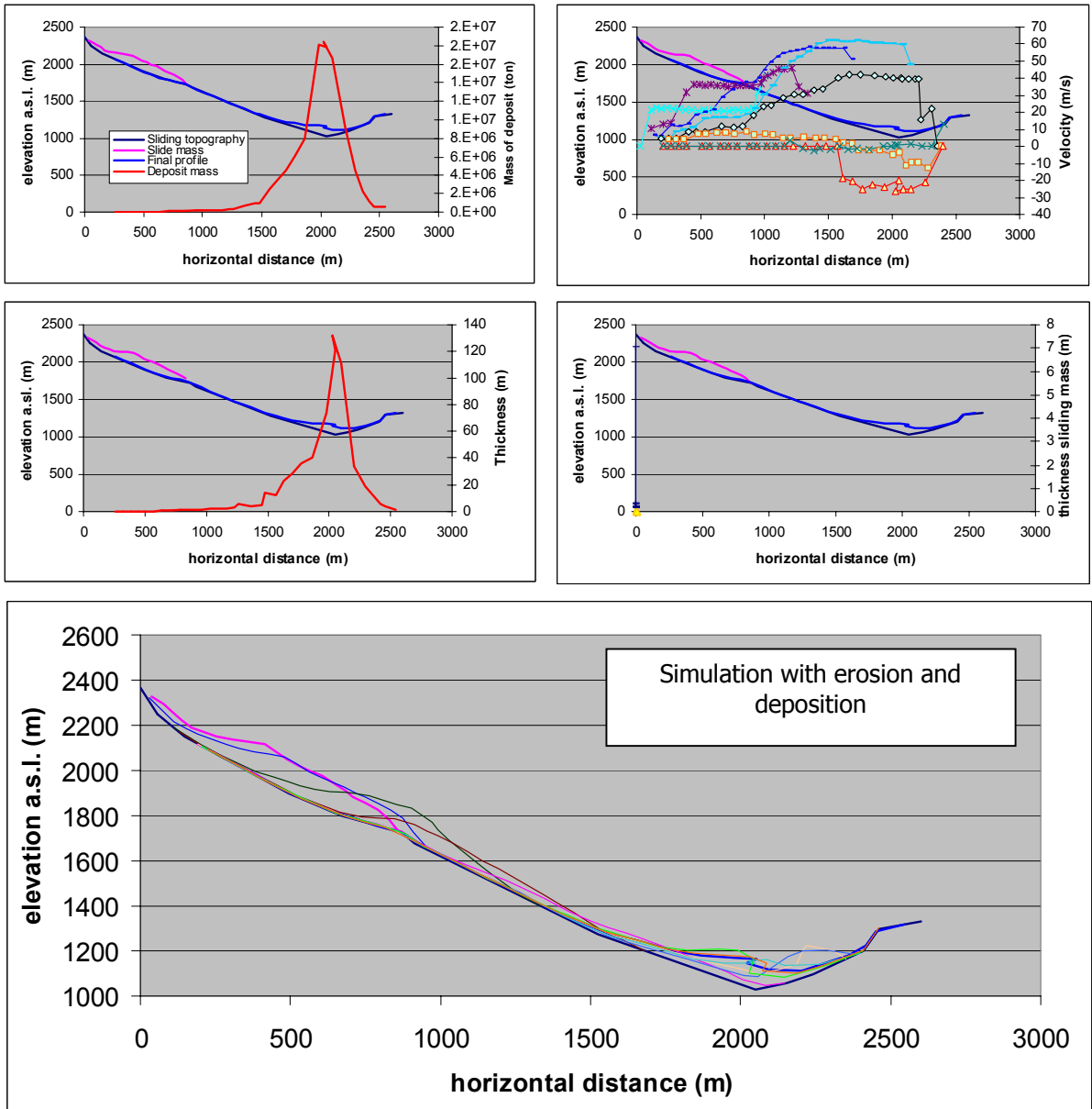


Figure 5.4: Results of the simulation for the Val Pola Landslide by means of the modified DAN model and considering erosion along the path.

5.2. Sesa landslide

The Sesa landslide is located in the Grigna valley, a left hand tributary of the Valcamonica (Oglio river, Lombardy region, northern Italy, CROSTA, 2001). The Grigna valley, as well as many other tributary valleys in the area, is characterised by the presence of a narrow and deep rocky gorge about 6 km in length. The upper catchment area is quite distinctive geologically because of the thick glacial deposits covering the hillslopes.

On October 1993, after a 15-day rainy period, the Sesa landslide started moving at greater velocity with renewed debris-flow activity along its left lower flank. Rainfall intensity was relatively low but the total antecedent rainfall was quite considerable if considering that a 100 yr recurrence time was calculated. In the early evening (20:15 hrs) of October 9, the landslide collapsed completely. A 2 Mm³ mass of glacial and fluvio-glacial deposits, with a thickness ranging from 60 to 80 m, was involved, together with about 2000-3000 m³ of tree trunks. Thick glacial deposits have been exposed along the main sub-vertical scarp where an 80-m-high sub-vertical face is still present 8 years after the failure. Beneath these deposits, the bedrock (mainly sandstone and siltstone) dips 30° to the north in the direction of the slope.

The initial movement was of the slump type, but some evidence (flow-like structures and damages to trees) suggests that a flow occurred in the intermediate and lower slope sectors. An evident flow superelevation, on the slide valley flank, just downstream of Ponte Sesa, (cross section A in figures 5.5 and 5.6) was observed in a rectilinear tract of the valley. No sign of impoundment of the creek was observed, and this is also supported by eye-witness reports. This last observation suggests that no landslide dam was created, and, as a consequence landslide dam collapse cannot be invoked as the origin of the subsequent debris flow.

The landslide material and the wood debris flowed within the main creek for about 7 km down to the mouth of the Grigna valley and continued downstream as a hyper-concentrated flood.

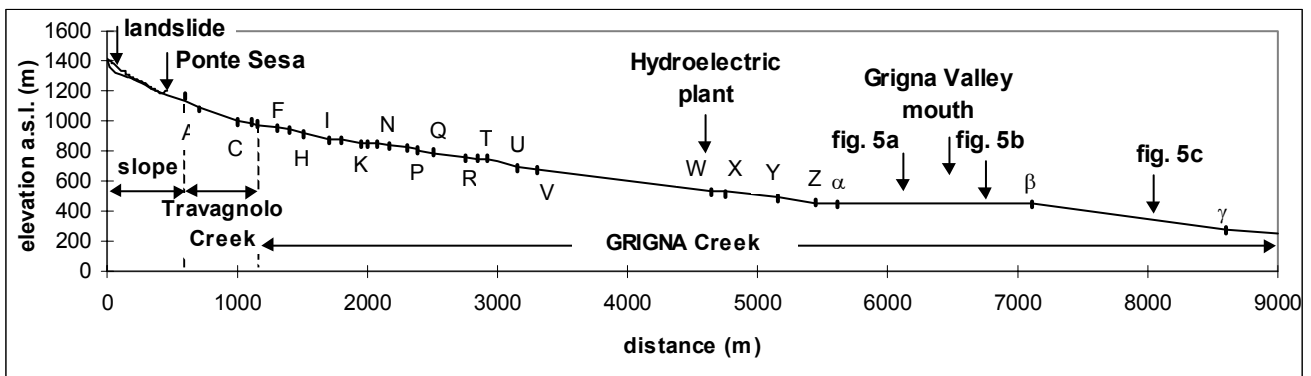


Figure 5.5: Profile along the flow path of the Sesa landslide with position of surveyed cross sections

Clear indications of a debris flow and finally of a hyper-concentrated flood (PIERSON and COSTA, 1987) were observed along the rocky gorge and the final alluvial fan area. Exceptional superelevation of the debris flow up to 30 m high occurred along the banks of Travagnolo Creek. Superelevation and changes in thickness have been rated along the entire flow path (**Figure**). Furthermore, alluvial debris and slope scouring, as well as deposition of coarse and fine materials were observed, described and measured. The total duration of the phenomenon was estimated to be about 17-20 minutes (an average velocity of 7.5 m s⁻¹) according to eye-witness reports and the time of occurrence of sequential damage at different structures (bridges, rural roads, water intake structures and damages and interruption of production at the hydroelectric power plant). located along the path at known elevations from the valley bottom. Total cost of the damage was about 2.5 million dollars.

Of the initial landslide mass (total volume 2 Mm³), about 1.6 Mm³ flowed along the gorge, 10% of it consisting of silt, as indicated by samples of slope material collected along the main scarp. This

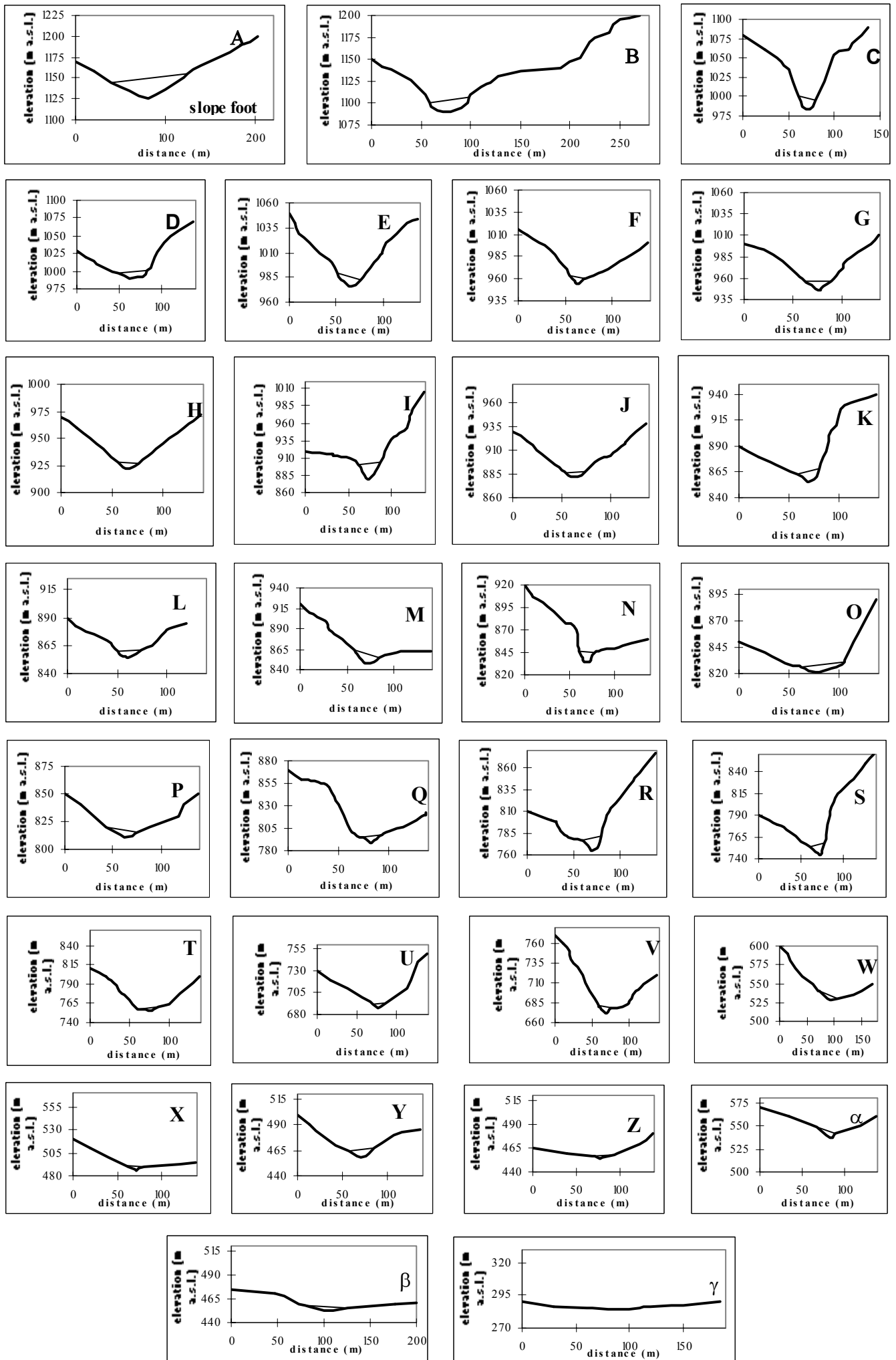


Figure 5.6: Surveyed cross sections along the Sesa flow path

mass of finer particles was transported farther downstream from mouth of the Grigna valley under conditions of hyper-concentrated flow, as indicated by the large deposits that occur downstream. About 0.8 Mm^3 of coarse debris have been deposited along the 6-km-long gorge and 713 m of topographic relief (i.e., fall height/travel distance: $H/L \approx 0.12$), and the flow has entrained more debris by bulking. All along this sector the deposits consist mainly (55%) of boulders (as much as almost 100 m^3 in size) with abundant gravel and sand (45%). These deposits are characterised by inverse grading, with undefined stratification, high density and compaction, gradual downstream decrease of the average grain size, and with larger grain size in corresponding to bends in the flow path. Their thicknesses of the deposits ranges from 0.5 to 3.5 m. However, actual flow thickness achieved much greater values, up to 30 m, with a gradual downstream decrease. Twenty eight cross sections have been located and surveyed along the gorge, describing for each the main sedimentological (grain-size distribution of the deposited and scoured materials; type of deposit) as well as the geometry of the flow mudline. These observations have been used to assess the average velocity and discharge along the path by analysing flow surface superlevation according to JOHNSON & RODINE (1984, see figure 5.7). Observing the results it is possible to say that the mass initially (from the origin to 400 m downslope) moved rapidly (between 9.7 and 19 m/s), slowing to the Travagnolo-Grigna Creek confluence (1100 m from the source). From this point to the hydroelectric power plant (4700 m from the source), the debris flowed at an average speed of 4.2-11 m/s with local changes in velocity and discharge due to morphological control and water inflow from tributary valleys. It is possible that the narrowness of the channel in the upper sector, with almost constant width and with frequent tight bends, might have caused pulsing of the flow.

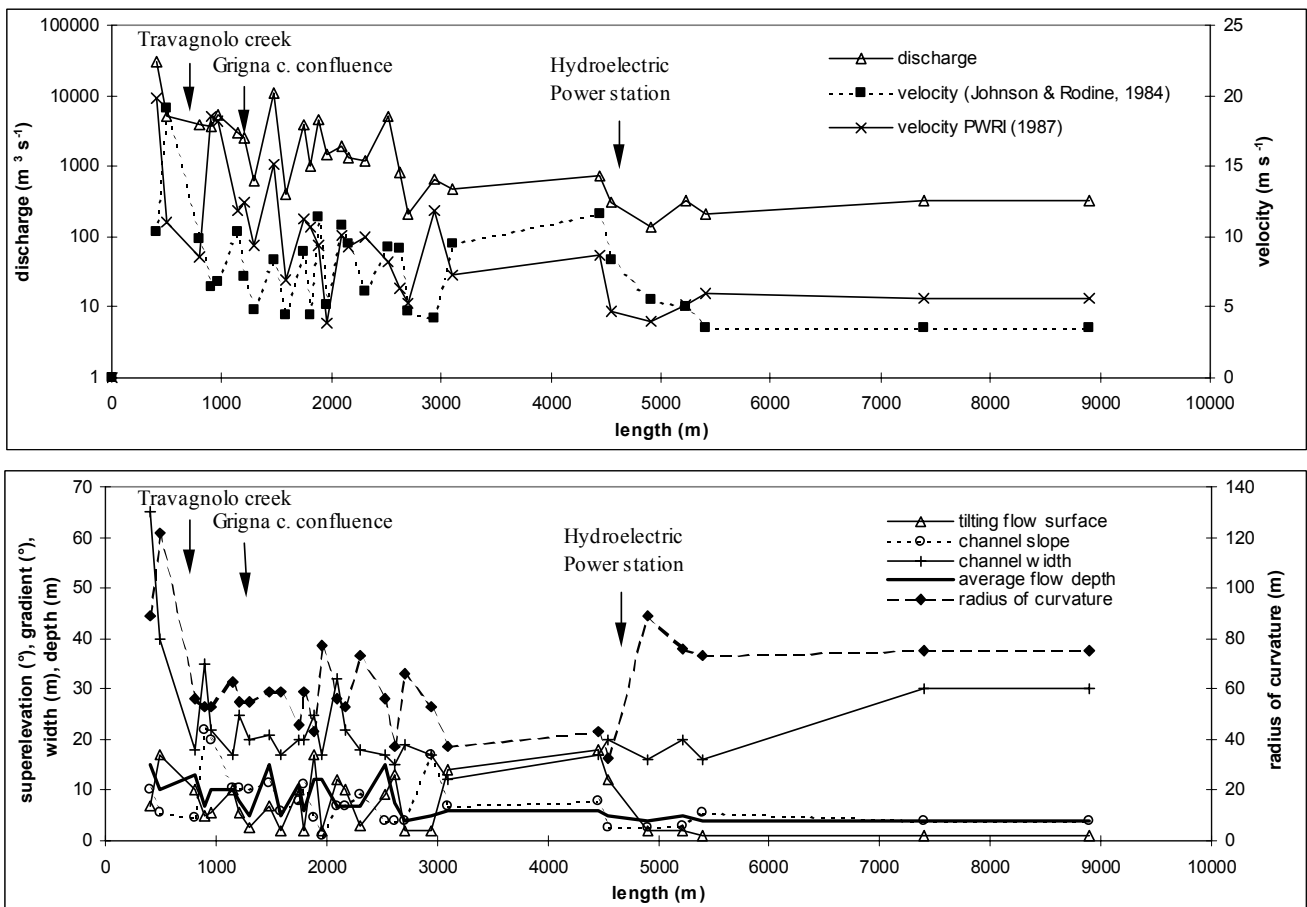


Figure 5.7: Flow velocity and discharge along the flow path of the Sesa landslide and main controlling parameters.

The second half of the path is more rectilinear with minor bending and a more continuous flow at almost constant velocity (about 3.3 m/s). Even at this lower velocity, damages to bridges and small crossings, as well as deposition and erosion occurred also downstream of the valley mouth (Bienno area).

The unit discharge relating to a specific maximum flow depth has been computed from the recorded data to evaluate the general flow behaviour (HUNGR et al., 1984; TAKAHASHI, 1991). The feasibility of this approach is based on the fact that the observable post-event mudline (i.e., trimline) corresponds to the point of maximum flow discharge. The debris flow discharge for the 28 cross sections has been computed using different methods (JOHNSON and RODINE, 1984; HUNGR et al., 1984; TAKAHASHI, 1991) and compared to data available in the literature (HUNGR et al., 1984; PIERSON, 1985; TAKAHASHI, 1991). **Figure 5.8** presents the unit discharge vs maximum flow-depth relationships, as well as the computed values. The data fall within the dilatant and laminar viscous flow fields as defined by HUNGR et al. (1984). They are also well fitted by a $q \propto h^{2.5}$ equation (e.g., $q = 0.38 h^{2.568}$) proposed for collisional material by ANCEY et al. (1999). For this collisional conditions, ANCEY et al. suggest that frictional interactions, throughout the network of particles in contact, are too weak to influence the bulk behaviour of the flowing material. This could be due both to the relative abundance of large blocks within the flowing mass and to the narrowness and roughness of the rocky gorge.

On the same plot are traced the theoretical curves for the laminar, dilatant, and turbulent flow cases for channels with the observed limit slope values (minimum 5° and maximum 22°).

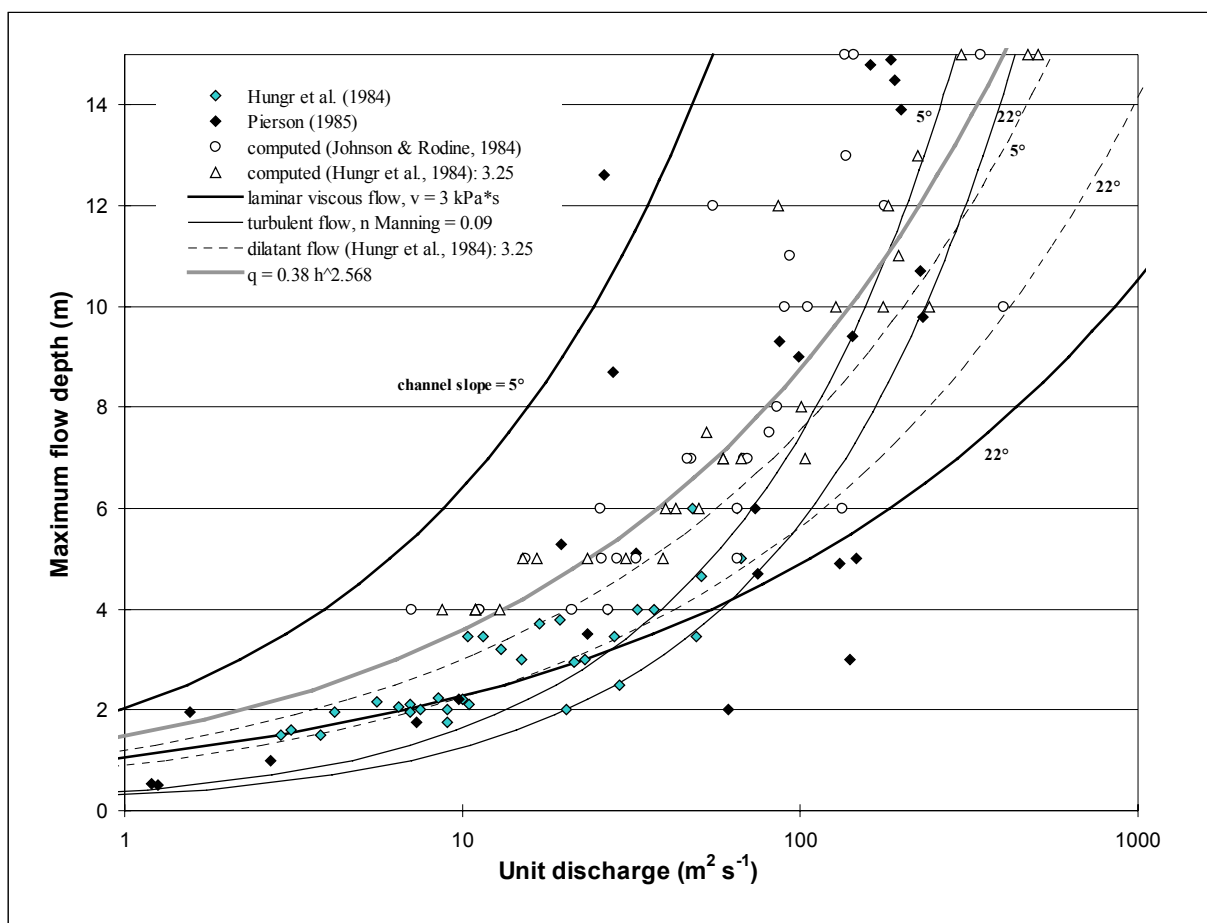


Figure 5.8: Unit discharge vs maximum flow-depth relationships with computed values for the Sesa event by means of different formulae (CROSTA, 2001)

By considering these results it can be seen that the rheological behaviour of the flow changed successively during the event (from landslide to hyper-concentrated stream flow) because of different factors. These plots however suggest only an approximate classification of the flow. Among these factors we can list: 1) progressive increase in the scouring action and resulting bulking as the flow moves downstream; 2) trapping of the largest blocks in major constrictions of the gorge; 3) deposition of large blocks by settlement and flow spreading in the lower gorge sector and at the alluvial fan apex, and 4) the final deposition of fine materials. At the same time, the length of the flow path and the tributary valleys can induce changes in the properties of flowing material by increasing the water content within the mass. As a consequence, matrix viscosity, hydrodynamic interactions, friction, and collisions may have played different roles in different sectors of the flow path (COUSSOT and PIAU, 1995).

5.2.1. Landslide dynamics

The numerical code developed and modified from the one by HUNGR (1995) allows the modelization of the frictional regime, typical of the initial movement (for the first 500 m along the slope profile). The successive changes to a turbulent regime, as witnessed by field evidence, and the gradual changes due to the increase of water content (inflow from tributary valleys, deposition along the path) have also been modeled.

Among the results we can list:

- evaluation of velocity (see figure 5.9),
- thickness of flow and deposit,
- total and partial times of flow; and
- mass distribution during flow and after deposition.

It must be stressed that, to model the turbulent flow along the main valley channel, a higher-than-common n Manning coefficient has been introduced (0.05 to 0.15). This is in good agreement with observations conducted by JARRETT & COSTA (1986) in the dam-break modeling of the Lawn Lake Dam ($n = 0.1-0.2$, on average 80% higher than found in their field survey) as well as from other researchers (HUNGR et al., 1984; TAKAHASHI, 1991).

The results have been compared to field observation and the model has also been successfully calibrated by means of this field check (computed from trimline data). This has also been allowed by knowledge of approximate partial duration time (since the slide occurrence up to the damaged hydroelectric power station) and total duration time of the event (since the slide occurrence up to the Grigna valley mouth).

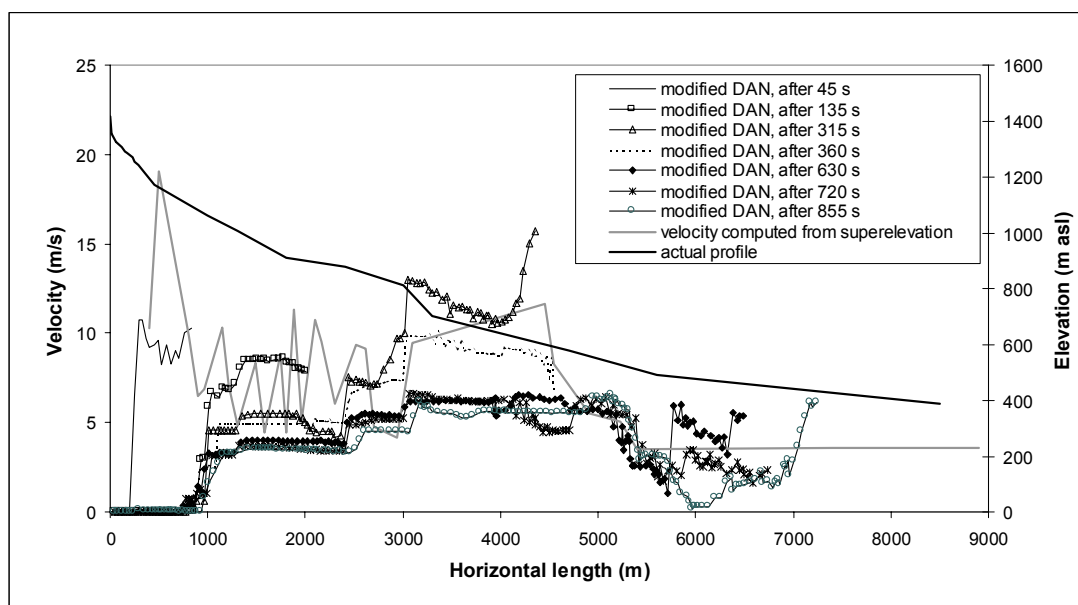


Figure 5.9: Velocity of flow for the material of the Sesa landslide as computed at different time steps

6. FINITE ELEMENT MODELLING

Finite element modeling of flow-like landslides is one of the possible approaches that can be used. As above mentioned, the models based on continuum mechanics and associated with a versatile rheological model have been preferred for the prediction of runout and relevant parameters. Nevertheless, analytical solutions inevitably consist of idealized physical models (eg. Depth averaged) and of simplifying assumptions for field behaviors. Numerical simulations are generally configured with finite difference schemes in the conventional Eulerian coordinates, whereas a Lagrangian frame of reference is more suitable for these problems.

Only CHEN & LEE (2000) seem to have used the combination of a Lagrangian frame and finite element methods for a 3D solution. Nevertheless their model makes use of a number of columns in contact to each other and with averaged properties with depth. The columns are free to deform but are fixed in volume when sliding down a slope and a constant bulk density is assumed. According to this approach, CHEN & LEE (2000) adopt a representation similar to the one introduced by HUTTER AND SAVAGE (1988) and used also in part by HUNGR (1995) in their 2D models.

A different approach has been used in our study. We have developed a 2D/3D finite element code to model movements characterized by very large displacements. The main computational characteristics include a combined Eulerian-Lagrangian calculation scheme, using triangular isoparametric finite elements (3 node triangular) and an Euler backward timestepping (for numerical stability in time).

State variables (stresses, strain, etc.) are transported in space by using a stabilizing algorithm. To help in following the large deformations maintaining a robust solution, an automatic method for optimization of the time-step size and number of iterations has been introduced on the basis of a force unbalance error. The idea was to be able to use different material laws already known, tested and verified for granular materials. The implemented material laws include classical elasto-plasticity, with a linear elastic part and different applicable yield surfaces (Mohr-Coulomb, Drucker-Prager, von Mises, etc.). Associated and non-associated flow rules are accepted to simulate granular materials.

The code allows for a large deformation material description introducing an updated Lagrangian scheme and it is incrementally objective to account for large rotations. The initial state of stress is determined by considering the material as elastic and by using a quasi static timestepping. Presently, the unstable mass is individuated by a pre-defined slip surface that is computed through a specific finite element simulation. This failure surface can be computed by lowering in time of material strength and also by imposition of dynamic disturbance.

The present code has pre- and post-processing capabilities (eg. Visualization of material flow in time, with possibility to produce a movie of the simulation, or of velocity patterns in time, etc.) and values of the state variables can be saved and plotted for any timestep.

Finally, the code is able to consider water action within the material but with a considerable increase in computational time. The same can be said about 3D modeling.

For consistency with what has been shown up to now in the document we will show the results for a 2D model realized for the Val Pola landslide. In the following figures we show the mesh for the discretization of the space domain (see figure 6.1), the landslide mass domain and the topographic and sliding surface.

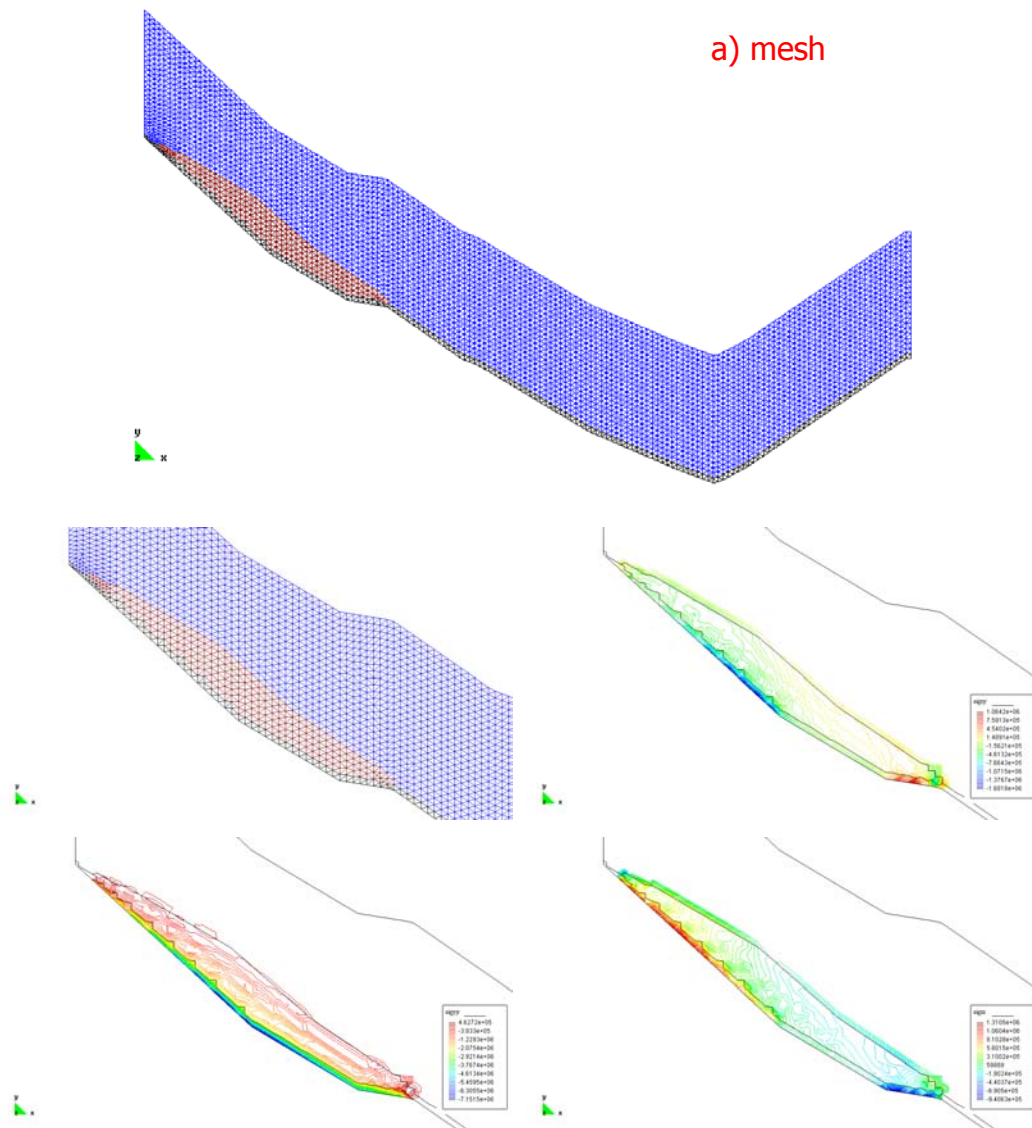


Figure 6.1: Mesh for the discretization of the val Pola landslide mass, slip surface and profile with representation of the initial stress state computed assuming elastic properties for the material

After this initial step we allowed the mass to move downslope by attributing the final properties to it and to the slip and topographic surface. The entire mass is followed during the flow and the state variables are saved and some of them are reported in the following figure (see figure 6.2a, b).

Some plots are also reported (see figure 6.3), and these results have been used for model calibration together with the actual duration of the phenomenon, the signs of debris passage and its distribution in space.

It is evident that this type of modeling is the one that seems more capable to catch flow characteristics and to simulate them with time and with changes in topographic and morphometry. The code is presently in development and its verification is also object of our researches.

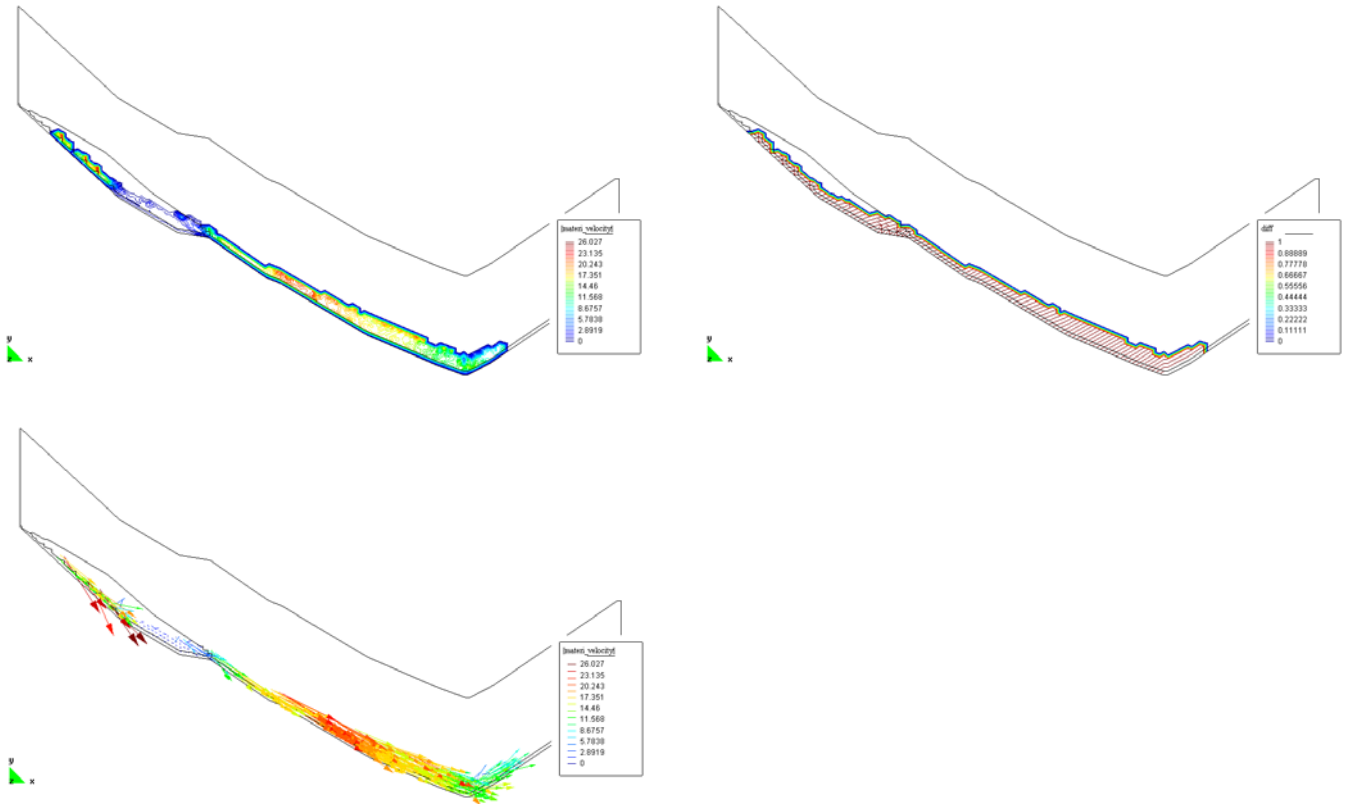
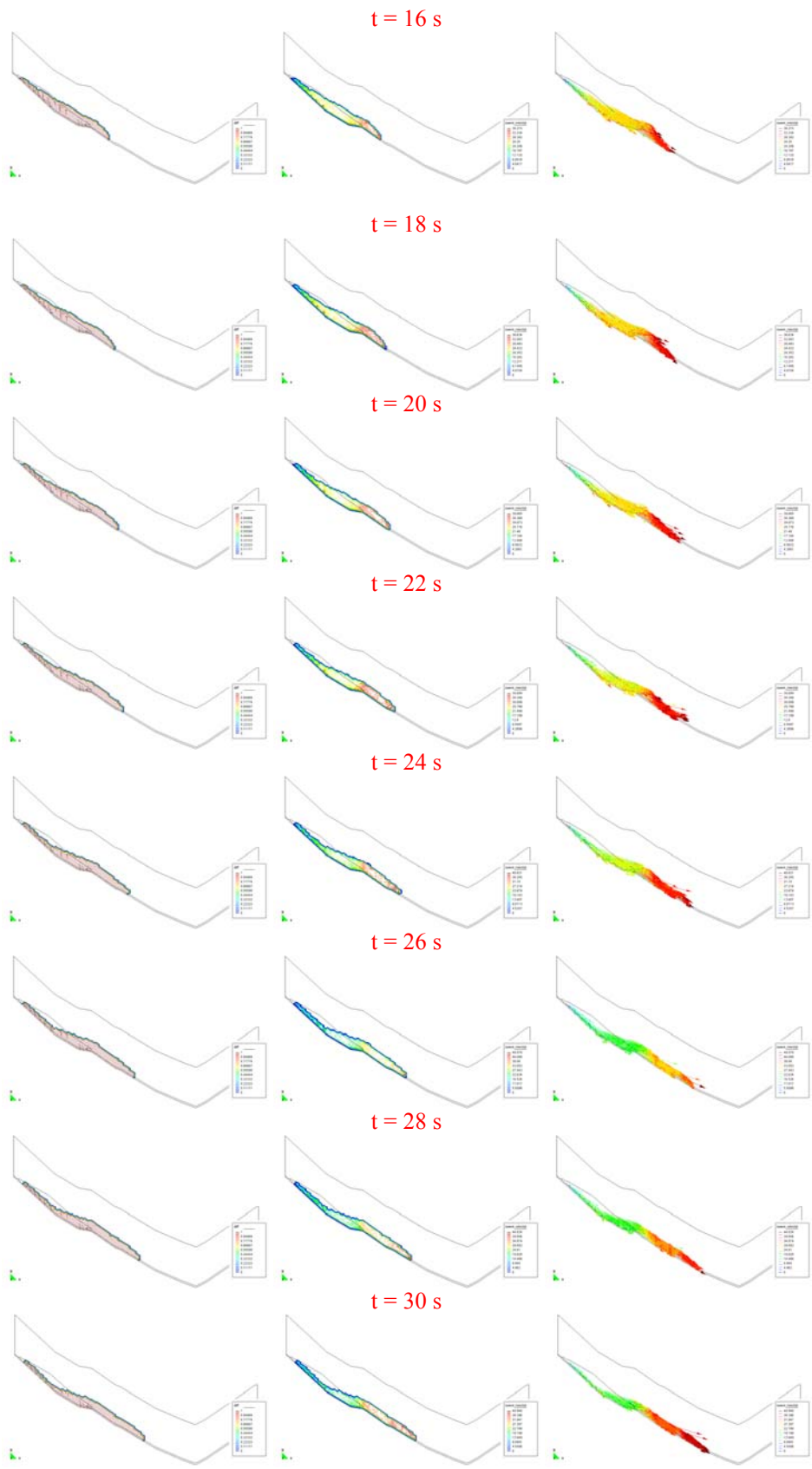


Figure 6.2a: Velocity, mass distribution and velocity vectors during flow of the Val Pola model



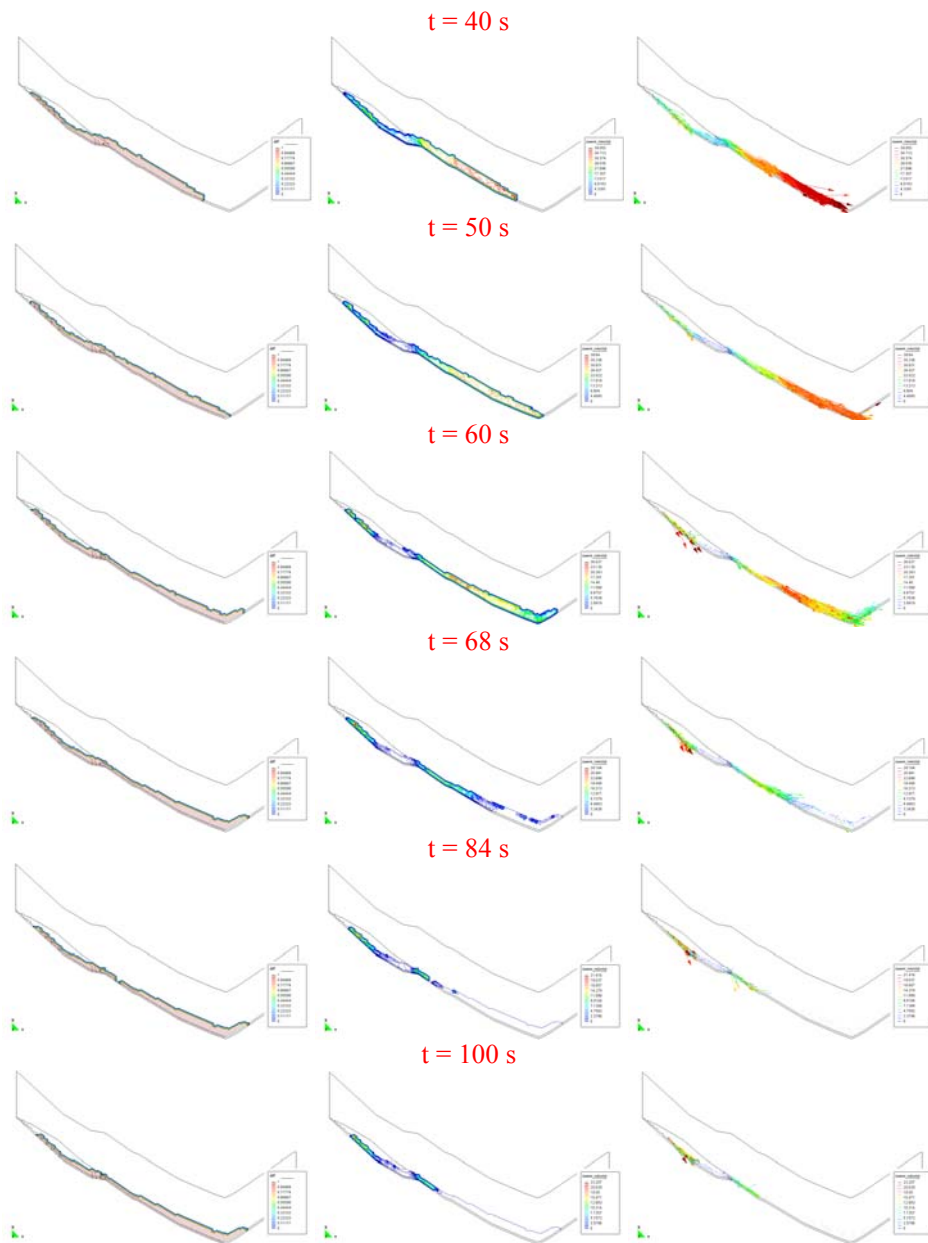


Figure 6.2b: Velocity, mass distribution and velocity vectors during flow of the Val Pola model (from 16 s to 100 s)

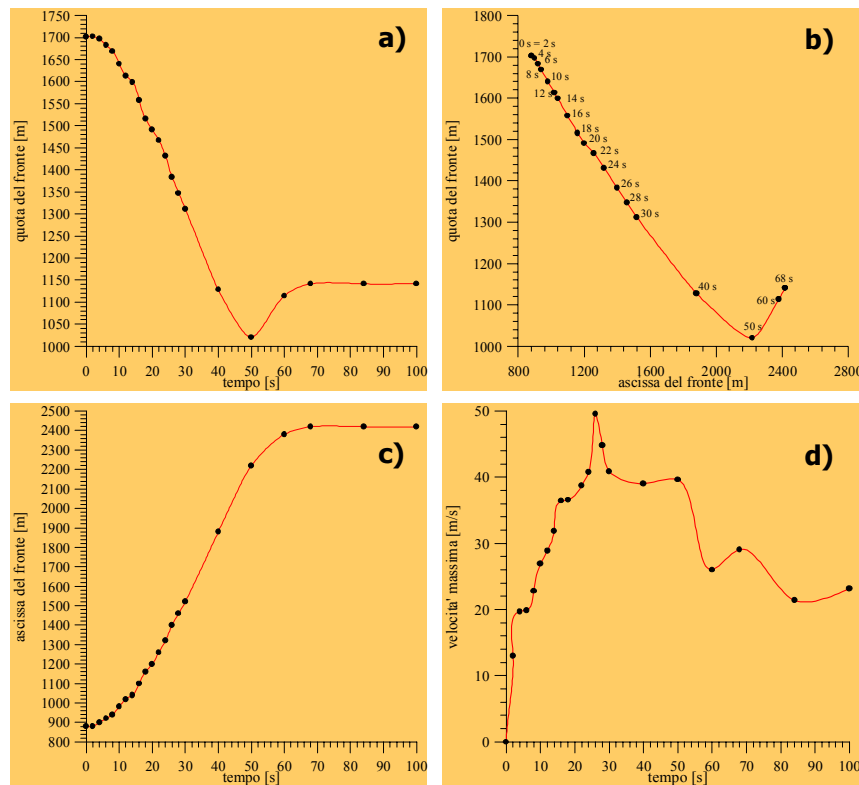


Figure 6.3: Example of output data for the Val Pola rock avalanche simulated with the finite element code. a) elevation of the rock avalanche front vs time, b) elevation of the rock avalanche front vs distance for different time instants, c) front velocity vs time d) max

7. EMPIRICAL AND SEMIEMPIRICAL RELATIONSHIPS

Hazard assessment on a fan or along the transportation path or the accumulation zone of a flow (debris flow, mudflow, lahar, rock avalanche, etc.) and the design of protective structures against them require an estimate of many important parameters. According to some researchers the assessment of debris flow hazard potential has to rely on semi-quantitative methods. RICKENMANN (1999) sustains that debris flow and granular flow processes in nature are too complex and therefore numerical simulation are still of limited use for practical applications. IVERSON et al. (1998) present, for example, a method of delineating lahar hazard zones in valleys that head on volcano flanks.

Empirical methods must be rapid, objective, and reproducible, and can be used where data, time, funding, or personnel are inadequate for application of more sophisticated methods. Delineation of hazard zones traditionally involves review of historical records as well as field identification of inundation limits of historic events. Interpolation and extrapolation of runout distance, inundation limits of past flow events provide the basis for predicting areas prone to inundation. Adopted tools for interpolation and extrapolation of available data are calibrated flow-routing models (e.g., LAENEN and HANSEN, 1988; MACEDONIO and PARESCHI, 1992; COSTA, 1997) as well as judgment. The central tenets of the empirical model proposed by different investigators are, namely: inundation by past events provides a basis for predicting inundation by future events; distal debris flow hazards are confined to valley outlets or valleys that head on volcano flanks; event volume largely controls the extent of inundation area downstream; voluminous flows occur less often than small

ones; and the size of any future event is extremely difficult to be precisely assessed and uncertainty must be considered in the analyses.

A complete empirical procedure, which makes use of multiple relationships, has to define the values expected for the maximum debris flow volume, the peak discharge, the flow velocity, the total travel and runout and/or runup distance.

Eventually, it must be stressed that the validation of an empirical and/or semi-empirical approach is usually difficult because of, namely: the variety in composition of the natural material, which limits their applicability to a narrow range of processes; the limited number of direct field observations and measurements; the difficulty in performing laboratory scaled tests

RICKENMANN (1995) proposed a two step procedure for the evaluation of debris flow hazard in a mountain catchment: the determination of the probability of occurrence of a debris flow event and the quantitative estimate of the most important parameters for hazard assessment. Information on past events are clearly fundamental as well as sediment availability and lithology.

7.1. Empirical relationships for debris flows

Debris flow volume is one of the most relevant parameters for debris flow hazard assessment. Nevertheless, relationships commonly found in the literature give quite different results when applied to the same area. These relationships are generally based on a series of different parameters such as: basin area, channel slope, geological index, etc. (HAMPEL, 1977, Takeji, 1980, KRONFELLNER-KRAUS, 1984, 1987, ZELLER, 1985, RICKENMANN & ZIMMERMAN, 1993, D'AGOSTINO, 1996) but for a better evaluation it is recommended to verify also the sediment availability or sediment potential by adopting geomorphological and engineering geological techniques.

Knowledge of the volume can help in evaluating also the *expected peak discharge* and the associated flow velocity at some interesting and more problematic points. Many investigators showed that a relationship exists between peak discharge (Q_p) and debris flow volume (or magnitude, M) (HUNGR et al., 1984, MIZUYAMA et al., 1992, TAKAHASHI et al., 1994).

RICKENMANN (1999) derived a semi-theoretical relationship by assuming that Froude scaling must be satisfied for flows of different size characterized by similar physical properties. The relationship can be written as:

$$Q_* = 0.1M_*^{5/6} = 0.1M_*^{0.833}$$

where $Q_* = Q_{p2}/Q_{p1}$ and $M_* = M_2/M_1$ with the two pedices 1 and 2 which refer to two flows of similar material properties but different size.

MIZUYAMA et al. (1992) suggested that different empirical relationships can be found for granular and for muddy debris flows. This observation is supported by other investigators. These investigators presented a series of empirical formulae among which we present the following ones.

Data sets	Formulas	Number of events	References
Granular debris flow - Japan	$Q_p = 0.135 M^{0.78}$	≈ 50	MIZUYAMA et al., 1992
Muddy debris flow - Japan	$Q_p = 0.0188 M^{0.79}$	≈ 100	MIZUYAMA et al., 1992
Merapi volcano - Indonesia	$Q_p = 0.00558 M^{0.831}$	≈ 200	JITOUSONO et al., 1996
Sakurajima volcano - Japan	$Q_p = 0.00135 M^{0.87}$	≈ 100	JITOUSONO et al., 1996
Landslide dam failure	$Q_p = 0.293 M_w^{0.56}$	9	COSTA, 1988
Glacial dam failure	$Q_p = 0.0163 M_w^{0.64}$	20	COSTA, 1988

Equations by RICKENMANN (1999) and by MIZUYAMA (1992) for granular debris flows give the maximum peak discharge values greater than those deriving from equations for finer volcanic debris flows. Rickenmann also suggests that the peak discharge of a debris flow surge should be related to the debris – water volume of the corresponding surge and not to the total debris flow volume.

Flow behaviour of debris flow has been described through a long series of approaches. Most of field observations concern the mean translational *velocity of the debris flow front* or the *maximum velocity*. It has also been observed that maximum flow velocity does not necessarily coincide with the part of the flow where maximum flow depth is recorded. This non-coincidence is usually neglected in semi-quantitative analyses.

Among the different approaches, proposed for the computation of the maximum mean cross sectional velocity of the frontal part of debris flows, we present some relationships that can generally expressed in the general form $V = C_x H^\alpha S^\beta$. C_x is here considered as an empirical constant that depends on the values of α and β .

Flow Type	Formulas	Notes	References
Newtonian laminar flow	$V = (1/3)\rho g H^2 S / \mu$	1/3: rectangular channel	
Dilatant grain shearing	$V = (2/3)\xi H^{1.5} S$	Bagnold type eq. For dilatant grain shearing, 2/3 for wide rectangular channel	
Newtonian turbulent flow	$V = (1/n)H^{2/3}S^{1/2}$	Manning Strickler equation	PWRI, 1988
Newtonian turbulent flow	$V = CH^{1/2}S^{1/2}$	Chezy equation	RICKENMANN, 1990
Empirical equation	$V = C_1 H^{0.3} S^{0.5}$	Unsteady debris flow surges	KOCH, 1998

In this table, V (m/s) is the cross-sectional mean flow velocity, H (m) is the maximum flow depth, S is the channel bed slope, ρ (kg/m^3) is the grain water mixture density, ξ ($1/(\text{sm}^{1/2})$) is a lumped coefficient depending on grain size and grain concentration, n ($\text{s/m}^{1/3}$) is the Manning coefficient ($\approx 0.1 \text{ s/m}^{1/3}$ for debris flows according to PIERSON, 1986, PWRI, 1988, RICKENMANN & ZIMMERMANN, 1993, with n greater for granular debris flows than for lahars), C ($\text{m}^{1/2}/\text{s}$) is the Chezy coefficient, and C_1 ($\text{m}^{0.7}/\text{s}$) is a dimensional empirical coefficient. The flow resistance coefficients or material parameters (eg.: μ , ξ , n , C , C_1) can be back-calculated as a function of peak discharge from available data and Rickenmann proposed a series of semi-theoretical relationships for their calculation:

Flow type	Formulas
Newtonian laminar flow	$\mu_* = 20 Q_*^{3/5}$
Dilatant grain shearing	$\xi_* = 150 Q_*^{-2/5}$
Newtonian turbulent flow: Manning Strickler	$n_* = 0.077 Q_*^{1/15}$
Newtonian turbulent flow: Chezy equation	$C_* = 22$
Empirical equation	$C_{1*} = 10 Q_*^{2/25}$

COSTA (1984) reports some other equations as proposed by investigators from Russia, China and Japan and each one obtained from an independent set of data. These equations are all in the $V = C_x H^\alpha S^\beta$ form with exponents ranging between: $0.5 < \alpha < 0.67$ and $0.25 < \beta < 0.5$.

Another type of relationship is the one relating the mean flow velocity with the discharge and the slope. For the debris flows has been proposed:

$$V = 2.1 Q^{0.33} S^{0.33}$$

The total travel distance or maximum runout or reach distance, L , can be fundamental in identifying potentially endangered areas. It has been shown by many authors that rockfalls and rock avalanches evidence a dependence of the H/L ratio on the mobilized volume (M). The H/L ratio is the ratio between the total fall height and the total runout distance. The same type of

relationship has been demonstrated as valid for debris flows. RICKENMANN (1999) presents the relationship that satisfy the geometric or Froude scaling approach:

$$L_* = 30 (M H)_*^{1/4}$$

where $M H$ represents an expression for the available potential energy. Rockfalls and rock avalanches usually show higher values for the H/L ratio and consequently a shorter maximum runout.

One more interesting parameter in debris flow hazard assessment is represented by the runout distance on the alluvial fan, L_f . This distance is described as the one between the fan apex and the lowest point of the debris flow accumulation. Always according to RICKENMANN (1999) and to his Froude or geometric scaling approach it can be shown that:

$$L_{f*} = 15 M_*^{1/3}$$

From in situ measurements of debris flows on scree slopes in the Upper Valtellina area (northern Italy, Central Alps, Lombardy, eg. Figure 7.1) a different relationship has been computed (CROSTA et al.).



Figure 7.1: Debris flows in Upper Valtellina

In fact all the measured debris flows plot below the relationship proposed by Rickenmann and are fitted by: $L \text{ (m)} = 7 M^{0.275}$ with volume in m^3 (figure 7.2).

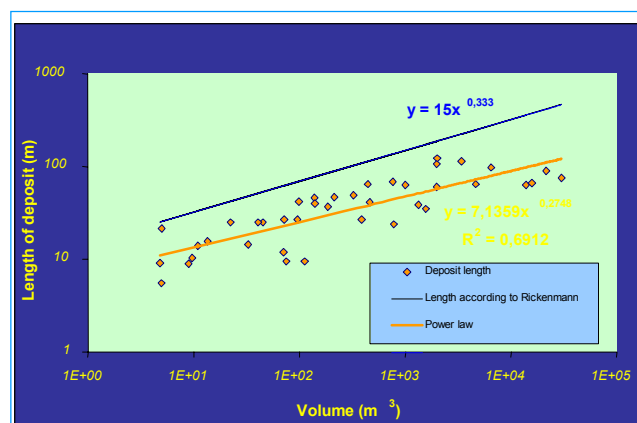


Figure 7.2: Plot of the length of debris flow deposits versus volume. Data collected by the authors in Upper Valtellina are fitted and compared with Rickenmann equation

The rationale for the method proposed by IVERSON et al. (1998) derives from scaling analyses of generic lahar paths and statistical analyses of 27 lahar paths documented at 9 volcanoes. Together these analyses yield semi-empirical equations that predict inundated valley cross-sectional areas

(A) and planimetric areas (B) as functions of flow volume (V). The predictive equations ($A = 0.05V^{2/3}$ and $B = 200V^{2/3}$) provide information necessary to calculate and plot inundation limits on topographic maps. A range of inundation limits can be plotted for debris flow events of increasing volume and decreasing probability

The method proposed by IVERSON et al. (1998) predicts inundation areas in distal valleys that head on volcano flanks, but distal lahars originate at proximal sources, and identification of source areas poses a preliminary problem. They assume that the source areas for sudden-onset lahars lie within a proximal hazard zone defined by the intersection of an "energy cone" with the volcano's topographic surface (MALIN & SHERIDAN, 1982). This energy cone has its apex at the volcano summit, and the cone slope is determined by the characteristic ratio of vertical descent (H) to horizontal runout (L) of events such as pyroclastic flows or rock avalanches that may spawn lahars (figures 7.3, 7.4). The boundaries of proximal hazard zones are included in the H/L range between 0.1 to 0.3, depending on the size and type of the proximal event. The authors assume that where the proximal hazard boundaries transect the valleys, these define the upstream boundaries of distal hazard zones. Iverson et al. suggest that in distal valleys lahar volume generally influences the size more than the shape of deposition areas. If the shape of all lahar paths were identical

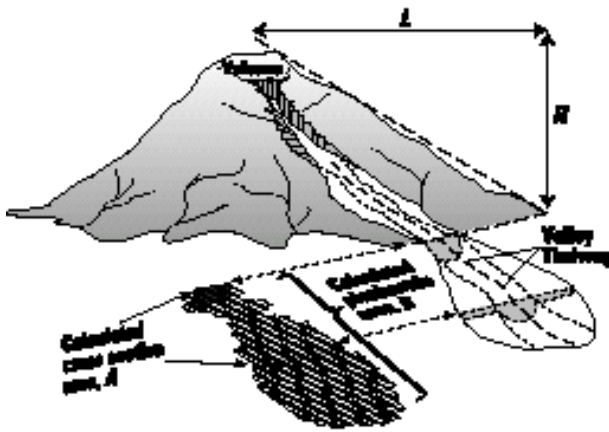


Figure 7.3: Lahar path and geometric relationships between h and L . This describes the extent of the proximal hazard zone. A and B , describe the extent of the distal lahar-inundation hazard zone. (IVERSON et al., 1998)

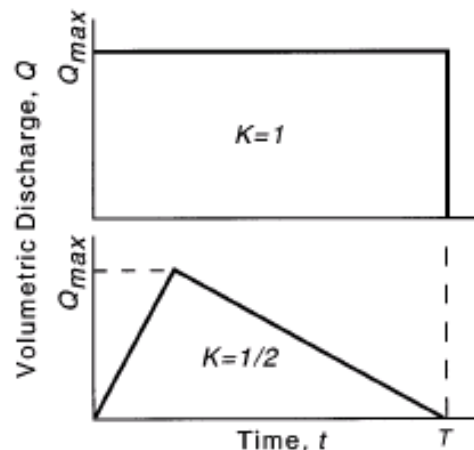


Figure 7.4: Idealized lahar hydrographs, with different shape parameters, K , defining lahar duration, T , and maximum instantaneous volumetric discharge Q_{max} , for hydrographs (IVERSON et al., 1998)

according to a fractal scaling law, geometric similarity would establish the validity of the relationships $A \propto V^{2/3}$ and $B \propto V^{2/3}$. However, because the shape of flow paths varies, it is useful to consider how the same relationships result from scaling analyses of lahar kinematics and geometries.

To assess the cross-sectional area of valley inundation, it is considered a lahar that moves downstream as an evolving, translating waveform of constant mass and constant bulk density. In such a case conservation of mass implies conservation of volume, expressed by

$$V = \int_T Q(t) dt = K Q_{max} T$$

where, V is the lahar volume, $Q(t)$ is the volumetric discharge at a valley cross section through which the flow passes, Q_{max} is the maximum instantaneous or peak volumetric discharge at the same cross section, t is time, and T is the total time required for the lahar to pass the cross section.

The shape of the lahar hydrograph determines the dimensionless parameter K ($0 < K < 1$), with values of $K \approx 1/2$ usually appropriate for debris flow hydrographs (with a rough triangular shape) It is also assumed that the maximum discharge produces the maximum inundation of valley cross-

sectional area. This value is of primary interest for delineating hazard zones. Q_{\max} and A_{\max} are related by $Q_{\max} = A_{\max}U$, where U is the velocity averaged over the valley cross section. In the scaling analysis it is important to know that U scales with the characteristic velocity \sqrt{gR} , in which g is the magnitude of gravitational acceleration and R is the hydraulic radius ($R = A/P$, where A is the valley cross-sectional area inundated and P is the valley wetted perimeter, figure 7.5).

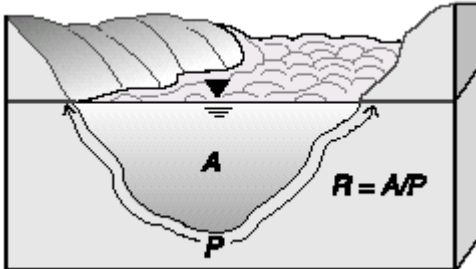


Figure 7.5: Sketch showing the definition of hydraulic radius $R = A/P$, where A is the valley cross-sectional area inundated and P is the valley wetted perimeter

The scaling $U \approx \sqrt{gR}$ is fundamental for both unsteady and steady flows of liquids in open channels (e.g., HENDERSON, 1966). IVERSON et al. show that \sqrt{gR} is the approximate translation speed of ideal monoclinal waves in such flows, and $U^* = U/\sqrt{gR}$ is a dimensionless velocity known as Froude number. This number describes the ratio of inertial and gravitational forces in such flows. In distal regions, where valley thalwegs slope less than 10° , the scaling $U \approx \sqrt{gR}$ appears appropriate whereas Savage and Bagnold numbers can be used in different areas.

By combining $Q_{\max} = A_{\max}U$ with $U \approx \sqrt{gR}$ is possible to obtain the peak discharge scaling $Q_{\max} \approx A_{\max}\sqrt{gR}$ that helps in defining the dimensionless peak discharge as

$Q_{\max}^* = \frac{Q_{\max}}{A_{\max}\sqrt{gR}}$ in which the characteristic length scale $\sqrt{A_{\max}}$ emerges as the counterpart to the characteristic velocity scale, \sqrt{gR} .

In turn, the characteristic time scale results from the quotient of the characteristic length and velocity scales. With this time scale we define the dimensionless lahar duration at a cross section as

$$T_{\max}^* = \frac{T}{\sqrt{A_{\max}} / \sqrt{gR}}$$

With a couple of more steps it yields:

$$A = CV^{2/3}$$

in which A is written as shorthand for A_{\max} . If we assume that C is constant, which is equivalent to assuming that flow hydrographs have constant shapes, then $A \propto V^{2/3}$.

Iverson et al. identify the distal extent of lahar deposits as the downstream limit of discernable overbank debris-flow deposition. A simple assumption is made to simplify the analysis, namely, the lahar volume leaving the proximal hazard area (V) matches the volume deposited downstream. This is a simplistic assumption, because a lahar may gain or lose sediment and/or water and thereby alter its volume gradually as it moves downstream.

As a consequence, $V = hB$ in which B denotes the total planimetric area of this path, and h denotes the lahar deposit thickness measured normal to the surface (figure 7.6). This last relationship can be simplified if $h \propto B^{1/2}$ applies for lahar paths of diverse shapes and sizes. If all lahar paths were geometrically similar (i.e., had identical shapes and differed only in size), $h \propto B^{1/2}$ would apply exactly. However, even if lahar paths differ significantly in planimetric shape, $h \propto B^{1/2}$ applies approximately if h/\sqrt{B} is approximately constant. Typically, $h/\sqrt{B} \ll 1$ because lahar paths and deposits are dominantly tabular. Adopting the notation $\varepsilon = h/\sqrt{B}$ and postulating that ε is a small

constant, Iverson et al. use $h = \varepsilon/\sqrt{B}$ and obtain $V = \varepsilon B^{3/2}$, or as $B = cV^{2/3}$ in which $c = \varepsilon^{-2/3}$ is a hypothetical constant, $c \gg 1$.

This equation expresses the desired relation between lahar volume and the planimetric area of inundation, but the validity of the equation and the constancy of c must be tested with data.



Figure 7.6: Idealized lahar-path geometries with $H = h/\sqrt{B}$ constant.

Testing of the equations involves statistical determination of whether the inundation areas A and B are proportional to $V^{2/3}$. Calibration of the equations proposed by IVERSON et al. (1998) involves statistical determination of the best-fit values of the proportionality coefficients c and C . The power-law equations: $A = CV^{2/3}$ and $B = cV^{2/3}$ suggest that it is possible to linearize the equations by logarithmic transformation prior to statistical testing and calibration.

Log transformation is appropriate because we expect the deviation of data values from a hypothetical trend to scale with the size of the data value, that is the magnitude of the standard error of predictive equations will increase by a factor of 10 as lahar volume increases by a factor of 10. Log transformation yields:

$$\begin{aligned} \log A &= \log C + 2/3 \log V \\ \log B &= \log c + 2/3 \log V \end{aligned}$$

where $2/3$ is the slope and $\log C$ is the A intercept (value of $\log A$ for $\log V = 0$) on a log-log plot (see figures 7.7, 7.8) of A as a function of V , $\log c$ is the intercept on a log-log plot of B versus V .

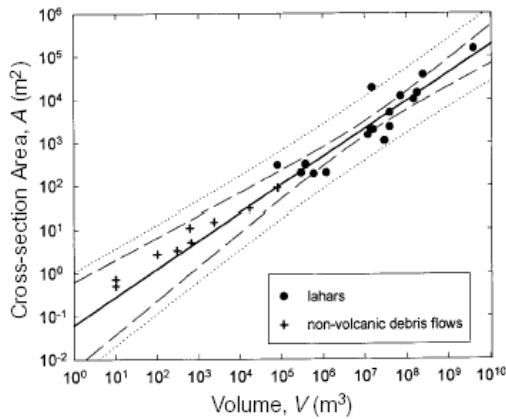


Figure 7.7: Scatter plot of inundated valley cross-section area A as a function of lahar volume V . The best-fit log-log regression line and 95% confidence intervals for regression (dashed lines) and prediction (dotted lines) are shown (IVERSON et al., 1998)

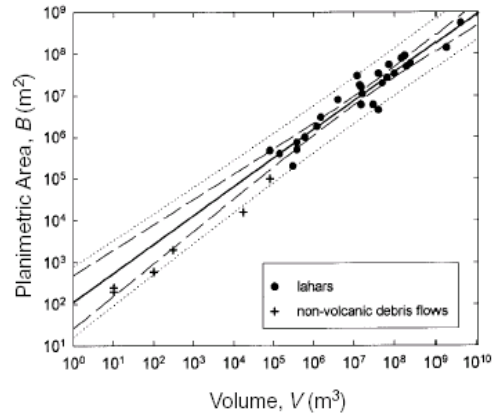


Figure 7.8: Scatter plot of inundated planimetric area B as a function of lahar volume V . The best-fit log-log regression line and 95% confidence intervals for regression (dashed lines) and prediction (dotted lines) are shown (IVERSON et al., 1998).

The lahar volumes adopted for the analyses by IVERSON et al. (1998) involve some uncertainty because flows can vary in volume as they move downstream, and downstream changes in volume are not necessarily monotonic (e.g., PIERSON, 1985, 1995; SCOTT et al., 1995).

The lahar volumes listed by IVERSON et al. provide estimates of the value most representative of the volume of any particular lahar as it enters the distal inundation area. It must be remembered that the use of log transformed data allows to minimize the effect of errors and inaccuracies and that maximum reported volumes are $V < 4 \times 10^7 \text{ m}^3$. Furthermore, Iverson et al. emphasize the difficulties encountered in collecting data for small lahars and debris flows even if these are the most frequent class of events. To overcome this problem they included data for nine nonvolcanic debris flows with $V < 8 \times 10^4 \text{ m}^3$.

These problems are quite common in any event magnitude estimate, for example for debris flow events in alpine and prealpine areas, and increase in relevance with the age of the reported events.

The predictive models for the cross-sectional and planimetric areas of inundation by lahars are:

$$A = 0.05V^{2/3}$$

$$B = 200V^{2/3}$$

BASIC DATA RANKED IN ORDER OF FLOW VOLUME as adopted by Iverson et al. (1998)

Name of event	Location and date	Data source	Flow	Inundated	Inundated
			volume, V (m^3)	cross section Area, A (m^2)	planimetric area, B (m^2)
Osceola	Mount Rainier, United States., 5000 B.P.	Vallance and Scott, 1997	4.0×10^9	1.5×10^5	5.5×10^5
Teteltzingo	Citlaltepeli, Mexico, 18000 B.P.	Carrasco-Núñez et al., 1994	1.8×10^9	N.D.	1.4×10^5
Electron	Mount Rainier, United States, 530–550 B.P	Crandell, 1971	2.5×10^8	3.7×10^4	6×10^7
Round Pass	Mount Rainier, United States, 2700 B.P	Crandell, 1971	2×10^8	N.D.	5×10^7
Dead Man Flat	Mount Rainier, United States, 1100 B.P.	K. Scott et al., 1995; J.W. Vallance, unpublished data	1.8×10^8	1.4×10^4	9.0×10^7
National	Mount Rainier, United States, 500–1800 B.P.	K. Scott et al., 1995; J.W. Vallance, unpublished data	1.5×10^8	1.0×10^4	7.8×10^7
Paradise	Mount Rainier, United States, 4500–5000 B.P.	Crandell, 1971	1×10^8	N.D.	3.4×10^7
Zigzag	Mount Hood, United States, 1700 B.P	J. W. Vallance, unpublished data	7.3×10^7	1.2×10^4	5.5×10^7
Trout Lake	Mount Adams, United States, 6000 B.P.	Vallance, 1998	6.6×10^7	N.D.	2.7×10^7
Middle Fork Nooksack	Mount Baker, United States, 6000 B.P.	Hyde and Crandell, 1978	5×10^7	N.D.	2×10^7
Kautz Creek	Mount Rainier, United States, 1947	Crandell, 1971; Scott and Vallance, 1995	4×10^7	5000	4.5×10^5
Azufrado	Nevado del Ruiz, Columbia, 1985	Fritz et al., 1986; Pierson et al., 1990	4×10^7	2300	3.4×10^7
Molinos Nereidas (Chinchina)	Nevado del Ruiz, Columbia, 1985	Fritz et al., 1986; Pierson et al., 1990	3×10^7	1100	6.0×10^5
Guali	Nevado del Ruiz, Columbia, 1985	Fritz et al., 1986; Pierson et al., 1990	1.6×10^7	2000	1.1×10^7
Salt Creek	Mount Adams, United States, 200 B.P.	Vallance, 1998	1.5×10^7	N.D.	1.6×10^7
Tahoma	Mount Rainier, United States, 400–500 B.P.	Scott et al., 1995	1.5×10^7	1.9×10^4	6.0×10^5
Pine Creek + Muddy River	Mount St. Helens, United States, 1980	Pierson, 1985	1.4×10^7	2100	1.8×10^7
South Fork Toutle	Mount St. Helens, United States, 1980	Janda et al., 1981; Fairchild and Wigmosta, 1983	1.2×10^7	1500	3×10^7
Whitney Creek	Mount Shasta, United States, 1935	Osterkamp et al., 1986	4×10^5	N.D.	8×10^5
Bolun Creek	Mount Shasta, United States, 1897	Osterkamp et al., 1986	1.5×10^5	N.D.	3×10^5
Mabinit Eruption Lahars	Mayon, Philippines, 1984	Rodolfo, 1989	1.2×10^5	200	1.8×10^5
Tahoma Creek	Mount Rainier, United States, 1988	Walder and Driedger, 1994; J.S. Walder, unpublished data	6×10^5	190	1×10^5
Blue Lake	Mount St. Helens, United States, 1980	Major, 1984; Major and Voight, 1986	3.8×10^5	320	7.5×10^5
Butte Canyon	Mount St. Helens, United States, 1980	Major, 1984; Major and Voight, 1986	3.8×10^5	300	5.0×10^5
Mabinit Typhoon Saling	Mayon, Philippines, 1985	Rodolfo, 1989; Rodolfo et al., 1989	3×10^5	200	2×10^5
Middle	Mount St. Helens, United States, 1980	Major, 1984; Major and Voight, 1986	1.4×10^5	N.D.	4.0×10^5
Polallie Creek	Mount Hood, United States, 1980	Gallino and Pierson, 1984; T. C. Pierson, unpublished data	8×10^4	300	4.7×10^5
West Dodson	Columbia Gorge, Oregon, United States, 1996	R. M. Iverson, unpublished data	8×10^4	90	1×10^5
Mayflower Gulch	Tenmile Range, Colorado, United States, 1961	Curry, 1966	1.7×10^4	30	1.6×10^4
Oddstad	Pacifica, California, United States, 1982	Howard et al., 1988	2300	15	N.D.
Big Bend	Pacifica, California, United States, 1982	Howard et al., 1988	660	5	N.D.
Yosemite	Pacifica, California, United States, 1982	Howard et al., 1988	610	11	N.D.
B1	Nigel Pass, Canada, recent	Owens, 1972	300	3.3	2000
N32	Nigel Pass, Canada, recent	Owens, 1972	100	2.7	600
N2	Nigel Pass, Canada, recent	Owens, 1972	10	0.7	200
USGS flume experiments	30 experiments, 1993–1996	Major, 1996; Iverson, 1997	10	0.4 – 0.6	200–300

Data for small, nonvolcanic debris flows provide another opportunity for comparing the inundation patterns of lahars with those of related phenomena. Debris flows exhibit a variety of compositions and behaviours intermediate between those of wet rock avalanches and sediment-laden water floods (IVERSON, 1997), but small debris flows commonly contain greater concentrations of large clasts than do large lahars (CRANDELL, 1971; TAKAHASHI, 1991).

The data for nonvolcanic debris flows used by Iverson et al. (1998) depart from the trend for lahars. This departure indicates that small, nonvolcanic debris flows inundate larger channel cross-sections, but are characterized by smaller planimetric areas. Non volcanic debris flows behave generally in a less fluid way leaving proportionately thicker deposits than do most lahars. This difference in inundation patterns could be the result of a scale effect (IVERSON et al., 1998), or of a minor mobility. A possible reason could lay in their high concentration of large clasts, which cause higher frictional resistance.

IVERSON et al. (1998) put in evidence how, on average, lahars of any volume inundate planimetric areas roughly 20 times larger than those inundated by rock avalanches of similar volume.

From in situ measurements of debris flows on scree slopes and in small channels in the Upper Valtellina area a different relationship has been computed (CROSTA et al.). These data show a strong difference with respect to those used by IVERSON et al. (1998) and suggest that, as pointed out by different authors, granular flows are less mobile than lahars. In fact all the measured debris flows plot below (see figure 7.9) the relationship proposed by Iverson et al. and are fitted by: $B (m) = 7 M^{0.66}$ with volume, M , in m^3 and by: $A (m^2) = 6.5 M^{0.69}$. On the contrary, a better correspondence has been found between data by IVERSON et al (1998) and those computed after the Sarno 1998 event.

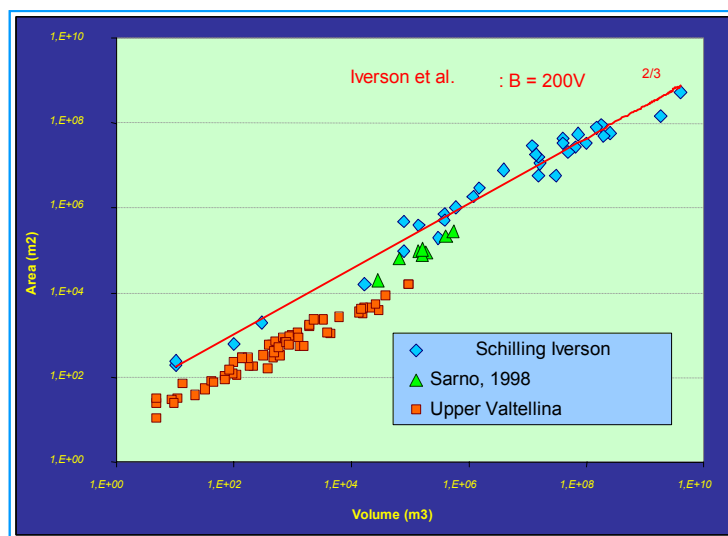


Figure 7.9: Area vs volume plot for data collected by the authors in Upper Valtellina and at Sarno, compared with those collected and published by IVERSON et al., 1998

IVERSON et al. (1998) implemented their method as a simple distributed approach by using GIS (LAHARZ). The model allows the definition of areas of maximum hazard by computing cross sections for each step along the flow path. An example of the results is shown in the following two figures (figure 7.10).

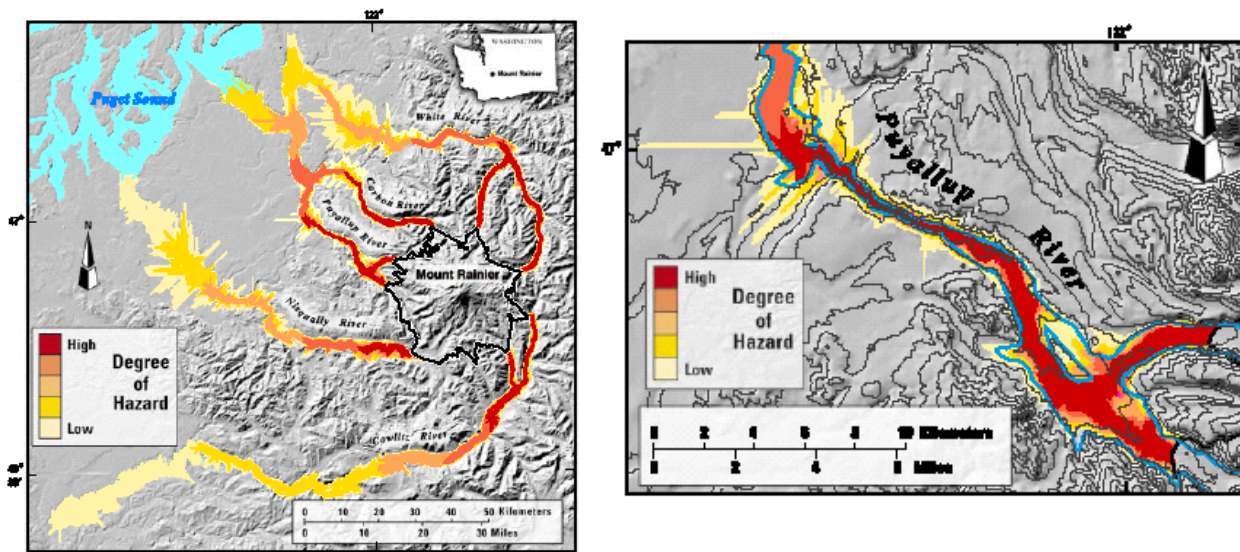


Figure 7.10: Lahar-inundation hazard map constructed by IVERSON et al. (1998) applying LAHARZ to the Mount Rainier area (western Washington). The proximal hazard zone is enclosed by the dark line surrounding Mount Rainier.

8. REFERENCES

- Adams, M. J. and Briscoe B. J. (1994) - Deterministic micromechanical modeling of failure or flow in discrete planes of densely packed particle assemblies: Introductory principles. In A. Mehta (ed). *Granular Matter*, pp. 259-291, Springer-Verlag, New York.
- Amarù, M. and Crosta, G. (1996) - La modellazione numerica per la previsione delle distanze di massimo espandimento di frane a rapida evoluzione. *Proc. V° Conv. Naz. Giov. Ricerc. Geol. Appl.*, 8-11 ottobre 1996. (in italian)
- Arguden, A. T. and Rodolfo, K. S. (1990) - Sedimentologic and dynamic differences between hot and cold laharcic debris flows of Mayon volcano, Philippines. *Geol. Soc. Am. Bull.*, 102:865-876.
- Atkin, R. J. and Craine, R. E. (1976) - Continuum theories of mixtures: Basic theory and historical development. *Q. J. Mech. Appl. Math.*, 29(2):209-244.
- Ayotte, D. and Hungr, O. (2000) - Calibration of a runout prediction model for debris flows and avalanches. In G.F. Wieczorek and N.D. Naeser (eds): *Proc. 2nd. International Conference on Debris Flows*, Taipei, 505-514, Balkema, Rotterdam.
- Ayotte, D., Evans, N. and Hungr, O. (1999) - Runout analysis of debris flows and avalanches in Hong Kong. *Proc. Slope Stability and Landslides, Vancouver Geotechnical Society Symposium*, May 1999, 39-46.
- Bagnold, R. A. (1954) - Experiments on a gravity-free dispersion of large solid spheres in a newtonian fluid under shear. *Proc. Royal Soc. of London, ser. A*, 225:49-63.
- Bagnold, R. A. (1956) - The flow of cohesionless grains in fluids. *Royal Society of London Philosophical Transactions, ser. A*, 249:235-297.
- Bambozzi, C. (1999) - Simulazione numerica della caduta massi. Tesi di Laurea. DIS Politecnico di Milano. (in italian)
- Battaglia, M. (1993) - On pyroclastic flow emplacement: *Journal of Geophysical Research*, 98(B12):22269-22272.
- Bear, J. (1972) - *Dynamics of Fluids in Porous Media*. Dover, Mineola, N.Y., 764 pp.
- Beatty, C. B. (1974) - Debris flows, alluvial fans, and a revitalized catastrophism. *Z. Geomorph, supplement*, 21:39-51.
- Best, J. L. (1992) - Sedimentology and event timing of a catastrophic volcanoclastic mass flow, volcan Hudson, southern Chile. *Bull. Volcanol.*, 54:299-318.
- Beverage, J. P. and Culbertson, J. K. (1964) - Hyperconcentrations of suspended sediment. *J. Hydraul. Division, Proc. Am. Soc. Civil Engin.*, 90:117-128.
- Bird, R. B., Stewart, W. E. and Lightfoot, E. N. (1960) - *Transport Phenomena*, John Wiley, New York, 780 pp.
- Bird, R. B., Dai, G. C. and Yaruso, B. J. (1982) - The rheology and flow of viscoplastic materials. *Rev. Chem. Eng.*, 1:1-70.
- Blackwelder, E. (1928) - Mudflow as a geologic agent in semiarid mountains. *Geological Society of America Bulletin*, 39:465-480.
- Blair, T. C. and McPherson, J. G. (1994) - Alluvial fan processes and forms. In A. D. Abrahams and A. J. Parsons (eds.): *Geomorphology of desert environments*. Chapman and Hall, London, 354-402.
- Brantley, S.R. and Waitt, R.B. (1988) - Interrelations among pyroclastic surge, pyroclastic flow, and lahars in Smith Creek valley during first minutes of 18 may 1980 eruption of Mount St. Helens, USA. *Bull. Volcanol.*, 50:304-326.
- Bromhead, E. N. (1986) - *The stability of slopes*. Chapman and Hall, New York, 374 pp.
- Broscoe, A. J. and Thomson, S. (1969) - Observations on an alpine mudflow, Steele Creek, Yukon. *Canadian Journal of Earth Sciences*, 6:219-229.
- Brown, R. L. and Richards J. C. (1970) - *Principles of Powder Mechanics*, 221 pp., Pergamon, Tarrytown, N. Y., 221 pp.
- Calhoun, D. and LeVeque, R. J. (2000). A Cartesian grid finite volume method for the advection-diffusion equation in irregular geometries, *J. Comput. Phys.*, 157:143-180.

- Campbell, C.S. (1989) - Self-lubrication for long runout landslides. *Jour. Geol.*, 97(6):653-665.
- Carslaw, H. S. and Jaeger J. C. (1959) - *Conduction of Heat in Solids* (2nd ed.). Oxford Univ. Press, New York, 510 pp.
- Caruso, P. and Pareschi, M. T. (1993) - Estimation of lahar-runout flow hydrograph on natural beds. *Environmental Geology*, 22:141-152.
- Casagrande, A. (1936) - Characteristics of cohesionless soils affecting the stability of slopes and earth fills. *Boston Society of Civil Engineers Journal*, 23:13-32.
- Chen, C. L. (1988) - Generalized viscoplastic modeling of debris flows. *Journal of Hydraulic Engineering*, 114:237-258.
- Costa, J. E. (1984) - Physical geomorphology of debris flows. In J.E. Costa and P.J. Fleisher (eds): *Developments and Applications of Geomorphology*. Springer, Berlin and N.Y., 268-317.
- Costa, J. E. (1991) - Nature, mechanics and mitigation of the Val Pola Landslide, Valtellina, Italy. *Z. Geomorph, N.F.*, 35(1):15-38.
- Costa, J. E. and Jarrett, R. D. (1981) - Debris flows in small mountain stream channels of Colorado and their hydrologic implications. *Bulletin of the Association of Engineering Geologists*, 18:309-322.
- Costa, J. E. and Williams, G. P. (1984) - Debris-flow dynamics (videotape): U.S. Geological Survey Open-File Report 84-606, 22 min.
- Coulomb, C. A. (1776) - Sur une application des regles de maximis & minimis à quelques problèmes de statique, relatifs à l'architecture, in *Memoires de Mathematique et de Physique*, Presented at the Royal Academy of Sciences, 1773, pp. 343-384, Imp. R. Acad. Sci., Paris.
- Cousot, P. and Meunier, M. (1996) - Recognition, classification and mechanical description of debris flows, *Earth-Sci. Rev.*, 40:209-227.
- Cousot, P. and Piau, J.M. (1993) - L'écoulement des boues. *La Recherche*, 24:1084-1090. (in french)
- Cousot, P. and Proust, S. (1996) - Slow unconfined spreading of a mudflow. *J. Geophys. Res.*, 101(B1):25217-25229.
- Crandell, D. R. (1971) - Postglacial lahars from Mount Rainier volcano, Washington. *U. S. Geol. Surv. Prof. Pap.*, n. 677, 74 pp.
- Crandell D. R. (1987) - Deposits of pre-1980 pyroclastic flows and lahars from Mount St. Helens volcano, Washington. *U. S. Geol. Surv. Prof. Pap.*, n. 1444, 91 pp.
- Cronin S. J., Neall V. E., Lecointre J. A. and Palmer A. S. (1997) - Changes in Whangaehu river lahar characteristics during the 1995 eruption sequence, Ruapehu volcano, New Zealand. *J. Volcanol. Geotherm. Res.*, 76:47-61.
- Cronin S. J., Neall V. E., Lecointre J. A. and Palmer A. S. (1999) - Dynamic interactions between lahars and stream flow: A case study from Ruapehu volcano, New Zealand. *Geol. Soc. Am. Bull.*, 111(1):28-38.
- Cronin S. J., Lecointre J. A., Palmer A. S. and Neall V. E. (2000) - Transformation, internal stratification, and depositional processes within a channelised, multi-peaked lahar flow. *New Zeal. Journ. Geol. Geophys.*, 43:117-128.
- Crosta G. (1991) - Studio di movimenti in massa. Modellazione teorica e sperimentale con osservazioni di campagna. Tesi di dottorato, Univ. Studi di Milano, Dip. Scienze della Terra.
- Cruden, D. M. and Hungr, O. (1986) - The debris of the Frank Slide and theories of rockslide-avalanche mobility. *Canadian Journal of Earth Sciences*, 23:425-432.
- Cruden, D. M. and Varnes, D. J. (1996) - Landslide types and processes. In A. K. Turner and R. L. Schuster (eds.): *Landslides investigation and mitigation*. Nat. Acad. Press, Washington D. C.
- Cundall, P. A. (1971) - A computer model for simulating progressive, large-scale movements in blocky rock systems. *Proc. Symp. Int. Soc. Rock Mech (Nancy)*, 2 art. 8.
- Cundall, P. A. (1987) - Distinct element models of rock and soil structures. In E.T. Brown (ed.): *Analytical and computational methods in engineering Rock Mechanics*. Allen & Unwin, 129-163.
- Cundall, P. A. and Strack, O. D. L. (1979) - A discrete numerical model for granular assemblies. *Géotechnique*, 29(1):47-65.

- Curry, R. R. (1966) - Observation of alpine mudflows in the Tenmile Range, central Colorado: Geological Society of America Bulletin, 77:771-776.
- DeGraff, J. (1994) - The geomorphology of some debris flows in the southern Sierra Nevada, California. *Geomorphology*, 10:231-252.
- Denlinger, R.P. and Iverson, R.M. (2001) - Flow of variably fluidized granular masses across 3-D terrain: 2. Numerical predictions and experimental tests: *Journal of Geophysical Research*, 106 (B1): 537-552.
- Desai, C. S. and Siriwardane H. J. (1984) - Constitutive laws for engineering materials, with emphasis on geologic materials. Prentice- Hall, Englewood Cliffs, N. J., 468 pp.
- Dinehart, R. L. (1997) - Sediment transport in the hyperconcentrated phase of the march 19, 1982, lahar. In T.C. Pierson (ed.): *Hydrologic Consequences of Hot-Rock/Snowpack Interactions at Mount St. Helens, Washington, 1982-1984*. U.S. Geol. Surv. Open-File Report, n. 96-179, 37-52.
- Drake, T.G. (1990) - Structural features in granular flows. *Journal of Geophysical Research*, 95(B6):8681-8696.
- Duran, J. (2000) - *Sands, Powders, and Grains - An Introduction to the Physics of Granular Materials*. Springer, N. Y., 214 pp.
- Eckersley, J. D. (1990) - Instrumented laboratory flowslides. *Geotechnique*, 40:489-502.
- Fink, J. H., Malin, M. C., D'Alli, R. E. and Greeley, R. (1981) - Rheological properties of mudflows associated with the spring 1980 eruptions of Mount St. Helens volcano, Washington. *Geophysical Research Letters*, 8:43-46.
- Einstein, A. (1906) - A new determination of molecular dimensions. *Annalen der Physik*, 19:289-306.
- Erismann, T. H. (1979) - Mechanism of large landslides. *Rock Mech.*, 12, 15-46
- Evans, S. G. and Hungr, O. (1993) - The assessment of rockfall hazards at the base of talus slopes. *Canadian Geotechnical Journal*, 30: 620-636.
- Evans, S. G., Hungr, O. and Enegegn, E. G. (1994) - The Avalanche Lake rock avalanche, Northwest Territories, Canada: description, dating and dynamics. *Canadian Geotechnical Journal*, 31:749-768.
- Evans, S. G., Hungr, O. and Clague J. J. (2001) - The 1984 rock avalanche from the western flank of Mt. Cayley, Garibaldi Volcanic Belt, British Columbia: description and dynamic analysis. *Engineering Geology*. In press
- Folk, R. L. (1984) - *Petrology of sedimentary rocks*. Hemphill, Austin, Texas, 184 pp.
- Fryxell, F. M. and Horberg, L. (1943) - Alpine mudflows in Grand Teton National Park, Wyoming. *Geological Society of America Bulletin*, 54:457-472.
- Gibson, R. E., Knight, K. and Taylor, P. W. (1963) - A critical experiment to examine theories of three-dimensional consolidation, in problems of settlements and compressibility of soils. *Proc. of the European Conference on Soil Mechanics and Foundation Engineering; Wiesbaden, Germany, v. I*, 69-76.
- Gidaspow, D. (1994) - *Multiphase flow and fluidization*. Academic, San Diego, Calif., 467 pp.
- Goguel, J. (1978) - Scale-dependent rockslide mechanisms, with emphasis on the role of pure fluid vaporization. In B. Voight (ed.): *Rockslides and avalanches, 1: Natural phenomena*, Chap. 20, Elsevier Amsterdam, 693-705.
- Gray, J. M. N. T., Wieland, M. and Hutter K. (1999) - Gravity driven free surface flow of granular avalanches over complex basal topography, *Proc. R. Soc. London, Ser. A*, 455:1841-1874.
- Hanes, D. M. and Inman, D. L. (1985) - Experimental evaluation of a dynamic yield criterion for granular fluid flows: *Journal of Geophysical Research*, 90(B5), 3670-3674.
- Hampton, M. A. (1979) - Buoyancy in debris flows: *Journal of Sedimentary Petrology*, 49:753-758.
- Harris, S. A. and Gustafson, C. A. (1993) - Debris flow characteristics in an area of continuous permafrost, St. Elias Range, Yukon Territory. *Z. Geomorph.*, 37:41-56.
- Hiiner, G. and Spencer, N. (1998) - Rubbing and scrubbing. *Physics Today*, 51(9):22-27.

- Hiscott, R. N. (1994) - Traction-carpet stratification in turbidites - fact or fiction?. *J. Sediment. Petrol.*, A64:204-208.
- Hiscott, R. N. (1995) - Traction-carpet stratification in turbidites - fact or fiction? Reply. *J. Sediment. Petrol.*, A65:704-705.
- Hoblitt, R. P. (1986) - Observations of the eruptions of July 22 and August 7, 1980, at Mount St. Helens, Washington. *U.S. Geol. Surv. Prof. Pap.*, 1335, 44 pp.
- Hodgson, K. A. and Manville, V. R. (1999) - Sedimentology and flow behavior of a rain-triggered lahar, Mangatoenui Stream, Ruapehu volcano, New Zealand, *Geol. Soc. Am. Bull.*, 111(5):743-754.
- Hsu, K. J. (1975) - Catastrophic debris streams (Sturzstroms) generated by rockfalls: *Geological Society of America Bulletin*, 86:129-140.
- Hsu, K. J. (1978) - Albert Hiem: Observations on landslides and relevance to modern interpretations. In Voight, B. (ed.): *Rockslides and avalanches*, 1: Natural phenomena. Amsterdam, Elsevier, 71-93.
- Hubbert, M. K. and Rubey, W. W. (1959) - Role of fluid pressures in mechanics of overthrust faulting, I: Mechanics of fluid-filled porous solids and its applications to overthrust faulting. *Geol. Soc. Am. Bull.*, 70:115-166.
- Huben, J. F. and Filipov, A. J. (1989) - Debris-flow deposits in alluvial fans on the west flank of the White Mountains, Owens Valley, California, USA: *Sedimentary Geology*, 61:177-205.
- Huguet, D., Thouret, J. C. and Nehlig, P. (1999a) - Lahar (volcanic debris flow) deposit from the Cantal stratovolcano (Massif Central, France), *J. of Conf., EUG X*, 321.
- Huguet, D., Thouret, J. C. and Nehlig, P. (1999b) - Les dépôts de lahars du strato-volcan du Cantal: essai de synthèse, *Doc. BRGM*, 291:20-23. (in french)
- Huguet, D., Thouret, J. C., Nehlig, P. and Raffy, J. (2000) - L'exhumation des paléo-formes en domaine volcanisé: l'exemple du strato-volcan du Cantal (Massif Central), *RST XVIII*, 153. (in french)
- Hui, K. and Haff, P.K. (1986) - Kinetic grain flow in a vertical channel: *International Journal of Multiphase Flow*, 12:289-298.
- Hungr, O. (1990) - Mobility of rock avalanches. *Reports of the National Research Institute for Earth Science and Disaster Prevention, Tsukuba, Japan*, 46: 11-20.
- Hungr, O. (1995) - A model for the runout analysis of rapid flow slides, debris flows and avalanches. *Can Geotech J*, 32(4):610-623.
- Hungr, O. (1997) - Analysis of the motion of a debris avalanche event. *Chikyu ("Earth") magazine, Japan, special issue focused on debris flow hazards*, H.Fukuoka, Ed., 19:661-665 (translated into Japanese).
- Hungr, O. (2000) - Analysis of debris flow surges using the theory of uniformly progressive flow. *Earth Surface Processes and Landforms* 25:1-13.
- Hungr, O. and Evans, S. G. (1996) - Rock avalanche runout prediction using a dynamic model. *Proc. 7th. International Symposium on Landslides, Trondheim, Norway*, 1:233-238.
- Hungr, O. and Evans, S. G. (1997) - A dynamic model for landslides with changing mass. In P.G. Marinos, G. C. Koukis, G. C. Tsiambaos, and G. C. Stournaras (eds.): *Proc. IAEG International symposium on engineering geology and the environment, Athens, June, 1997*, 1:719-724.
- Hungr, O. and Morgenstern, N. R. (1984a) - Experiments on the flow behavior of granular materials at high velocity in an open channel. *Géotechnique*, 34: 405-413. Discussion and Reply, 35: 383-385.
- Hungr, O. and Morgenstern, N. R. (1984b) - High velocity ring shear tests on sand. *Géotechnique*, 34: 415-421.
- Hungr, O., Morgan, G. C. and Kellerhals, R. (1984) - Quantitative analysis of debris torrent hazards for design of remedial measures. *Can. Geotech. J.*, 21: 663-667.
- Hungr, O., Salgado, F. M. and Byrne P. M. (1989) - Evaluation of a three-dimensional method of slope stability analysis, *Can. Geotech. J.*, 26, 679-686.

- Hungr, O., Dawson, R., Kent, A., Campbell, D. and Morgenstern, N. R., 2000. Rapid flow slides of coal mine waste in British Columbia, Canada. In Geological Society of America Reviews (ed.) Catastrophic Landslides. Engineering Geology 14 (in press, 17 msp., 22 figures).
- Hutchinson, J. N. (1986) - A sliding-consolidation model for flow slides. *Can. Geotech. J.*, 23:115-126.
- Hutchinson J. N. (1992) - Landslide hazard assessment. Proc. 6th Int. Symp. on Landslides, Christchurch, New Zealand, 3.
- Hutter, K., Koch, T., Pluss, C. and Savage, S. B. (1995) - The dynamics of avalanches of granular materials from initiation to runout. Part II. Experiments. *Acta Mechanica*, 109, 127-165.
- Inrnan, D. L (1952) - Measures for describing the size distribution of sediments: *Journal of Sedimentary Petrology*, 22:125-145.
- Itasca Consulting Group (1996). Particle flow code in 2-D (PFC-2D), version 1.1. User's manual.
- Iverson, R. M. (1985) - A constitutive equation for mass-movement behavior. *J. Geol.*, 93:143-160.
- Iverson, R. M. (1997a) - The physics of debris flows. *Reviews of Geophysics*, 35(3):245-296.
- Iverson, R. M. (1997b) - Hydraulic modeling of unsteady debris-flow surges with solid-fluid interactions. In C. L. Chen (ed.): *Debris flow hazards mitigation: Mechanics, prediction, and assessment: American Society of Civil Engineers, Proc of 1st International Conference, San Francisco*, 550-560.
- Iverson, R. M. and Denlinger, R. P. (2001) - Flow of variably fluidized granular masses across 3-D terrain: I. Coulomb mixture theory: *Journal of Geophysical Research*, 106(B1), 553-566
- Iverson, R. M. and LaHusen, R. G. (1989) - Dynamic pore-pressure fluctuations in rapidly shearing granular materials. *Science*, 246:796-799.
- Iverson, R. M. and LaHusen, R. G. (1993a) - Friction in debris flows: Inferences from large-scale flume experiments. In H. W. Shen, S. T. Su and F. Wen (eds.): *Hydraulic Engineering '93, Proc. of ASCE 1993 conference, San Francisco, California*, 1604-1609.
- Iverson, R. M. and LaHusen, R. G. (1993b) - Pore-pressure dynamics in debris-flow experiments [abs.]. *Eos (Transactions American Geophysical Union)*, 74:310.
- Iverson, R. M., LaHusen, R. G. and Costa, J. E. (1992) - Debris-flow flume at H. J. Andrews Experimental Forest, Oregon. U.S. Geological Survey Open-File Report, 92-483, 2 p.
- Iverson, R. M., LaHusen, R. G., Major, J. J., and Zimmerman, C. L. (1994) - Debris flow against obstacles and bends: Dynamics and deposits [abs.]. *Eos (Transactions American Geophysical Union)*, v. 75, p. 274.
- Iverson, R. M., M. E. Reid, and R. G. LaHusen (1997) - Debris-flow mobilization from landslides. *Ann. Rev. Earth Planet. Sci.*, 25:85-138.
- Jaeger, H. M., Nagel, S. R. and Behringer, R. P. (1996) - Granular solids, liquids, and gases: *Reviews of Modern Physics*, 68:1259-1272.
- Jakob, M., Hungr, O. and Thomson, B. (1997) - Two debris flows with anomalously high magnitude. In C. L. Chen (ed.): *Debris Flow Hazards Mitigation, Mechanics, Prediction and Assessment. Proc. of The First International Conference on Debris Flow Hazards ASCE, San Francisco*, 382-394.
- Jakob, M., Anderson, D., Fuller, T., Hungr, O. and Ayotte, D. (2000) - An Unusually Large Debris Flow at Hummingbird Creek, Mara Lake, British Columbia. *Can. Geotech. J.*, 38 (in press)
- Janda R. J., Scott K. M., Nolan M. and Martinson H. A. (1980) - Lahar movement, effects and deposits. In P.W. Lipman and D. R. Mullineaux (eds.): *The 1980 eruptions of Mount St. Helens, Washington. U.S. Geol. Surv. Prof. Pap.*, n. 1250, 461-478.
- Johnson, A. M. (1970) - *Physical processes in geology. Freeman, Cooper and Co., San Francisco*, 576p.
- Johnson, A. M. (1984) - Debris flow. In D. Brunsten and D. B. Prior (eds.): *Slope instability. John Wiley and Sons, N. Y.*, 257-361.

- Johnson, S. E., (1997) The 1996 Thenalt Creek debris flows and debris avalanches in the Columbia River Gorge east of Ponland, Oregon. C. L. Chen (ed.): Debris Flow Hazards Mitigation, Mechanics, Prediction and Assessment. Proc. of The First International Conference on Debris Flow Hazards ASCE, San Francisco, 395-404.
- Kirn, S. B., Chough, S. K. and Chun, S. S. (1995) - Bouldery deposits in the lowermost part of the Cretaceous Kyokpori Formation, SW Korea: Cohesionless debris flows and debris falls on a steep-gradient delta slope. *Sedimentary Geology*, 98:97-119.
- Kohlbeck, F., Mojica, J. and Scheidegger, A.E. (1994) - Clast orientation of the 1985 lahars of the Nevado del Ruiz, Colombia and implications for depositional processes. *Sedimentary Geology*, 88:175-183.
- Kuntz, M.A., Rowley, P.D., MacLeod, N.S., Reynolds, R.L., McBroome, L.A., Kaplan, A.M., and Lidke, D.J. (1981) - Petrography and particle size distribution of pyroclastic flow, ash cloud and surge deposits. In P.W. Lipman and D.R. Mullineaux (eds.): The 1980 eruptions of Mount St Helens, Washington. U.S. Geological Survey Professional Paper, 1250:525-539.
- Laberg, J S. and Vorren T. O. (1995) - Late Weichselian subnarine debris flow deposits on the BearIsland Trough Mouth Fan. *Marine Geology*, 127:45-72.
- Lambe, T. W. and R. V. Whitman (1979) - Soil Mechanics, SI Version. John Wiley, New York, 553 pp.
- Lavigne, F. (1998) - Les lahars du volcan Merapi, Java Central: déclenchement, budget sédimentaire, dynamique et risques associés. Thèse de Doctorat (géographie physique), Université Blaise Pascal, Clermont-Ferrand, 539 pp. (inédit).
- Lowe, D. R. (1975) - Water escape structures in coarse-grained sediments. *Sedimentology*, 22:157-204.
- Lowe, D. R. (1976) - Grain flow and grain flow deposits. *Journal of Sedimentary Petrology*, 46:188-199.
- Lowe, D. R. (1976) - Grain flow and grain flow deposits. *Journal of Sedimentary Petrology*, 46:188-199.
- Ivohrig, D., Whipple, K. X., Hondzo, M., Ellis, C. and Parker, G. (1998) - Hydroplaning of subaqueous debris flows. *Geological Society of America Bulletin*, 110:387-394.
- Major, J. J. (1996) - Experimental studies of deposition by debris flows: process, characteristics of deposits and effects of pore-fluid pressure. Ph.D. thesis, Seattle, University of Washington, 341 pp.
- Major, J. J. (1997) - Depositional processes in large-scale debris-flow experiments. *Jour. of Geol.*, 105:345-366.
- Major, J. J. (1998) - Pebble orientation on large, experimental debris-flow deposits. *Sediment. Geol.*, 117:151-164.
- Major, J. J. (in press) - Gravity-driven consolidation of granular slurries: implications for debris-flow deposition and deposit characteristics. *Journal of Sedimentary Research*.
- Major, J. J. and Voight, B. (1986) - Sedimentology and clast orientation of the 18 may 1980 southwest-flank lahars, Mount St. Helens, Washington. *J. Sedim. Petrol.*, 56 (5):691-705.
- Major, J. J. and Newhall, C. G. (1989) - Snow and ice perturbation during historical volcanic eruptions and the formation of lahars and floods: a global review. *Bull. Volcanol.*, 52:1-27.
- Major, J. J. and Pierson, T. C. (1992) - Debris flow rheology: experimental analysis of fine-grained slurries. *Water Resources Research*, 28:841-857.
- Major, J. J and Iverson, R. M. (1999) - Debris-flow deposition: effects of pore-fluid pressure and friction concentrated at flow margins. *Geol. Soc. Am. Bull.*, 111 (10):1424-1434.
- Major, J. J., Iverson, R. M., McTigue, D., Macias, S. and Fiedorowicz, B. K. (1997) - Geotechnical properties of debris-flow sediments and slurries. In C.L. Chen (ed.): Debris flow hazards mitigation: mechanics, prediction, and assessment. American Society of Civil Engineers, Proceedings of First International Conference, August 7-9, San Francisco: 249-259.
- Masson, D. G., Huggett, Q. J. and Brunsdon, D. (1993) - The surface texture of the Saharan debris flow deposit and some speculations on submarine debris flow processes. *Sedimentology*, 40:583-598.

- Melosh, H.J. (1979) - Acoustic fluidization: a new geological process?. *Jour. Geophys. Res.*, 84:8097-8113.
- Middleton, G. V. and Hampton, M. A. (1976) - Subaqueous sediment transport and deposition by sediment gravity flows. In D.J. Stanley and D. J. P. Swift (eds.): *Marine sediment transport and environmental management*, New York, John Wiley and Sons: 197-218.
- Middleton, G. V. (1993) - Sediment deposition from turbidity currents. *Annual Review of Earth and Planetary Sciences*, 21:89-114.
- Mills, H. H. (1984) - Clast orientation in Mount St Helens debris-flow deposits, North Fork Toutle River, Washington. *J. Sediment. Petrol.*, 54:626-634.
- Monon, D. M. and Campbell, R. H. (1974) - Spring mudflows at Wrightwood, Southern California. *Quarterly Journal of Engineering Geology*, 7:377-384.
- Mothes, P.A., Hall, M.L. and Janda, R.J. (1998) - The enormous Chillos Valley Lahar: an ash flow-generated debris flow from Cotopaxi volcano, Ecuador, *Bull. Volcanol.*, 59, 233-244.
- Naylor, M.A. (1980) - The origin of inverse grading in muddy debris flow deposits-a review. *J. Sedim. Petrol.*, 50 (4):1111-1116.
- Nemec, W. and Steel, R. J. (1984) - Alluvial and coastal conglomerates. Their significant features and some comments on gravelly mass-flow deposits. In E.H. Koster and R. J Steel. (eds.): *Sedimentology of gravels and conglomerates*. Canadian Society of Petroleum Geologists Memoir, 10:1-31.
- Nieuwenhuijzen, M. E. and Van Steijn, H. (1990) - Alpine debris flows and their sedimentary properties. A case study from the French Alps. *Permafrost and Periglacial Processes*, 1:111-128.
- O'Brien, J. S. and Julien P.Y. (1988) - Laboratory analysis of mudflow properties. *J. Hydraul. Eng.*, 114:877-887.
- Okuda, S., Suwa, H., Okunislù, K., Yokoyama, K. and Nakano, M. (1980) - Observations on the motion of a debris flow and its geomorphological effects. *Z. Geomorph.*, 35:142-163.
- Okuda, S., Suwa, H., Okunislù, K. and Yokoyama, K. (1981) - Depositional processes of debris flow at Kanùkanlihorì fan, Northern Japan Alps. *Japanese Geomorphological Union Transactions*, 2:353--361.
- Palladino, D. M. and Valentine, G. A. (1995) - Coarse tail vertical and lateral grading in pyroclastic flow deposits of the Latera Volcanic Complex (Vulsini, Central Italy): Origin and implications for flow dynamics. *Journal of Volcanology and Geothermal Research*, 69:343-364.
- Palmer, B. A., Alloway, B. V. and Neall, V. E. (1991) - Volcanic debris-avalanche deposits in New-Zealand: lithofacies organisation in unconfined, wet-avalanche flows. In R.V. Fisher and G.A. Smith (eds.): *Sedimentation in Volcanic Settings*, SEPM Spe. Publ., 45:89-98.
- Pariseau, W.G. and Voight, B. (1978) - Rockslides and avalanches: basic principles, and perspectives in the realm of civil and mining operations. In B. Voight (ed.): *Rockslides and avalanches*, 2 Engineering sites, Elsevier, Amsterdam:1-86.
- Passman, S. L. and McTigue, D. F. (1986) - A new approach to the effective stress principle. In S. K. Saxena (ed.): *Compressibility Phenomena in Subsidence*, Eng. Found., New York: 79-91.
- Phillips, C. J. and Davies, T. R. H. (1991) - Determining rheological parameters of debris flow material. *Geomorphology*, 4:101-110.
- Pierson, T. C. (1980) - Erosion and deposition by debris flows at Mt. Thomas, North Canterbury, New Zealand. *Earth Surface Processes*, 5:227-247.
- Pierson, T. C. (1981) - Dominant particle support mechanisms in debris flows at Mt. Thomas, New Zealand, and implications for flow mobility. *Sedimentology*, 28:49-60.
- Pierson, T. C. (1984) - Why debris flows stop. *Geological Society of America Abstracts with Programs*, 16:623.
- Pierson, T. C. (1985) - Initiation and flow behavior of the 1980 Pine Creek and Muddy River lahars, Mount St. Helens, Washington. *Geol. Soc. Am. Bull.*, 96:1056-1069.
- Pierson, T. C. (1986) - Flow behaviour of channelized debris flows, Mount St Helens, Washington, in Abrahams A.D. (ed): *Hillslope Processes*, Allen and Unwin, Boston: 269-296.

- Pierson, T. C. (1995) - Flow characteristics of large eruption-triggered debris flows at snow-clad volcanoes: constraints for debris-flow models. *J. Volcanol. Geotherm. Res.*, 66:283-294.
- Pierson, T. C. (1997) - Transformation of water flood to debris flow following the eruption-triggered transient-lake breakout from the crater on March 19, 1982. In T.C. Pierson (ed.): *Hydrologic Consequences of Hot-Rock/Snowpack Interactions at Mount St. Helens, Washington, 1982-1984*, U.S. Geol. Surv. Open-File Report, 96-179:19-36.
- Pierson, T. C. (1998) - An empirical method for estimating travel times for wet volcanic mass flows. *Bull. Volcanol.*, 60:98-109.
- Pierson, T. C. and Scott, K. M. (1985) - Downstream dilution of a lahar: transition from debris flow to hyperconcentrated streamflow. *Water Resour. Res.*, 21 (10):1511-1524.
- Pierson, T. C. and Costa, J. E. (1987) - A rheologic classification of subaerial sediment-water flows. In J.E. Costa and G.F. Wieczorek (eds.): *Debris Flows/Avalanches: process, recognition and mitigation*. *Rev. Eng. Geol., Geol. Soc. Am., Boulder, Co.*, 7:1-12.
- Pierson, T. C. and Waitt, R. B. (1997) - Dome-collapse rockslide and multiple sediment-water flows generated by a small explosive eruption on February 2-3, 1983. In T.C. Pierson (ed.): *Hydrologic Consequences of Hot-Rock/Snowpack Interactions at Mount St. Helens, Washington, 1982-1984*. U.S. Geol. Surv. Open-File Report, 96-179:53-68.
- Pierson, T. C., Janda, R., Thouret, J. C. and Borrero, C. A. (1990) - Perturbation and melting of snow and ice by the 13, November 1985 eruption of Nevado del Ruiz, Colombia, and consequent mobilization, flow and deposition of lahars. *J. Volcanol. Geotherm. Res.*, 41:17-66.
- Pierson, T. C., Daag, A. S., Delos Reyes, P. J., Regalado, M., Soludum R. U. and Tubianosa, B. S. (1996) - Flow and deposition of post-eruption hot lahars on the East side of Mount Pinatubo, July-October 1991. In C.G. Newhall and R.S. Punongbayan (eds.): *Fire and Mud, Eruptions & Lahars of Mount Pinatubo, Philippines*. Philippines Institute of Volcanology & Seismology, Quezon City and University of Washington Press, Seattle.
- Pouliquen, O. and Delour, J. and Savage, S.B. (1997) - Fingering in granular flows: *Nature*, 386:816-817.
- Pringle, P.T. and Cameron, K.A. (1997) - Eruption-triggered lahar on May 14, 1984. In T.C. Pierson (ed.): *Hydrologic Consequences of Hot-Rock/Snowpack Interactions at Mount St. Helens, Washington, 1982-1984*. U.S. Geol. Surv. Open-File Report, 96-179:81-103.
- Punongbayan, R. S., Newhall, C. G. and Hoblitt, R. P. (1996) - Photographic record of rapid geomorphic change at Mount Pinatubo, 1991-94. In C.G. Newhall and R.S. Punongbayan (eds.): *Fire and mud. Eruptions and lahars of Mount Pinatubo: Quezon City, Philippine Institute of Volcanology and Seismology, Seattle, University of Washington Press*:21-66.
- Rankine, W. J. M. (1857) - On the stability of loose earth, *Philos. Trans. R. Soc. London*, 147:9-27.
- Reid, M. E. and Iverson R.M. (1992) - Gravity-driven groundwater flow and slope failure potential, 2: Effects of slope morphology, material properties, and hydraulic heterogeneity. *Water Resour. Res.*, 28: 939- 950.
- Reid, M. E., R. G. LaHusen, and R. M. Iverson, *Debris-flow initiation experiments using diverse*
- Rickmers, W. R. (1913) - *The Duab of Turkestan*. Cambridge University Press, 563 pp.
- Rodolfo, K. S. (1989) - Origin and early evolution of lahar channel at Mabinit, Mayon volcano, Philippines. *Geol. Soc. Am. Bull.*, 101:414-426.
- Rodolfo, K. S., Arguden, A. T., Solidum, R. U. and Umbal, J. V. (1989) - Anatomy and behaviour of a post-eruptive rain lahar triggered by a typhoon on Mayon Volcano, Philippines. *International Association of Engineering Geology Bulletin*, 40:55-66.
- Rodolfo, K. S. and Arguden, A. T. (1991) - Rain-lahar generation and sediment-delivery systems at Mayon volcano, Philippines. In G.A. Smith and R.V. Fisher (eds.): *Sedimentation in Volcanic Settings*. *SEPM Spe. Publ.* 45:71-87.
- Savage, S.B. (1984) - The mechanics of rapid granular flows. *Advances in Applied Mechanics*, 24:289-366.
- Savage, S.B. and Sayed, M. (1984) - Stresses developed in dry cohesionless granular materials sheared in an annular shear cell. *Journal of Fluid Mechanics*, 142:391-430.

- Savage, S.B. and McKeown, S. (1983) - Shear stresses developed during rapid shear of dense concentrations of large spherical particles between concentric cylinders: *Journal of Fluid Mechanics*, 127: 453-472.
- Savage, S.B. and Hutter, K. (1989) - The motion of a finite mass of granular material down a rough incline. *Journal of Fluid Mechanics*, 199:177-215.
- Savage, S. B. and Hutter, K. (1991) - The dynamics of avalanches of granular materials from initiation to runout. Part I: Analysis. *Acta Mechanica*, 86:201-223.
- Scheidegger, A.E. (1973) - On the prediction of the reach and velocity of catastrophic landslides. *Rock Mech.*, 5:231-236.
- Schonfeld, B. (1996) - Roll waves in granular flows and debris flows. Master's thesis, Montreal, Canada, McGill University, 160 pp.
- Schrincke, H. U. (1967) - Graded lahars in the type sections of the Ellensburg Formation, south-central Washington. *Journal of Sedimentary Petrology*, 37:438--448.
- Schwab, W. C., Lee, H. J., Twichell, D. C., Locat, J., Nelson, C. H., McArthur, W. G., and Kenyon, N. H. (1990) - Sediment mass-flow processes on a depositional lobe, Outer Mississippi Fan. *Journal of Sedimentary Research*, 66:916--927.
- Schiffman, R. L., Chen, A. T. F. and Jordan, J. C. (1969) - An analysis of consolidation theories. *American Society of Civil Engineers Proceedings, Journal of the Soil Mechanics and Foundation Division*, SMI:285-312.
- Scott, K. M. (1988a) - Origins, behavior and sedimentology of lahar-runout flows in the Toutle-Cowlitz River system. *U.S. Geol. Surv. Prof. Pap.*, 1447-A, 74 pp.
- Scott, K. M. (1988b) - Magnitude and frequency of lahars and lahars-runout flows in the Toutle-Cowlitz River system, U.S. Geol. Surv. Prof. Pap., 1447-B, 33 pp.
- Scott, K. M., Vallance, J. W. and Pringle, P. T. (1995) - Sedimentology, behavior, and hazards of debris flows at Mount Rainier, Washington. *U.S. Geol. Surv. Prof. Pap.*, 1547, 56 pp.
- Sharp, R. P. and Nobles, L. H. (1953) - Mudflow of 1941 at Wrightwood, southern California. *Geological Society of America Bulletin*, 64:547-560.
- Shreeve, R. L. (1968) - Leakage and fluidisation in air lubricated avalanches. *Geol. Soc. Am. Bull.*, 79:653-658.
- Singewald, J. T. (1928) - Mudflow as a geologic agent in semiarid mountains. *Comrnent. Geological Society of America Bulletin*, 39:480--483.
- Smith, G. A. and Fritz, W. J. (1989) -Volcanic influences on terrestrial sedimentation. *Geology*, 17:375-376.
- Smith, G. A. and Lowe, D.R. (1991) - Lahars: volcano-hydrologic events and deposition in the debris flow-hyperconcentrated flow continuum. In G.A. Smith R.V. Fisher (eds.). *Sedimentation in Volcanic Settings*, SEPM Spe. Pub., 45:59-69.
- Sohn, Y. K. (1997) - On traction-carpet sedimentation. *J. Sediment. Res.*, 67 (3):502-509.
- Sousa, J. and Voight, B. (1991) - Continuum simulation of flow failures. *Geotechnique*, 41:515-538.
- Suwa, H. (1988) - Focusing mechanism of large boulders to a debris-flow front. *Japanese Geomorphological Union Transactions*, 9:151-178.
- Suwa, H. and Okuda, S. (1983) - Deposition of debris flows on a fan surface, Mt Yakedake, Japan. *Z. Geomorph.*, supplement, 46:79-101.
- Takahashi, T. (1978) - Mechanical aspects of debris flow. *American Society of Civil Engineers Proceedings, Journal of the Hydraulics Division*, 104:1153-1169.
- Takahashi, T (1991) - Debris flow. Balkema, Rotterdam, Netherlands, 165 pp.
- Tanner, L. H. and Huberl, J. F. (1991) - Basalt breccias and conglomerates in the lower McCoy Brook Formation, Fundy Basin, Nova Scotia: Differentiation of talus and debris-flow deposits. *Journal of Sedimentary Petrology*, 61:15-27.
- Terzaghi, K. (1923) - Die Berechnung der Durchliissigkeitsziffer des Tones aus dem Verlauf der Hydrodynamischen Spannungsercheinungen. *Akademie der Wissenschaften in Wien, Sitzungsberichte: Mathematisch-Naturwissenschaftliche Klasse, part IIa*, 132 (314):125-128.
- Terzaghi, K. (1943) - Theoretical soil mechanics. NewYork, John Wiley and Sons, 510 pp.

- Terzaghi, K. (1956) - Varieties of submarine slope failures. Proceedings of Eighth Texas Conference on Soil Mechanics and Foundation Engineering, Austin, University of Texas, Bureau of Engineering Research, Special Publication 29, September 14-15:3.1-3.41.
- Thouret, J. C. (1993) - Des paléo-volcans aux volcans actifs. *Bull. Assoc. Géogr. Franç.*, 4:326-365.
- Thouret, J. C., Abdurachman, K.E., Bourdier, J.-L. & Bronto, S. (1998) - Origin, characteristics, and behaviour of lahars following the 1990 eruption of Kelud volcano, Eastern Java (Indonesia). *Bull. Volcanol.*, 59:460-480.
- Vallance, J. W. (1994) - Experimental and field studies related to the behavior of granular mass flows and the characteristics of their deposits. Ph.D. thesis, Houghton, Michigan Technological University, 197 pp.
- Vallance, J.W. (2000) - Lahars. In Sigmanson et al. (eds.): *Encyclopedia of Volcanoes*. Academic Press:601-616.
- Vallance, J. W. and Scott, K.M. (1997) - The Osceola mudflow from Mount Rainier: sedimentology and hazard implication of a huge clay-rich debris flow. *Geol. Soc. Am. Bull.*, 109 (2):143-163.
- Vallance, J. W. and Savage, S.B. (2000) - Particle segregation in granular flows down chutes. In A. Ro-sato and D. Blackmore (eds.): *Segregation in granular flows*. International Union of Theoretical and Applied Mechanics symposium, Dordrecht, Netherlands:31-51.
- Vallejo, L. E. (1979) - An explanation for mudflows. *Geotechnique*, 29:351-354.
- VanDine, D. F., Hungr, O., Lister, D. R. and Chatwin, S. C. (1997) - Channelized debris flow mitigative structures in British Columbia, Canada. In C. Chen (ed.) *Debris Flow Hazards Mitigation, Mechanics, Prediction and Assessment*. Procs., The First International Conference on Debris Flow Hazards ASCE, San Francisco:606-615.
- Varnes, D. J. (1978) - Slope movement types and processes. In *Landslides, analysis and control*. Transportation Research Board, Washington, D.C., Special Report 176:11-33.
- Vignaux, M. and Weir, G.J. (1990) - A general model for Mt. Ruapehu lahars. *Bull. Volcanol.*, 52:381-390.
- Walton, A.W. and Palmer, B.A. (1988) - Lahar facies of the Mount Dutton Formation (Oligocene-Miocene) in the Marysvale volcanic field, Southwestern Utah. *Geol. Soc. Am. Bull.*, 100:1078-1091.
- Wasson, R. J. (1978) - A debris flow at Reshun, Pakistan Hindu Kush. *Geografiska Annaler*, 60:151-159.
- Webb, R. H., Pringle, P. T., Reneau, S. L., and Rink, G. R. (1988) - Monument Creek debris flow, 1984. Implications for formation of rapids on the Colorado River in Grand Canyon National Park. *GeoIogy*, 16:50-54.
- Whipple, K.X. and Dunne, T. (1992) - The influence of debris-flow rheology on fan morphology, Owens Valley, California. *Geological Society of America Bulletin*, 104:887-900.
- Wilson, L. and Head, J.W. (1981) - Morphology and rheology of pyroclastic flows and their deposits, and guidelines for future observations. In P.W. Lipman and D.R. Mullineaux (eds.): *The 1980 eruptions of Mount St. Helens, Washington*. U.S. Geological Survey Professional Paper, 1250:513-524.
- WP/WLI (1993) - Multilingual landslide glossary. Int. Geotechnical Societies, UNESCO Working Party on World Landslide Inventory. Bitech publ., Richmond, B.C.
- Yano, K. and Daido, A. (1965) - Fundamental study on mudflow. *Kyoto, Disaster Prevention Research Institute Bulletin*, 14 (2):69-83.
- Youd, T. L. (1973) - Liquefaction, flow, and associated ground failure. U.S. Geological Survey Circular 688, 12 pp.